Molecular Relaxations and Crystallization Kinetics of Amorphous Pharmaceuticals using Broadband Dielectric Spectroscopy

Thesis submitted to
the University of Calicut in partial fulfillment of the
requirements for the award of the degree of

DOCTOR OF PHILOSOPHY IN PHYSICS

by
SAHRA MOHAMED

Under the guidance of
Dr. Mohamed Shahin Thayyil

DEPARTMENT OF PHYSICS
UNIVERSITY OF CALICUT
KERALA- 673635
INDIA
JULY, 2019

UNIVERSITY OF CALICUT
Department of Physics

Calicut University P.O.,
Kerala, 673635, INDIA
✆ 0494 2407416, 9961824725
Email : shahin@uoc.ac.in
www.universityofcalicut.info

Dr. Mohamed Shahin Thayyil
Assistant Professor

CERTIFICATE

Certified that the corrections / suggestions from the adjudicators of the Ph. D. thesis entitled "**Molecular Relaxations and Crystallization Kinetics of Amorphous Pharmaceuticals using Broadband Dielectric Spectroscopy**" *submitted by Mrs. Sahra Mohamed, research scholar of Department of Physics under my supervision and guidance, have been incorporated in this copy of the thesis and has been checked for plagiarism, using* ***URKUND*** *software at CHMK library, University of Calicut. The contents in the hardcopy and softcopy are same.*

University of Calicut

Dr. MOHAMED SHAHIN THAYYIL
(Supervisor)

DECLARATION

It is hereby declared that the thesis entitled "**Molecular Relaxations and Crystallization Kinetics of Amorphous Pharmaceuticals using Broadband Dielectric Spectroscopy**" submitted herewith is an authentic record of the research work carried out by me under the supervision of **Dr. Mohamed Shahin Thayyil**, Assistant Professor, Department of Physics, University of Calicut, in partial fulfillment of the requirements for the award of the degree of Doctor of Philosophy in Physics under the Faculty of Sciences, University of Calicut, Kerala. The contents of this thesis have not been submitted to any other institute or University for the award of any degree or diploma.

Place: Calicut University

Date:

SAHRA MOHAMED

UNIVERSITY OF CALICUT
Department of Physics

Calicut University P.O.,
Kerala, 673635, INDIA
✆ 0494 2407416, 9961824725
Email : shahin@uoc.ac.in
www.universityofcalicut.info

Dr. Mohamed Shahin Thayyil
Assistant Professor

CERTIFICATE

This is to certify that the thesis entitled "**Molecular Relaxations and Crystallization Kinetics of Amorphous Pharmaceuticals using Broadband Dielectric Spectroscopy**" is an authentic record of the research work carried out by **Ms. SAHRA MOHAMED** under my guidance for the award of the degree of Doctor of Philosophy in Physics under the faculty of Sciences, University of Calicut, Kerala and the same has not been submitted elsewhere for any degree or diploma.

University of Calicut

Dr. MOHAMED SHAHIN THAYYIL
(Supervisor)

UNIVERSITY OF CALICUT
CERTIFICATE ON PLAGIARISM CHECK

1.	Name of the research scholar	SAHRA MOHAMED		
2.	Title of thesis/dissertation	Molecular Relaxations and Crystallization Kinetics of Amorphous Pharmaceuticals using Broadband Dielectric Spectroscopy.		
3.	Name of the supervisor	Dr. Mohamed Shabin Thayyil		
4.	Department/Institution	Department of Physics University of Calicut		
5.		Introduction/ Review of literature	Materials and Methods	Result/ Discussion/Summary/ Conclusion
	Similar content (%) identified	2%	9%	1%
	Acceptable maximum limit (%)	25 /35	25	10
6.	Software used	Urkund		
7.	Date of verification	22/6/2019		

**Report on plagiarism check, specifying included/excluded items with % of similarity to be attached.*

Checked by (with name, designation & signature)

Dr. Vinod V.K.
Assistant Librarian
University of Calicut

Name & Signature of the Researcher SAHRA MOHAMED

Name & Signature of the Supervisor

25/06/2019.

Dr.MOHAMED SHAHIN THAYYIL
ASST. PROFESSOR
Department of Physics, University of Calicut
Kerala (India), Pin: 673635

The Doctoral Committee* has verified the report on plagiarism check with the contents of the thesis, as summarized above and appropriate measures have been taken to ensure originality of the Research accomplished herein.

Dr. M. Vinodkumar
Prof. & Head,
Department of Physics
University of Calicut
Kerala-673635, India.

12/7/19

Name & Signature of the HoD/HoI (Chairperson of the Doctoral Committee)

** In case of languages like Malayalam, Tamil, etc. on which no software is available for plagiarism check, a manual check shall be made by the Doctoral Committee, for which an additional certificate has to be attached*

ACKNOWLEDGEMENT

The completion of my work would not have been possible without the inspiration, support and encouragement of great many people. I take this opportunity to owe my gratitude to all those people.

I would like to express my sincere gratitude to my supervisor, Dr. Mohamed Shahin Thayyil for his guidance, constant support and valuable suggestions. He did whatever was required, for the successful completion of the endeavor, allowing me the room to work in my own way.

With a sense of regard and reverence, I would like to express my deep gratitude and heartfelt thanks to Dr. A. K. Bansal, Professor and Head, Department of Pharmaceutics, National Institute of Pharmaceutical Education and Research, Punjab, India, for providing necessary facilities, help and support for completing this work.

I owe my heartfelt thanks to Dr. K.L Ngai, Dipartimento di Fisica, Università di Pisa, Largo B. Pontecorvo 3, I-56127 Pisa, Italy, for his motivation and indispensable suggestions.

I would like to thank our present Head of the Department, Dr.A.M Vinodkumar and our former HOD's for offering personal and institutional support. I express my sincerest thanks to all other faculty members of the Department for their perceptive encouragement. I am also greatful to all the past and present non teaching staff in the department of Physics for their kindness and assistance.

I would like to express my sincere gratitude to my beloved colleagues and superior officers in Forensic Science Laboratory, Thiruvananthapuram. Without their support and co-operation, I would not have been able to complete this work.

I would like to acknowledge all the teachers and mentors I met from since my childhood. Each of your time, energy, and expertise had made me what I am today. I gratefully acknowledge University Grant Commission, India for providing financial assistance through MANF scheme.

I also thank my friends (too many to list here!! So gals and guys please excuse) for the fabulous memories and unfailing support through the years. I especially thank Safna for her endorsement during the last period of my work and Jini for her warmthness and delicious food. I also extend my gratitude to Sulaiman and Shabeeba. I offer my thanks to all my lab mates and friends in department of Physics.

Finally my deep and sincere gratitude to my family for inspiring me to follow my dreams. I know I always have my family to count on when times are rough. My parents deserve special mention for their continuous and unparalleled love, never ending encouragement and emotional support. I always knew that they believed in me and wanted the best for me. This journey would not have been possible if not for them, and I dedicate this work to them.

Sahra Mohamed

PREFACE

Cooling a liquid below its melting point usually results in crystallisation. However, if the system is exposed to high enough cooling rates, the molecules do not get sufficient time to rearrange themselves and the crystallization may be bypassed and it continues to be in supercooled liquid phase. On further cooling the dynamics become kinetically frozen and eventually become glass or amorphous solid. During this process of glass formation, the characteristic time for molecular motion in a liquid in picoseconds regime elongates to some few hundred seconds around the glass transition temperature (T_g), where molecular dynamics falls out of equilibrium in laboratory time scales. Below the glass transition temperature the material is locked in non-equilibrium state. Experimental techniques used for probing the dynamics of the glass forming systems include dielectric spectroscopy, Differential Scanning Calorimetry (DSC), Nuclear Magnetic Resonance (NMR), X-ray diffractometry, Fourier Transform Infrared spectroscopy (FTIR) *etc*. Among the experimental techniques broadband dielectric spectroscopy (BDS) is a very important and useful tool for monitoring the dynamic susceptibility of a system over a broad frequency range of up to 15 decades. Among the various relaxations observed in time or frequency window, the slowest of these processes is usually called as main or structural α-relaxation as it causes all correlations within the liquid to disappear and characterising the glass transition. The time constant of this process can be related to the overall viscosity of the material. On shorter timescales, additional secondary processes appear between the α-relaxation and microscopic dynamics, depending on the flexibility or intra-molecular degrees of

freedom of the molecules. These intra-molecular degrees of freedom are the backbone of the applicability of a polymer for practical purposes. However, even in case of the simplest rigid molecules, having no intra-molecular degrees of freedom, there appears secondary β-relaxation of intermolecular origin called Johari-Goldstein (JG) relaxation. JG relaxation is a matter of intense debate among the researchers, as their microscopic origin and their significance for the overall relaxation behaviour are by no means well understood.

Solubility and absorption of the active pharmaceutical ingredient with body fluids is important for getting the effect of a drug. During last decade about 40% of examined pharmaceutical drugs turned out to be poorly water-soluble, this results in their inadequate bioavailability. Improving the bioavailability (dissolution rate and solubility) of a pharmaceutical, especially life saving drugs, is the major issue the modern pharmaceutical industry has been addressing. Common methods adopted are usages of cyclodextrins, polymorphism or solvated compounds, nanotechnology, micronization, spray drying etc. The other alternative is to prepare drugs in the amorphous form, which is found to be more soluble, and have better dissolution rate and in consequence improved bioavailability. For commercial use, amorphous drugs must be stable for at least 3 –5 years. But, in many occasions practical advantages of amorphous drugs are lost because of the thermodynamic instability in the amorphous phase. During storage it may get converted to its stable crystalline form. Understanding the major factors responsible for recrystallization of the amorphous pharmaceutical can give insights to bypass this problem and would help the industry to develop amorphous drugs which are physically and chemically stable for a

longer shelf life. So critical study of broadband dielectric spectroscopy and other phase information will give insight to the basic physics and give way to device better technology for these issues.

In this work we present, the thermal and spectroscopic investigations of three hydrogen bonded active pharmaceutical ingredients (APIs) namely, clofoctol, droperidol and probucol. Glass forming ability of the samples were analyzed using DSC. The relaxation dynamics of APIs were investigated in supercooled and glassy states over broad frequency and temperature ranges at ambient pressure using BDS. To find the origin of the secondary relaxations, CM predictions were used. It was further verified from the computational investigations with the help of density functional theory. The pharmaceuticals, chosen for study have significantly broader structural dispersion than the majority of the drugs investigated so far and thus we have carried out the anti-correlation study between the width of the structural loss peak at T_g to the polarity of the drugs in the light of dipole-dipole interaction to the attractive part of the intermolecular potential. They are instrumental in testing the anti-correlation within the family of molecular pharmaceuticals as part of the totality of molecular glass formers studied by dielectric spectroscopy. Also the isothermal crystallization kinetics of clofoctol and droperidol were investigated using BDS and was analyzed using Avrami and Avramov models. The thesis is organized as follows.

Chapter 1 : Gives general introduction about glass, applications of amorphous systems in various fields including amorphous pharmaceuticals, literature review of

amorphous pharmaceuticals, advantages and challenges of amorphous formulation.

Chapter 2 : Elucidate about glass transition, dielectric theories, coupling model, models used to analyze isothermal crystallization kinetics *etc.*

Chapter 3 : Discusses the materials and methods used for this study.

Chapter 4 : Discuss about the glass forming ability, crystallization tendency and molecular dynamics of probucol.

Chapter 5 : Describe about thermal and spectroscopic studies and crystallization kinetics of amorphous clofoctol.

Chapter 6 : Elucidate about the glass forming ability, molecular dynamics and isothermal crystallization kinetics of amorphous droperidol.

Chapter 7 : Discuss about the correlation between β_{KWW} and $\Delta\varepsilon(T_g)$ as proposed by Paluch and co-workers, stability prediction using β_{KWW} (Shamblin's criteria) and fragility comparison of the three studied pharmaceuticals with other pharmaceuticals.

Chapter 8 : Conclusions and future perspective of the work are presented in Chapter 8.

ABBREVIATIONS

API	Active Pharmaceutical Ingredient
BCS	Biopharmaceutical Classification System
BDS	Broadband Dielectric Spectrometer
CC	Cole-Cole
CD	Cole-Davison
CM	Coupling Model
DSC	Differential Scanning Calorimetry
FDSE	Fractional Debye-Stokes-Einstein
FTIR	Fourier Transform Infrared Spectroscopy
HN	Havriliak-Negami
JG	Johari-Goldstein
JMAK	Johnason-Mehl-Avrami-Kolomogorov
KWW	Kohlrausch-William-Watts
TGA	Thermogravimetric Analysis
T_g	Glass transition temperature
T_K	Kauzmann temperature
TSDC	Thermally Stimulated Depolarization Currents
VFT	Vogel-Fulcher-Tammann
PXRD	Powder X-ray Diffraction
NMR	Nuclear Magnetic Resonance

CONTENT

LIST OF FIGURES

LIST OF TABLES

LIST OF PAPERS PUBLISHED

1. M Sahra, M. Shahin Thayyil, A.K Bansal, K L Ngai, M.K Sulaiman, G Shete , and KP Safna Hussan; Dielectric spectroscopic studies of three important active pharmaceutical ingrediants-clofoctol, droperidol and probucol. *J. Non-Cryst. Solids*. 505, 28-36 (2019).

2. M Sahra, M. Shahin Thayyil and A.K Bansal; Molecular relaxations and isothermal cold crystallization kinetics of amorphous clofoctol (Communicated).

3. M Sahra, M. Shahin Thayyil and S. Cappaccioli; Molecular relaxations in amorphous phenylbutazone. *AIP Conference Proceedings*. 1731, 070026 (2016).

4. M. Sahra, K. Jumailath, M. Shahin Thayyil, and S. Capaccioli; Relaxation dynamics of amorphous dibucaine using dielectric studies. *AIP Conference Proceedings*. 1665, 070035 (2015)

5. Sahra Mohamed, M. Shahin Thayyil, and S. Capaccioli; Molecular dynamics in amorphous ergocalciferol. *AIP Conference Proceedings*. 1591, 825(2014).

6. Sahra Mohamed, Jumailath Karuthedath, M. Shahin Thayyil, and S. Capaccioli; Molecular dynamic in amorphous atropine and tolnaftate. *Res. J. Recent.Sci*, 5(3), (2016).

PAPERS PRESENTED IN CONFERENCES.

1. Glass forming fragility predictions on important amorphous pharmaceuticals. National Conference on Material science & nanotechnology, MAR 18-20, 2019, MES Ponnani College.

2. Molecular relaxations in amorphous phenylbutazone. 60^{th} DAE Solid state symposium, DEC 21-25, 2015, Amity University, Noida.

3. Relaxation dynamics of amorphous dibucaine using dielectric studies. 59^{th} DAE Solid State symposium, DEC 16-20, 2014, VIT University, Vellore.

4. Study of amorphous tolnaftate using broadband dielectric spectroscopy. 26^{th} Kerala Science Congress, JAN-28-31, 2014, KVAS University, Wayanad.

5. Molecular dynamics in amorphous atropine and tolnaftate. 3^{rd} International Science Congress, DEC 8-9, 2013, Karunya University, Coimbatore.

6. Molecular dynamics in amorphous ergocalciferol. 58^{th} DAE Solid State symposium, DEC 17-21, 2013, Thapar University, Patiala.

Chapter 1
Introduction

Glass is an amorphous (non-crystalline) solid having short range molecular order with physical properties differing from their respective crystalline counterparts. Even though the atomic structure of glass is close to supercooled liquid, below the glass transition temperature (T_g) it behaves as solid. The theory behind glass transition is an all time interesting topic for the scientific community and there is still no generally accepted and perfectly satisfying theory of the glass transition. The study of glass transition and amorphous structural materials has been of great interest in various fields like pharmacy, medicine, food industry, electronics, metallurgy, geosciences, nanoscience, materials for energy source applications *etc.*

While cooling a liquid below its melting point crystallization occurs and if the cooling rate is high enough to surpass the crystallization, it becomes supercooled liquid and on further cooling, it turns into glassy state. Glasses are very fascinating material due to its dual nature, *i.e.,* mechanical properties of solids and molecular disorder characteristics of liquids. The temperature at which the transformation from liquid to glassy state occurs is known as glass transition temperature (T_g). At T_g molecular motions slows down to the time scale of hundred seconds and below T_g molecular rearrangement is too slow and the molecules fails to reach its equilibrium positions. Molecular mobility of amorphous solids are usually studied by using methods such as broadband dielectric spectroscopy (BDS), differential scanning calorimetry (DSC), nuclear magnetic resonance (NMR) *etc.,* out of which dielectric spectroscopy is particularly useful as it gives information about molecular dynamics in supercooled and glassy states in a wide range of frequency, temperature and even pressure.

Molecular relaxations in glass forming systems are mainly characterized by two kinds of motions. They are termed as primary or α-relaxation process, which is observed near the glass transition and the secondary relaxation processes, which are observed below the glass transition temperature. The α-relaxation process is due to the cooperative rearrangement of molecules and is related to the liquid-glass transition and also become kinetically frozen below T_g. The secondary relaxations are the local non-cooperative relaxations which are relatively faster process and the change of relaxation time with temperature is slower than that of structural relaxations. In some cases, the secondary relaxations are intramolecular in origin *i.e.,* from the motion of some molecular subgroup dynamically decoupled from the rest

of the molecule, while in some systems the secondary relaxation originates from the local motion of the whole molecule (intermolecular origin) and were usually termed as the Johari-Goldstein, JG-relaxation.

1.1. Applications of amorphous systems

Amorphous systems have enormous application in various fields such as polymer engineering, plastic crystals, ionic liquids, magnetic materials, semiconductors, food industry and pharmaceutics *etc.* In 1986, Angell *et al.* studied the fast ion transport in glassy and amorphous materials and emphasized the significance of studying the fast ion motions by mechanical response, in addition to electrical response measurements.[1] B. Zhang *et al.* studied cerium-based bulk metallic glasses with an exceptionally low glass transition temperature, similar to or lower than that of many polymers and reported that these materials can be regarded as metallic plastics. They have adequate lifetime at room temperature and they combine both behaviors of polymer like thermoplastic and distinctive properties of metallic glasses, thus providing possible potential applications.[2] M. Orita *et al.* prepared a range of amorphous films $InGaO_3(ZnO)_m$ (where $m < 4$) using a pulsed-laser deposition method with the purpose of creating ZnO-based amorphous transparent conductors. The films for m = 1-4 were confirmed to be amorphous phases.[3]

B. J. P. Jansen *et al.* prepared rubber modified glassy amorphous polymers through chemically induced phase separation and prepared a blend of poly(methyl methacrylate) (PMMA) with a dispersed rubbery epoxy phase.[4] Van Eerdenbrugh *et al.* in 2011applied the molecular recognition framework of crystal engineering to amorphous binary systems and devised an approach to prevent crystallization in organic systems. The study indicated that fundamental principles governing hydrogen bond directed molecular recognition events, adapted from the field of crystal engineering, can be applied to design of solids in which crystallization is prevented.[5] B. Krause *et al.* studied microcellular foaming of amorphous high T_g Polymers polysulfone (PSU), poly(ether sulfone) (PES), and cyclic olefin copolymer (COC) films using carbon dioxide as a physical blowing agent. They further investigated the plasticization phenomena by foaming poly(ether sulfone) sample and a cyclic olefin copolymer. The obtained results confirm that the dominating factor controlling the foam formation is the ability of the carbon dioxide to plasticize the polymer matrix.[6]

C. A. Angell in his review about dynamic process in ionic glasses concluded that decoupled ion motions in glassy solids lead to a rich variety of relaxation phenomena and stated that in all relaxations, evidence for a constant frequency independent loss between

resonance and relaxation frequency domains which may be connected to fracton dynamics endemic to the glassy state.[7] According to V. Baranchugov *et al.* amorphous Si can be used as high capacity anode material for rechargeable Li batteries, with neat, additive free, ionic liquid electrolytes, based on derivatives of piperidinium bis(trifluoromethylsfonyl) imide molten salt.[8]

T. Egami *et al.* reviewed about the structure, preparation and mechanical properties of amorphous metallic alloys specifically low field properties of engineering interest and reported that such alloys have low coercive fields and very square hysteresis loops; the effective magnetization in low fields is greatly increased by the application of a tensile stress.[9]

E. A. Davis et al. assessed about the experimental evidence concerning the density of states in amorphous semiconductors and the ranges of energy in which states are localized which includes dc and ac conductivity, drift mobility and optical absorption.[10] Hosono in 2006 fabricated thin film transistors which are transparent and flexible on a polyethylene terephthalate (PET) film substrate with an ionic amorphous oxide semiconductor (IAOS) in an In_2O_3-ZnO-Ga_2O_3 system. The field effect mobility of the fabricated transistors is reported to be 10 cm^2 $(V\ s)^{-1}$. This reported value is higher than that of hydrogenated amorphous Si and pentacene transistors by an order of magnitude. They also discussed about the chemical design concept of ionic amorphous oxide semiconductors and gave details regarding its unique electron transport properties, and electronic structure, in comparison with that of conventional amorphous semiconductors.[11]

Though amorphous systems have vast applications in various fields, our study particularly aims in studying about amorphous pharmaceuticals.

1.2. Classification of pharmaceuticals

Drugs are usually made up of two core components; the active pharmaceutical ingredient (API), which is the central ingredient, and the chemically inactive excipients which are the substances other than the drug that helps deliver the medication. Active pharmaceutical ingredient (API), is the term used to refer to the biologically active component of a drug product. According to U. S. Food and Drug Administration, such substances are intended to furnish pharmacological activity or other direct effects in the diagnosis, cure, mitigation, treatment, or prevention of disease or to affect the structure or function of the body.

Drugs can be categorized based on their therapeutic use, chemical structure, mechanism or mode of action *etc.* Drugs can be further classified into four categories based on their solubility and permeability to bio-membranes, first proposed by Amidon *et al.* in 1995.[12] This particular classification is known as the Biopharmaceutical Classification System (BCS). According to BCS, APIs are divided into four classes as follows.

Table 1.1. BCS classification of pharmaceuticals.

Class I	High solubility	High permeability
Class II	Low solubility	High permeability
Class III	High solubility	Low permeability
Class IV	Low solubility	Low permeability

Class I drugs are favored by pharmaceutical industry, because of the fast dissolution and rapid bioavailability of such APIs. They are considered as ideal for controlled drug delivery if they meet the pharmacodynamic and pharmacokinetic criterions.[13] Class II drugs required enhancement in dissolution rate since their solubility is low. Class III drugs usually exhibit low bioavailability and permeability enhancement is needed. Class IV drugs have poor and variable bioavailability and normally not suitable for oral drug delivery.[13]

Biard *et al.* in 2010 studied a group of organic molecules and separated them into three groups to assess the crystallization tendency from undercooled melt based on the existence or absence of crystallization while heating or cooling or reheating.[14] Class I shows crystallization on cooling from the undercooled melt while class II does not shows crystallization on cooling from the undercooled melt below glass transition temperature, but shows crystallization on reheating above glass transition temperature. Class III molecules do not show crystallization on either cooling below glass transition temperature or on reheating up to the melting point.

1.3. Amorphous pharmaceuticals

Most of the drugs are prepared in thermodynamically stable crystalline form and their physiochemical properties remain intact for longer period providing better shelf life. But most of the drugs in crystalline form is barely water soluble and have poor bioavailability. According to Kawabata *et al.* (2011), in recent years, the number of insoluble active

pharmaceutical ingredients (APIs) is increased and almost 70% of the newly developed drugs shows poor water solubility.[15] Strategies for enhancing the dissolution rate and hence bioavailability of poorly water soluble drugs is a key challenge to pharmaceutical industry.[16,17] Nowadays various techniques are employed to enhance the solubility, dissolution rate and bioavailability of APIs, such as use of co-solvents, use of surfactants, chemical modification of drug, amorphous formulation, micronization, alteration of pH of solvents, freeze drying, nanosuspension, self dispersing lipid formulation, lipid based delivery systems, solid dispersion system *etc.,* out of which amorphous formulation of API is a promising method for improving solubility of drugs.[14]

1.3.1. Advantages of amorphous pharmaceuticals

Recently, pharmaceutical industry has been focusing on the development of amorphous pharmaceuticals because of their desirable pharmaceutical properties. Solubility plays an important role in drug formulation. Low aqueous solubility of drug forces high dosage to achieve pharmacological response. Solubility also had great impact on the parenteral formulation of drugs. There are many techniques to improve the solubility of drugs. It includes physical modifications such as particle size reduction, amorphous formulation and cocrystallization, solid dispersion *etc.,* and chemical modifications such as salt formation, change of pH, use of buffer *etc.,* as well as miscellaneous methods such as novel excipients, use of adjuvant like surfactant, solubilizers *etc.*[18] Amorphous pharmaceuticals exhibit higher solubility[19] compared to its crystalline counterpart providing better pharmaceutical effect.

Bioavailability is one of the important pharmacokinetic properties, defined as the fraction of unchanged active drug ingredient that reaches the systemic circulation. Improving drug solubility and drug permeability are the two main methods to increase the bioavailability of APIs. Studies confirmed that amorphous pharmaceuticals provide improved bioavailability[20] than its crystalline counterpart.[21–30] Also amorphous pharmaceuticals have four or five times faster drug absorption time, faster dissolution rate[31,32] and better mechanical properties[33] compared to its crystalline form.

1.3.2. Challenges in amorphous formulation

Though amorphous pharmaceuticals play a major role in enhancing the solubility and bioavailability of APIs, it has some limitations also. Amorphous solids are less physically and chemically stable. Amorphous materials have higher free energy and are in non-equilibrium

state. They are thermodynamically unstable; hence, the physical stability and shelf life of most of the amorphous drugs are incredibly low. One of the major issues is the onset of crystallization at a later stage during product shelf life.[34] Another disadvantage is that amorphous drugs are habitually reactive and unstable to mechanical and thermal stresses.[35] Also they are extraordinarily sensitive to water sorption.[36] Due to this instability, amorphous pharmaceuticals are not extensively marketed as the crystalline one[23,37] and thus the understanding of the molecular dynamics and mechanism of crystallization from the amorphous state is inevitable in the development of amorphous pharmaceuticals for practical applications.

1.4. Review in amorphous pharmaceuticals

Amorphous materials can be prepared by using various methods including freeze-drying[38], quench cooling the melt[39,40], spray drying[41], solid dispersion[42], addition of impurities[43], rapid precipitation by antisolvent addition[44,45], grinding or milling of crystalline solids at low temperatures[40,46] and desolvation of crystalline materials[47] *etc*. Present study aims at preparing amorphous pharmaceuticals by quench cooling method and studying its molecular dynamics in supercooled liquid and glassy forms using broadband dielectric spectroscopy (BDS). Further, this study also focuses on understanding the crystallization kinetics of the amorphous state using BDS.

F. Melani *et al.* studied the nonsteroidal anti-inflammatory drug naproxen. Solid combinations of naproxen with amorphous hydroxypropyl derivatives of α, β and γ -cyclodextrin were prepared and conducted studies on drug crystallinity, thermal behavior and dissolution rate. Also studies about phase solubility analysis and computer-aided molecular modeling were performed to study the inclusion complexation of naproxen with hydroxypropyl cyclodextrins. No relationship was found between the decrease in crystallinity of the drug dispersed in the amorphous carrier matrix and the geometrical features of the cyclodextrin macrocycle.[48] C. Schebor *et al.* investigated the thermal stability of enzymes namely lactase and invertase in dried, amorphous matrices of-trehalose, maltose, lactose, sucrose and raffinose-sugars and in some other polymers such as casein, PVP and milk. They reported that trehalose showed the best degree of enzyme stabilization.[49]

D. Zhou *et al.* in their work related the thermodynamic quantities configurational enthalpy, entropy and free energy with reciprocal of relaxation time for five amorphous compounds including ritonavir, ABT-229, fenofibrate, sucrose, and acetaminophen. Heat capacities of the amorphous and crystalline phase of each compound were measured as a

function of temperature using modulated temperature DSC.[50] D. Lechuga-Ballesteros *et al.* measured the interactions between water vapor and amorphous pharmaceuticals-saccharides like Sucrose, α-lactose monohydrate, trehalose dihydrate, and raffinose pentahydrate, and indomethacin-using microcalorimetric technique. The moisture-induced thermal activity traces (MITATs) provides information about the mode of interaction between water vapor and the amorphous solids.[51]

In 2005, G. P. Johari *et al.* conducted dielectric relaxation studies on amorphous acetaminophen. They measured the dielectric permittivity and dielectric loss spectra of amorphous and supercooled acetaminophen over the frequency range 10 Hz-0.4 MHz.[29] The molecular mobility of amorphous ibuprofen was studied using broadband dielectric relaxation spectroscopy for different temperatures. The results show that ibuprofen has a complex relaxation map including two secondary relaxations, γ and β, a main α-process associated with the dynamic glass transition and a Debye-like process. The β-relaxation is verified as Johari-Goldstein relaxation. The two secondary relaxations showed Arrhenius temperature dependence while two Vogel-Fulcher-Tamman-Hesse (VFTH) regimes are observed for α-relaxation separated by a crossover temperature at 265 K.[52] K. Adrjanowicz *et al.* also conducted studies on dielectric relaxation and also crystallization kinetics of amorphous ibuprofen at ambient and elevated pressure. The crystallization kinetic studies revealed extension in crystallization time and induction time under high pressure compared to that crystallized at ambient pressure, which was due to the shift of the optimal nucleation and crystal growth process to higher temperatures with pressure.[53]

T. El Goresy *et al.* studied amorphous nifedipine and an equimolar binary mixture of nifedipine and acetaminophen were studied by dielectric spectroscopy in its supercooled liquid and in its glassy state. The α-relaxation process of the binary mixture occurs at a significantly lower temperature as compared to pure nifedipine and the supercooled liquid states were characterized by a relatively large steepness index m.[54] A. C. Rodrigues *et al.* studied the molecular mobility of amorphous S-flurbiprofen using BDS. Amorphous S-flurbiprofen was prepared by quench cooling. The fragility or steepness index was calculated as $m = 113$, classifying S-flurbiprofen as a fragile glass former.[55]

K Adrjanowicz *et al.* in 2010 determined the structural α-relaxation times deep in the glassy state of the pharmaceutical, Telmisartan using the approach suggested by Casalini and Roland. The values of structural relaxation time were compared with those predicted by the coupling model (CM).[56] K. Adrjanowicz *et al.* again conducted studies on molecular dynamics of amorphous telmisartan. In this study, they prepared amorphous samples by

cryomilling and by quench cooling of the melt and a comparative study of molecular dynamics of samples prepared in both ways were carried out. The long term stability of amorphous telmisartan was confirmed using X-ray diffraction analysis. Also solubility studies verified the better solubility of amorphous telmisartan than from the crystalline form.[40]

Z. Wojnarowska *et al.* performed broadband dielectric measurements on the pharmaceutical indomethacin at ambient and elevated pressure. A well resolved intramolecular secondary relaxation (γ) was observed, which was found to be pressure insensitive. Another slow secondary relaxation (β) was obtained in the vicinity of the T_g while analyzing the dielectric spectra at ambient pressure. And from CM prediction, it was classified as JG-relaxation[57]. V. Andronis *et al.* investigated the crystal nucleation and growth rates of polymorphs of indomethacin from amorphous state.[58]

Molecular dynamics studies were carried out on the antibiotics-azithromycin, clarithromycin and roxithromycin-in their supercooled liquid and glassy forms by using dielectric spectroscopy. A number of relaxation processes of different molecular origin were reported. The activation energies of the secondary processes and fragility index of all the three antibiotics found to be approximately similar, which in turn indicate the probable similar molecular dynamics. Also stability of amorphous forms was confirmed by X-ray diffraction.[59]

Z. Wojnarowska et al. studied the molecular dynamics of a common local anesthetic drug, lidocaine hydrochloride (LD-HCl), and its water mixtures by using BDS. From the calorimetric measurements, it was observed that even a small addition of water causes a significant effect on the relaxation dynamics of analyzed protic ionic liquid.[60]

The crystallization tendency and physical stability of a group of drugs after storage above and below the glass transition temperature and its relationship to glass forming ability was analyzed by A. Alhalaweh *et al.* Class III compounds remained amorphous under the studied dry conditions while most of Class II compounds crystallized when stored at 20 K above the T_g but remained amorphous when stored at 20 K below the T_g. They concluded that glass transition temperature was feebly correlated to physical stability and stated that molecular properties have significant impact on glass forming ability and glass stability.[61] The amorphous forms of erythromycin free base (ED) and its salts namely, stearate (ES), phosphate (EP) and thiocyanate (ET) were generated by K. Nanakwani *et al.* using in situ melt quenching and their crystallization tendency were evaluated. Kinetics of crystallization followed the order as ES > EP > ET > ED.[62]

By using broadband dielectric spectroscopy, U. Sailaja *et al.* studied the dielectric properties and molecular dynamics of two pharmaceuticals, namely nizatidine and perphenazine. Both samples had structural alpha relaxation above T_g and intramolecular gamma relaxation below T_g while JG -relaxation was supposed to be hidden under the structural relaxation peak.[63] Thermal characteristics and molecular dynamics of amorphous fenofibrate were studied using DSC and BDS. The sample does not show any tendency of crystallization during cooling and reaches it in the glassy state. The structural relaxation showed VFT temperature dependence and the drug was reported as fragile.[64] U. Sailaja *et al.* also conducted dielectric spectroscopic investigations on amorphous captopril. The sample was found to be highly unstable in the amorphous state.[65] Molecular relaxation studies on amorphous ketoprofen using BDS over wide temperature and frequency range revealed multiple relaxation processes-the primary α-relaxtion and the non JG γ-relaxation. Also solubility test proved that the amorphous form is more soluble than the crystalline phase.[39] Dielectric studies of supercooled cimetidine revealed well pronounced α-relaxation process above the glass transition temperature and the solubility of amorphous sample found to be double than that of its crystalline part.[66]

The molecular dynamics in the supercooled amorphous state of cimetidine, nizatidine, and famotidine were carried out using DSC, thermally stimulated depolarization currents (TSDC), and dielectric relaxation spectroscopy. Multiple relaxation processes were observed by relaxation study. Nizatidine was categorized as a fragile liquid and cimetidine as moderately fragile, while molecular mobility in amorphous famotidine could not be studied as it decomposes near the melting temperature.[67]

Dielectric measurements of supercooled and glassy nonivamide were carried out using BDS at various isobaric and isothermal conditions. The study revealed very narrow α-loss peak and unresolved secondary relaxations appearing in the form of an excess wing on the high frequency flank. Due to the unusual structure of nonivamide, the fragility index was found to be nearly constant on varying pressure.[68] J. Knapik-Kowalczuk *et al.* studied the physical stability of pure amorphous probucol and also studied the physical stability of amorphous probucol by mixing it with atorvastatin as a crystallization inhibitor.[69]

Z.Wojnarowska *et al.* carried out dielectric measurements of pharmaceuticals-procaine hydrochloride and procainamide hydrochloride-which are glass-forming as well as ionically conducting materials, to study the dynamics of the ion conductivity relaxation. They pointed the vital importance of β-conductivity relaxation as it is crucial as the precursor of the α-conductivity relaxation, analogous to the relation found between the Johari-Goldstein β-

relaxation and the structural α-relaxation in non-ionic glass forming systems.[70] G. Chawla *et al.* studied the molecular dynamics, hygroscopicity studies and physical stability studies of crystalline and amorphous irbesartan and opined it as a probable candidate for the drug development, since it showed high physical stability.[71]

R. Surana *et al.* prepared amorphous anhydrous trehalose in four different methods viz., freeze drying, spray drying, dehydration, and melt quenching. The sample prepared by dehydration was less resistant to crystallization, while melt quenched sample showed better resistance to crystallization.[72] K. Kaminski *et al.* studied the molecular mobility of leucrose at ambient and high pressure using BDS. Two types of secondary relaxations were observed in this disaccharide. The slower one was sensitive to pressure while the faster one was not indicating that it originates from the intramolecular motion.[73]

J. Knapik *et al.* prepared coamorphous drug-drug compositions of different molar ratios of ezetimib and indapamid and studied using BDS, DSC and X-ray diffraction (XRD). With this study they are able to stabilize amorphous form of easily recrystallizing ezetimib by adding even a small amount of indapamid.[74] Z. Wojnarowska *et al.* analyzed the solid-state properties of the vitrified, cryomilled and ball-milled amorphous indapamide samples using XRD, NMR, Fourier transform infrared spectroscopy (FTIR), DSC and BDS. The position as well as shape of the structural relaxation process, was found to be similar in all cases, but the molecular dynamics of milled and melt-quench samples below T_g found to differ from each other profoundly. All cases revealed only one well pronounced secondary relaxation process, but differ in its molecular origin.[75]

K. Adrjanowicz *et al.* studied the molecular dynamics of the pharmaceutical posaconazole in the supercooled liquid and glassy states. Structural α-relaxation was detected above the glass transition temperature and secondary relaxations (β and γ) were detected in the vicinity and below the glass transition temperature. From the dielectric and shear mechanical studies, it was confirmed that posaconazole is an extremely fragile glass former.[76] K. Kamiński *et al.* measured the dielectric relaxation spectra of amorphous and supercooled nicotine over a wide frequency range. Nicotine showed two kinds of relaxations-the structural α-relaxation and the precursor of it, the Johari-Goldstein β-relaxation. The sample showed good correspondence between the Johari-Goldstein relaxation time τ_{JG} and the calculated primitive relaxation time of the coupling model.[77]

G. Shete *et al.* investigated the dielectric relaxation of amorphous hesperetin using dielectric spectroscopy and also assessed the crystallization kinetics of amorphous hesperetin above the glass transition temperature. Amorphous hesperetin exhibited both structural

α-relaxation and more local β-relaxation.[78] With the help of dielectric spectroscopy, K. Grzybowska et al. investigated the molecular dynamics and crystallization tendency of amorphous celecoxib. This study stated that the structural relaxation seems to be responsible for devitrification of celecoxib if stored at room temperature $\sim$ 293 K. Also the crystallization can be considered to ultimately be affected by the β-process (JG-relaxation) because it is the precursor of the structural α-relaxation.[79]

Molecular dynamics and structural properties on the crystallization tendency of three 1,4-dihydropyridine derivatives, namely nifedipine, nisoldipine, and nimodipine were studied in their supercooled states using DSC and BDS. Isothermal crystallization kinetics of supercooled nifedipine and nimodipine were also investigated using BDS and found that nimodipine exhibits much slower crystallization in comparison to nifedipine. The coamorphous drug-drug system of nifedipine-nimodipine found to be stable and thus nimodipine act as an effective crystallization inhibitor for nifedipine.[80]

Ajay K. R. Dantuluri *et al.* studied the role of α-relaxation toward isothermal crystallization of amorphous celecoxib using dielectric relaxation spectroscopy. Crystallization kinetics of amorphous celecoxib were performed for different temperatures and analyzed using Avrami model.[81] K. Kolodziejczyk *et al.* investigated molecular relaxations and crystallization kinetics of amorphous Sildenafil in both supercooled liquid and glassy state. The cold crystallization mechanism of amorphous Sildenafil found to be similar in both the isothermal and non-isothermal conditions.[82]

1.5. Objectives of the study

1. To investigate glass forming ability and mechanical stability of amorphous pharmaceuticals using differential scanning calorimetry.
2. To understand the physiochemical aspects of glass transition phenomena by systematic investigation of glass forming materials using broadband dielectric spectroscopy.
3. To elucidate the basic aspects of glass transition phenomena and different relaxation processes in amorphous pharmaceuticals from the broadband dielectric spectroscopy.
4. To investigate the fundamentality and universality of Johari-Goldstein secondary relaxation, its properties and correlation with primary or structural relaxation.
5. To study the isothermal crystallization kinetics of amorphous pharmaceuticals using broadband dielectric spectroscopy.

1.6. Present work

In this work we present, the thermal and spectroscopic investigations of three hydrogen bonded active pharmaceutical ingredients (APIs) namely, clofoctol, droperidol and probucol. Glass forming ability of the samples were analyzed using DSC. The relaxation dynamics of APIs were investigated in supercooled and glassy states over broad frequency and temperature ranges at ambient pressure using BDS. To find the origin of the secondary relaxations, CM predictions were used. It was further verified from the computational investigations with the help of density functional theory. The pharmaceuticals, chosen for study have significantly broader structural dispersion than the majority of the drugs investigated so far and thus we have carried out the anti-correlation study between the width of the structural loss peak at T_g to the polarity of the drugs [83,84] in the light of dipole-dipole interaction to the attractive part of the intermolecular potential. They are instrumental in testing the anti-correlation within the family of molecular pharmaceuticals as part of the totality of molecular glass formers studied by dielectric spectroscopy. Also the isothermal crystallization kinetics of clofoctol and droperidol were investigated using BDS and was analyzed using Avrami and Avramov models.

The thesis is organized as follows. Chapter 1 gives general introduction about glass, applications of amorphous systems in various fields and particularly amorphous pharmaceuticals. Classification of pharmaceuticals, advantages and limitations of amorphous formulation and an outline of the present works are also described in Chapter 1. Theoretical overview about glass transition, dielectric theories and coupling model are presented in Chapter 2. The different models used for the analysis of isothermal crystallization kinetics are also discussed in Chapter 2. Materials and methods used are discussed in Chapter 3. Chapter 4 discuss about the glass forming ability, crystallization tendency and molecular dynamics of probucol. Chapter 5 and 6 describe about thermal and spectroscopic studies and also crystallization kinetics of amorphous clofoctol and droperidol respectively. Test of correlation between β_{KWW} and $\Delta\varepsilon(T_g)$ as proposed by Paluch and co-workers and stability prediction using β_{KWW} (Shamblin's criteria) and fragility comparison of the three studied pharmaceuticals with other pharmaceuticals are discussed in Chapter 7. Overall conclusion and an idea about the future perspective of the work are presented in Chapter 8.

Chapter 2

Theoretical Overview

2.1. Glass transition

Cooling a liquid from high temperature to low temperature below the melting point usually leads to crystallization. But if we provide sufficiently high cooling rate, then crystallization may be bypassed and the liquid becomes supercooled liquid. On further cooling, the dynamics become kinetically frozen and eventually become glass or amorphous solid. The transformation from liquid to amorphous glassy state occurs at so called glass transition temperature, T_g. The structures of glassy or amorphous systems are similar to that of liquid and they lack long range structural order. However the macroscopic behavior of amorphous systems is more similar to that of solid. Glass transition is accompanied by changes in thermodynamic quantities such as heat capacity, volume, entropy, enthalpy, viscosity and thermal expansion coefficient *etc.*

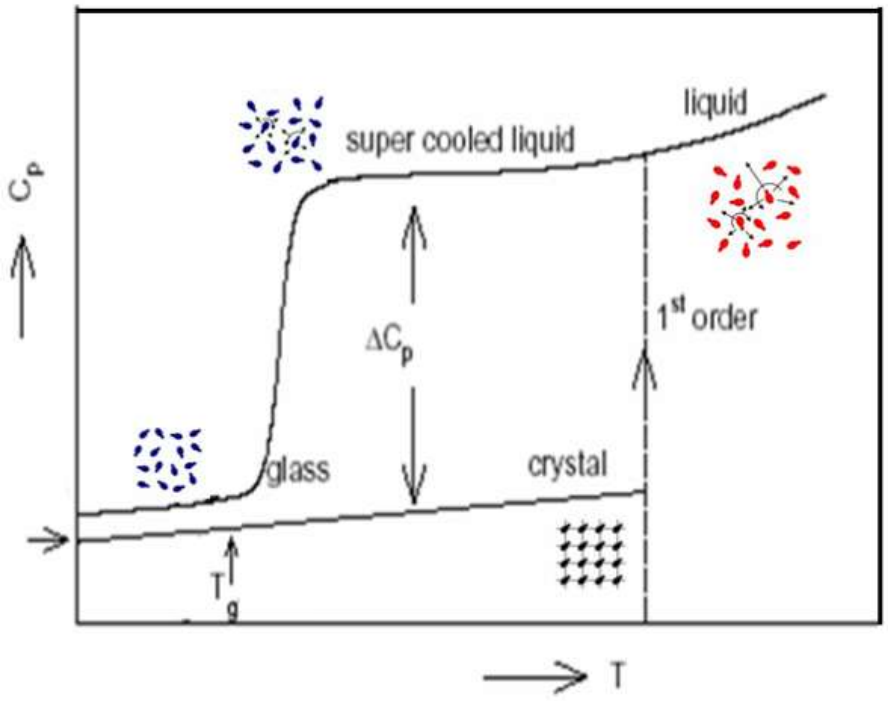

Figure 2.1. Variation of specific heat with temperature during glass transition.

Glass formation also influences the molecular dynamics with respect to temperature and pressure. The dramatic increase in the structural relaxation time (the time required for the system to recover to equilibrium after an external perturbation) is the unique feature of molecular dynamics of glass forming liquids. The typical time scale for molecular rearrangements in normal liquid is of the order of picoseconds, which changes up to hundreds of seconds in the vicinity of glass transition temperature.[85,86] The diffusion constant or viscosity also behaves in the same manner during glass transition. The glass transition temperature varies according to the rate of cooling. If it cools very slowly, it crystallizes.

2.2. Dielectric relaxations in glass forming systems

The term dielectric relaxation accounts for the return of the macroscopic system to the thermodynamic equilibrium subsequent to the removal of the external perturbation-electric field. On applying an electric field, the polar molecules will align in the direction of the applied field. On removal of the applied field, the molecules do not return to random orientation immediately. Relaxation time is the time taken by the molecules to randomly orient after the removal of the applied electric field. The characteristics relaxations are named by the order of their appearance, using the Greek letters *α, β, γ, δ etc,* Dielectric relaxations can be further classified according to their time scale as shown in figure 2.2. Different characteristics feature, not necessarily all simultaneously present in a single glass former.

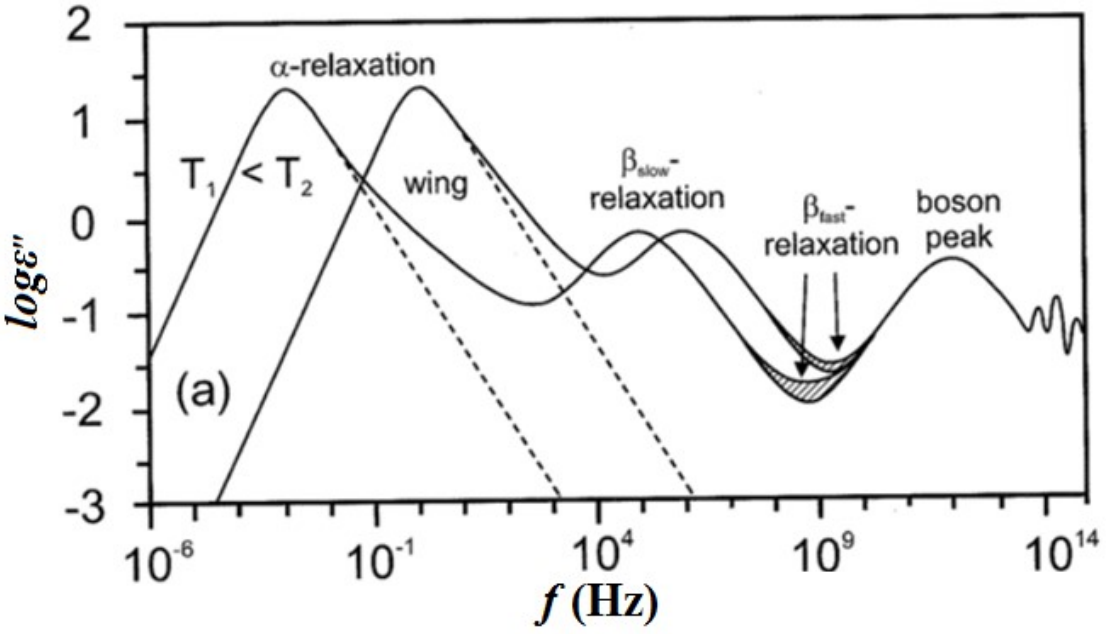

Figure 2.2. Schematic view of different relaxations in glass forming system.[87] The imaginary part of the complex dielectric function *vs.* frequency for temperatures T_1 and T_2.

The structural α-relaxation process, which is the main common dynamical process associated with the glass transition, shifts rapidly to higher frequencies with increasing temperature. In some glass forming systems, an excess wing is observed in the high frequency power law flank of the α-peak[88], while in some systems further relaxation process leads to additional peaks named as secondary relaxations or β-peak (or γ, δ…..relaxations if there are more than one). The amplitudes of all these processes further than the α-process are relatively small compared to the universal α-relaxation.

At frequencies around some THz, another loss peak shows up that can be acknowledged with the so called boson peak identified from neutron and light scattering.[87–89] The boson peak is a universal characteristic of glass forming systems and corresponds the vibrational density of state.

2.2.1. The structural relaxation

The structural α-relaxation is due to the collective, cooperative motions of molecules that involve the rearrangement of groups of molecules. These cooperative motions slow down dramatically on approaching the glass transition by decreasing temperature T or increasing pressure P and become kinetically frozen upon cooling the liquid to form a glass. Thus, the glass transition temperature is the temperature range where the structural relaxation motions take place on a time scale of the order of 10^2s. The most prominent features of the α-relaxation process include the non-exponential relaxation pattern and the non-Arrhenius temperature dependence.[90,91]

The non-exponential time dependence behavior of α-relaxation can be explained using the empirical stretched exponential or the Kohlrausch-Williams-Watts (KWW) function.[92,93]

$$\varphi(t) = \varphi(0) exp\left[-\left(\frac{t}{\tau_{KWW}}\right)\beta_{KWW}\right] \quad (2.1)$$

The quantities $\varphi(t)$ and $\varphi(0)$ are the dynamic response after a perturbation at time t and 0 respectively, τ_{KWW} is a characteristic time and the exponent β is the stretching parameter whose value generally lies in the range between 0 and 1. The response is an exponential function with $\beta = 1$ for the simple Debye relaxation process.

Another characteristic feature of the structural α-relaxation process is the deviation of its temperature dependence from the Arrhenius law, which is the general expected behavior for thermally activated processes. The temperature dependence of the α-relaxation time are very well described by the Vogel-Fulcher-Tammann equation[94–98] given by,

$$f_\alpha = f_0^\alpha \, e^{(-B/(T-T_0))} \tag{2.2}$$

where T_0 is the limiting temperature which indicates the divergence of the relaxation time at infinite viscosity corresponding to the complete blocking of the structural relaxation, f_0^α is a constant and $B = DT_0$, D is the strength parameter whose value is related to the degree of deviation of the τ_α (T) curve from the Arrhenius equation.[98] The extent of this deviation from Arrhenius behavior is incredibly different for different glass-forming materials. Oldekop and later Laughlin and Uhlmann[99] were the first to use T_g as a corresponding state parameter for liquid viscosity η to compare the flow behavior of different liquids. Angell[100] was the first who recognized the significance of the Laughlin-Uhlmann plot as a means to classify the transport properties of glass-formers. Fragile glasses show a bent curve in the normalized activation plot $log\tau$ versus T_g /T, which indicates that on decreasing T, the apparent activation energy increases. Now, the expressions strong and fragile are often used to express the curvature or location of either log η or $log\ \tau$ of the glass formers in the Oldekop-Laughlin-Uhlmann-Angell (OLUA) plot. Typical fragility plot or Angell plot for strong and fragile liquids are shown in figure 2.3.

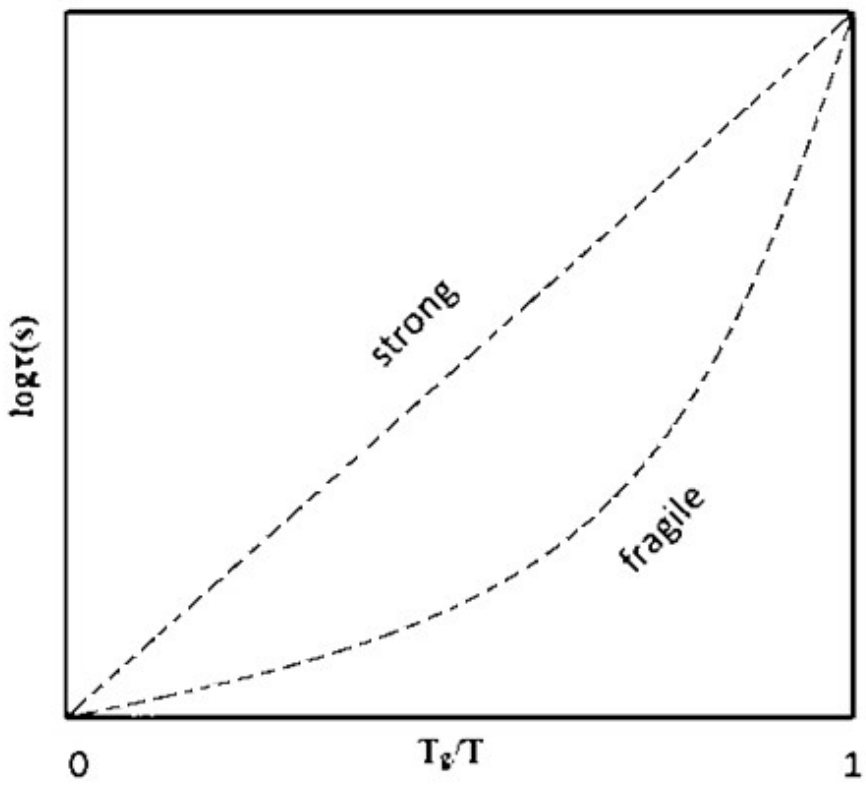

Figure 2.3. Angell plot of fragility for strong and fragile liquids.

The fragility or steepness index, *m* can be calculated from VFT fit and is defined as the slope of the relaxation time curve *vs*. T_g /*T* at the glass transition temperature T_g in the Oldekop-Laughlin-Uhlmann-Angell (OLUA) plot, given by[101]

$$m = \frac{dlog(\tau)}{d\left(\frac{T_g}{T}\right)}\Big|_{T=T_g} = \frac{DT_0T_g}{\left(T_g-T_0\right)^2 ln10} \quad (2.3)$$

If the value of *m* is less than 45 then such system belongs to strong liquids and if m is greater than 75 such system belongs to fragile liquids.[102] In fragile liquids near the glass transition temperature, molecular mobility changes rapidly with temperature indicating weak thermodynamic stability and consecutively leads to a larger tendency toward crystallization of amorphous systems.[82]

2.2.2. The secondary relaxations

In general, different dynamic features can be seen in the amorphous systems. In some cases, an excess wing is observed in the high frequency power law flank of the α-relaxation peak, while in other systems a slow β-peak show up. The secondary relaxation process present even in t1he amorphous glassy state is generally more localized and the molecular motions are non-cooperative. Dielectric loss spectra of secondary relaxations appear as a broad peak and are more often symmetrical, slowly moving at lower frequency on decreasing temperature.[88] In the microscopical point of view, the β-process can be contributed by two different mechanisms. Sometimes the secondary relaxation is due to the motions of molecular subunits that can relax independently from the whole molecules (intra-molecular origin). In some other materials, the secondary relaxation is due to the motion of the whole molecule (intermolecular origin).

In 1970, G. Johari and co-workers[103], found a particular type of secondary relaxation process in simple glass forming systems with no internal degree of freedom. Two approaches have been proposed to elucidate the origin of these intermolecular β-relaxations, which later called as Johari-Goldstein (JG) relaxation. Johari considered the concept of the islands of mobility, which are the isolated regions of loosely packed molecules caged in the glassy matrix, as the reason for the β-process. Consequently, in the glassy state, only molecules within these regions have enough space to execute the relatively fast and independent motions which appear as the β-relaxation. According to Johari's model, the β-relaxation originates only from molecules within the islands of mobility[104,105] and is a non-homogenous process. A totally different explanation was later put forward by Williams and Watts.[106] They

proposed that the β-process could be attributed to a faster, small angle (thermally-activated) reorientational motion of all molecules and have a homogenous nature, in contrast to Johari's concept. In some small molecular glass formers, JG β-relaxation is present but unresolved, because it is sandwiched between the more intense α-relaxation and a faster but non JG secondary γ-relaxation. Thayyil *et al.* showed in benzophenone and dimethyl phthalate that by dissolving either glass former in a host with a much higher glass transition temperature, the α-relaxation moved further from the γ-relaxation.[107]

At temperatures below the glass transition temperature when the structural relaxation process moved out of the frequency interval of the measurement, the linear temperature dependence of the secondary β-relaxations is well described by the Arrhenius equation.

$$f_\beta = f_0^\beta exp\,(\frac{-\Delta E_\beta}{RT}) \tag{2.4}$$

where R is the gas constant (R = 8.314 J mol^{-1} K^{-1}), f_0^β is the pre-exponential factor related to the lattice vibrational frequency and ΔE_β is the activation energy to overcome the energy barrier.

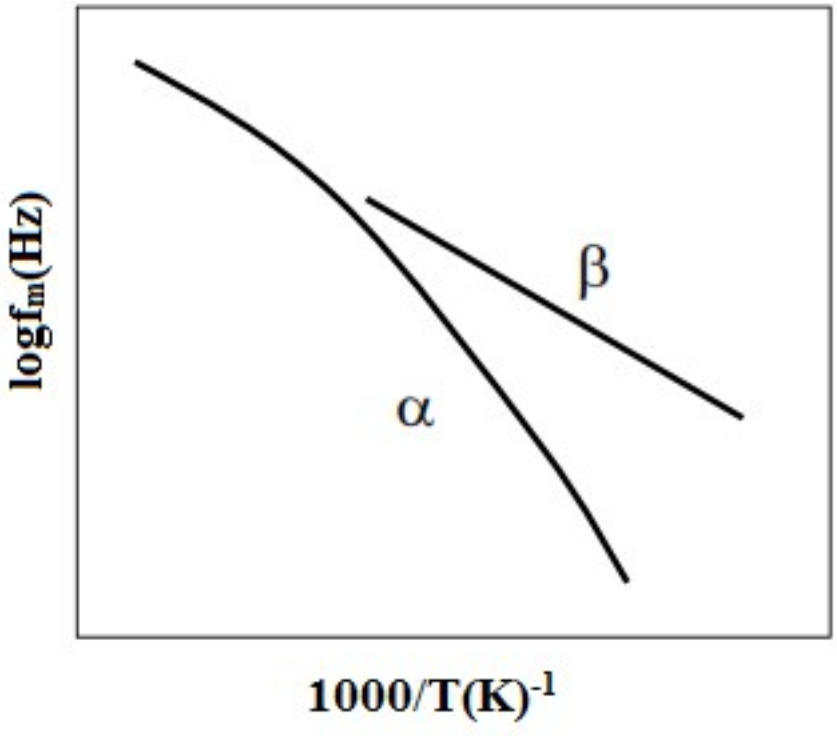

Figure 2.4. Temperature dependence of primary and secondary relaxation.

2.3. Dielectric relaxation theories

The dielectric constant or relative permittivity is the measure of distortion or polarization of the electric charge distribution in a material due to the application of the electric field. It depends on the frequency of the applied field and the polarizability of the material. Dipoles follow the field at low frequencies and the orientation polarization attains equilibrium so the dielectric permittivity will be high. The motion of the dipoles increases with the increase in the applied frequency of the field and a phase lag between the applied field and orientation of dipoles develops due to intermolecular forces. This causes the dielectric material to draw energy from the source of electricity, which is dissipated as heat, which in turn increases the dielectric loss. Thus dielectric permittivity decreases with increase in the frequency of the applied field. When the frequency of the applied field is sufficiently high, the molecular dipoles rotate as fast as they can and a peak occurs in the dielectric loss. The frequency corresponding to this peak is called dielectric relaxation frequency. The variation in dielectric permittivity and dielectric loss with the variation in frequency over a broad band of frequencies of the applied electric field is called dielectric dispersion. Also, the dielectric permittivity of a dielectric falls with the increase in temperature because rise in temperature causes increase in disorder of the molecular dipoles. Rotational motion of each dipole represents a characteristics relaxation time, which is an important parameter in dielectric spectroscopy. The relaxation may be due to the motion of a whole molecule or a functional group attached to a large molecule. The relaxation time depends on the intermolecular forces and the molecular size and varies inversely with temperature since all type of molecular movements become faster at higher temperatures. The dielectric relaxation behavior of glass forming systems can be explained using various models such as Debye, Cole-Cole, Cole-Davidson and Havriliak-Negami models.

2.3.1. Debye model

Debye proposed that for a dipolar system in non-equilibrium, the relaxation occurs with a rate that increases linearly with the distance from equilibrium. Debye model is suitable for systems having single relaxation time. He mathematically described the nature of dielectric dispersion *i.e.,* variation of dielectric constant with frequency and absorption for polar materials by a single relaxation time.[108] The relation for the complex permittivity at angular frequency ω is given by the equation

$$\varepsilon^* = \varepsilon'(\omega) - i\varepsilon''(\omega) = \varepsilon_\infty + \frac{\varepsilon_0 - \varepsilon_\infty}{1 + i\omega\tau} \quad (2.5)$$

where ε_∞ is the high frequency dielectric constant, ε_0 is the static dielectric constant and τ is the macroscopic relaxation time. This is the familiar Debye dispersion equation. The characteristic shapes of real and imaginary parts of ε^* against the frequency of the outer electrical field $\upsilon = \omega/2\pi$ for this model are plotted in figure 2.5. The imaginary part exhibits a symmetric peak with a maximum value at $\omega_{max}\tau = 1$ and has an amplitude given by $\varepsilon''_{max} = (\varepsilon_0-\varepsilon_\infty)/2$.

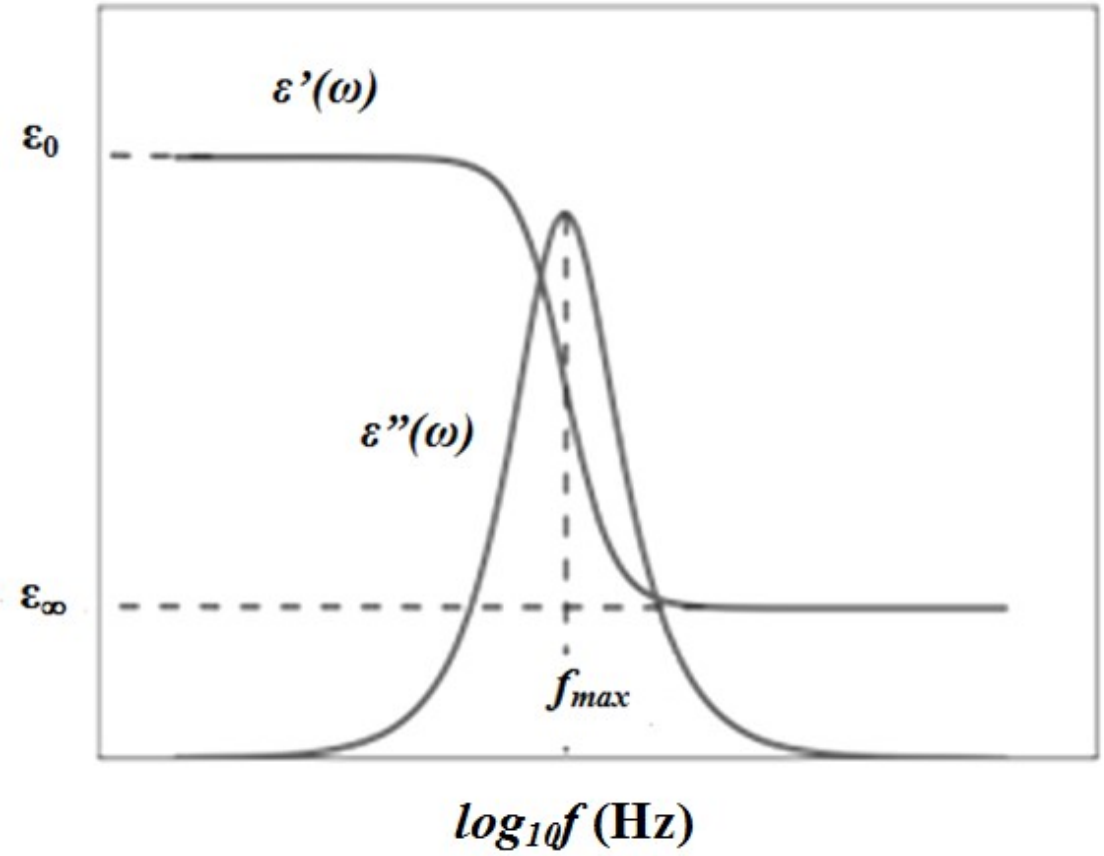

Figure 2.5. Frequency dependence of the real (ε') and imaginary (ε'') parts of permittivity in the Debye process.

The plot of the imaginary part of permittivity ε'' on the vertical axis *vs*. real part of permittivity ε' on the horizontal axis is known as Cole-Cole plot. The Cole-Cole plot of the Debye relaxations assumes the shape of a symmetric semicircular arc with center at $\left(\frac{\varepsilon_0+\varepsilon_\infty}{2}, 0\right)$ and radius $\left(\frac{\varepsilon_0-\varepsilon_\infty}{2}\right)$. Debye model response is observed in very few materials and for more complex systems such as polymers, this model fails to represent experimental data.

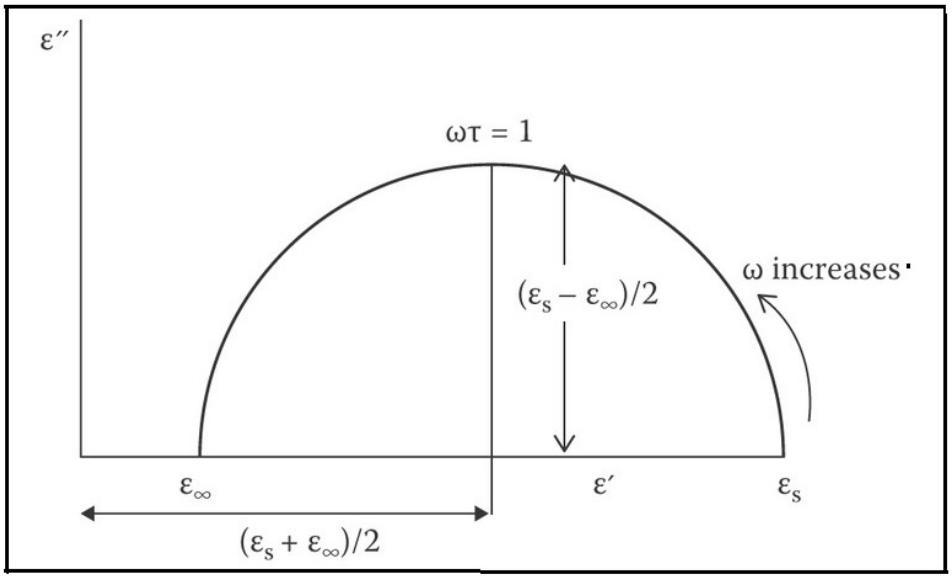

Figure 2.6. Cole-Cole plot for Debye process

Usually, the measured dielectric responses in most systems are non-Debye in nature, where the spectra are broader, asymmetric or showing the signatures of both. They are often described as Cole-Cole (CC)[109], Cole-Davidson (CD)[110,111], and Havriliak-Negami (HN)[93,112,113] shape functions.

2.3.2. Cole-Cole model

Experimental observations in long chain polar molecules showed a depressed or broadened semicircle, which could only be explained by introducing a fractional power in the imaginary part of the Debye function, put forwarded by K.S Cole and R.H. Cole. The center of the semi-circle lies not in the abscissa, but below it. Most of the secondary relaxations in almost all complex systems showed this behavior. This can also be explained in terms of the distribution of relaxation times of slightly varied dipoles. The complex dielectric function is described as

$$\varepsilon^*(\omega) - \varepsilon_\infty = \frac{\varepsilon_0 - \varepsilon_\infty}{1 + (i\omega\tau)^{1-\alpha}} \tag{2.6}$$

where α is the relaxation time distribution parameter which measures the broadening of the loss curve. The value of α lies between 0 and 1, *i.e.,* $0 \leq \alpha \leq 1$. When $\alpha = 0$, the Cole-Cole model reduces to the Debye model. When $\alpha > 0$, the relaxation is stretched, *i.e.,* is extends over a wider range on a logarithmic ω scale than Debye relaxation.

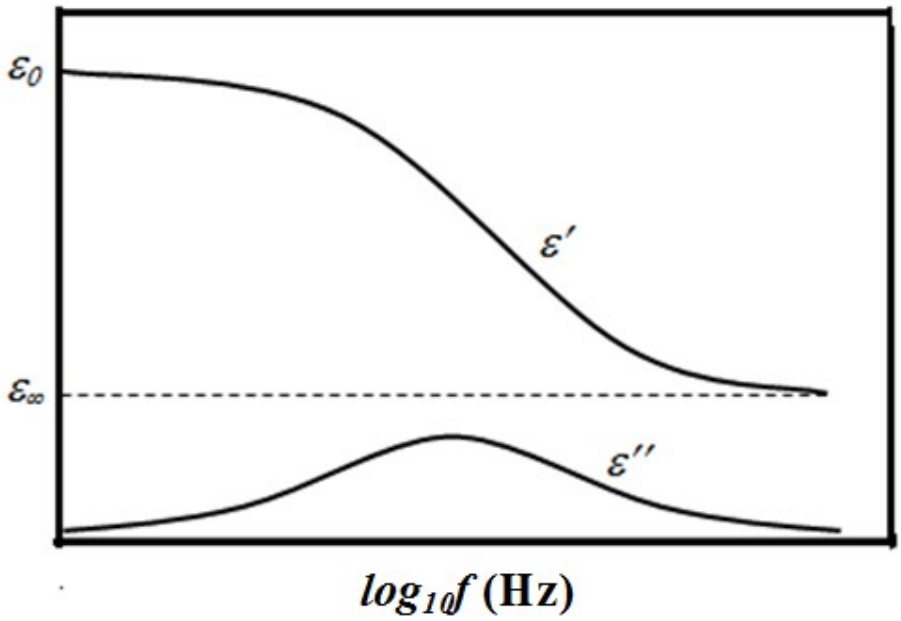

Figure 2.7. Frequency dependence of the real (ε′) and imaginary (ε″) parts of dielectric permittivity in a Cole-Cole process.

In this model also the loss curve is symmetric, but in Cole-Cole relaxations, the value of ε' decreases more slowly near the relaxation frequencies as compared to Debye relaxation.

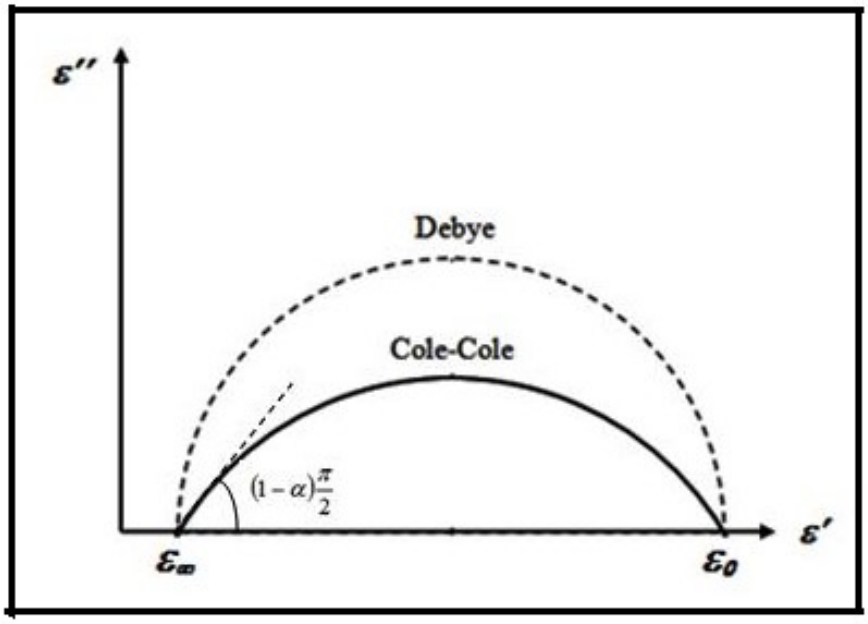

Figure 2.8. Cole-Cole plot for Cole-Cole process

2.3.3. Cole-Davidson model

Most of the supercooled glass forming system show a skewed arc with a high-frequency straight line and a low-frequency circular arc, where the spectra could only be explained by introducing a fractional power to the denominator, put forwarded by Davidson and Cole[111] given by

$$\varepsilon^*(\omega) - \varepsilon_\infty = \frac{\varepsilon_0 - \varepsilon_\infty}{(1+i\omega\tau)^\beta} \tag{2.7}$$

The above equation is known as Cole-Davidson equation. β is the shape parameter whose value changes between $0 < \beta \leq 1$. When $\beta = 1$, the above equation become Debye equation and for values $\beta < 1$, the arc is skewed to the right. The frequency dependence of real and imaginary parts of permittivity is shown in figure 2.9. From the figure, it can be clearly seen that the loss curve is asymmetric near relaxation frequencies.

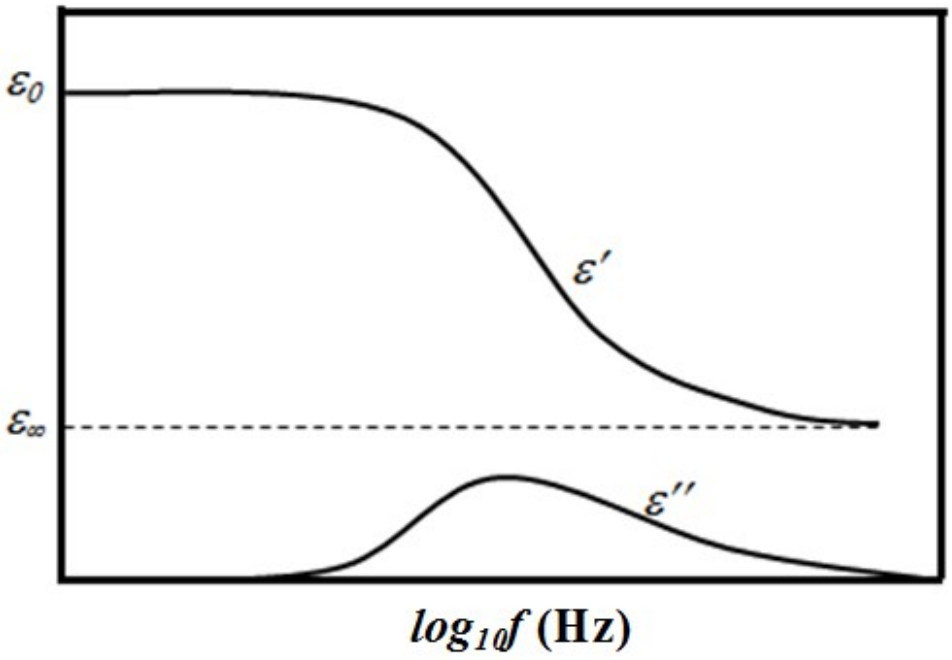

Figure 2.9. Frequency dependence of the real (ε′) and imaginary (ε″) parts of dielectric permittivity in a Cole-Davidson process

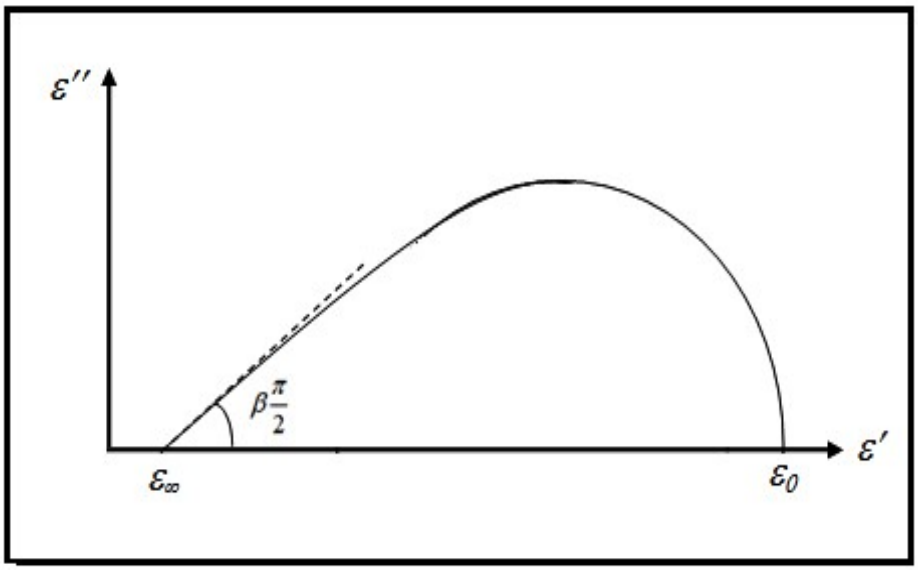

Figure 2.10. Cole-Cole plot for Cole-Davidson process

2.3.4. Havriliak-Negami model

Havriliak-Negami relaxation model accounts for both the broadness and asymmetry of the dielectric dispersion curve. The model was initially employed to describe the dielectric relaxation of some polymers[113] by adding two exponential parameters to the Debye equation.

$$\varepsilon^*_{HN}(\omega) = \varepsilon_\infty + \frac{\Delta\varepsilon}{(1+(i\omega\tau_{HN})^{1-\alpha_{HN}})^{\beta_{HN}}} \tag{2.8}$$

The exponents α and β are the shape parameters which describe the width or broadness and the asymmetry of the corresponding spectra respectively. Also $\Delta\varepsilon = \varepsilon_0 - \varepsilon_\infty$. For $\alpha = 0$ and $\beta = 1$, the Havriliak-Negami (HN) equation reduces to Debye equation. Also for $\beta = 1$, the HN equation reduces to the Cole-Cole equation and for $\alpha = 0$ to the Cole-Davidson equation.

Most of the dielectrics possess conductivity due to the motion of charges, which gives rise to the conduction current and additionally polarizes the dielectric. Adding the contribution dc conductivity σ, the dielectric permittivity can be expressed as[114]

$$\varepsilon^*_{HN}(\omega) = \varepsilon' - i\varepsilon'' = \varepsilon_\infty + \sum_k \left(\frac{\Delta\varepsilon}{(1+(i\omega\tau_{HNk})^{1-\alpha_{HNk}})^{\beta_{HNk}}}\right) - i\left(\frac{\sigma}{\omega\varepsilon_0}\right)^s \tag{2.9}$$

where s characterizes the conduction process. The conductivity term increases with decreasing frequency. An increase in absorbed moisture or in the case of polymers, the onset

of dc conductivity at higher temperature, dramatically increases the loss factor at lower frequencies. The conductivity term added to the imaginary part of the HN fit function can be subtracted from it after the fit. The use of Σ in the above equation stands for the summation over multiple relaxations.

The characteristic relaxation time τ_{HN} is related to the frequency of maximal loss f_{max}. The relaxation time τ can be calculated using the equation

$$\tau = \tau_{HN} \times \left[\sin\left(\frac{\alpha_{HN}\pi}{2+2\beta_{HN}}\right)\right]^{-1/\alpha_{HN}} \left[\sin\left(\frac{\alpha_{HN}\beta_{HN}\pi}{2+2\beta_{HN}}\right)\right]^{1/\alpha_{HN}} \quad (2.10)$$

For secondary relaxation process, $\beta_{HN} = 1$, and thus HN function becomes Cole-Cole function. Frequency dependence of the real (ε′) and imaginary (ε″) parts of dielectric permittivity in HN model and Cole-Cole plot for typical HN relaxation are shown in figure 2.11 and 2.12, respectively.

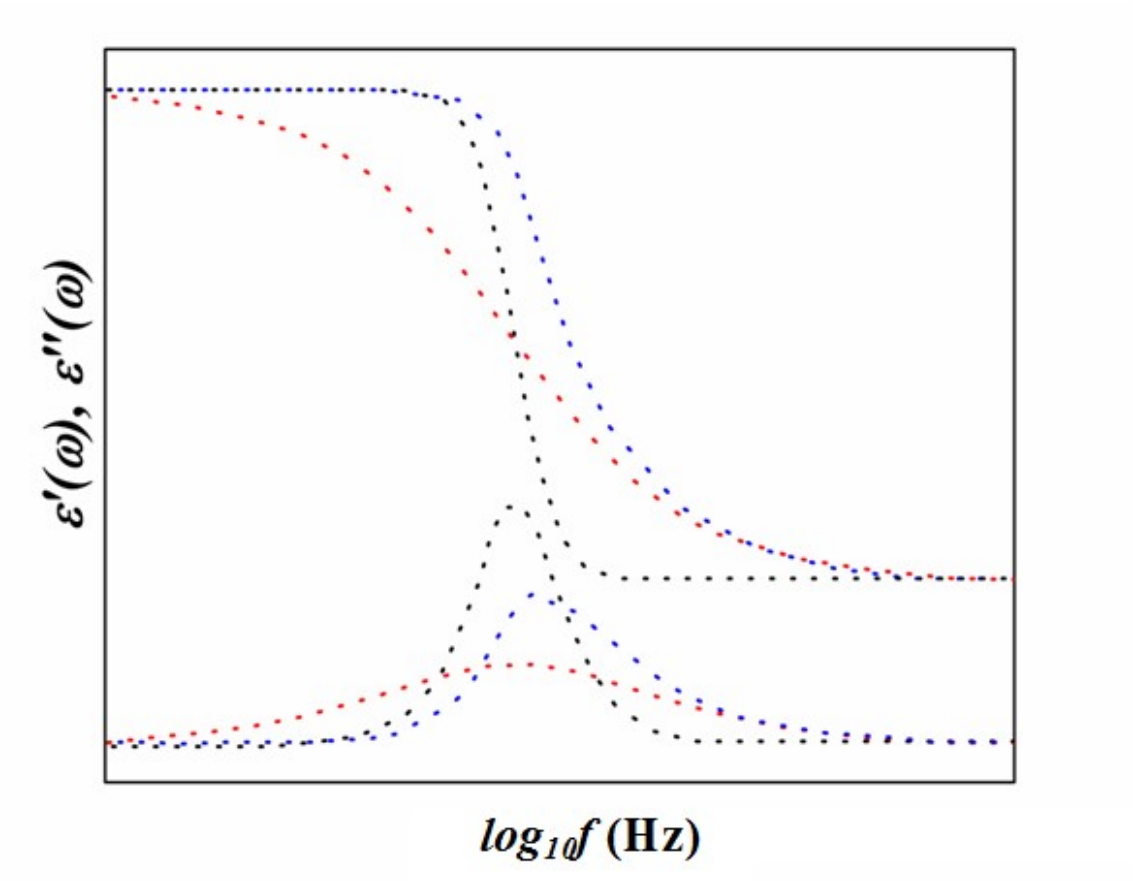

Figure 2.11. Frequency dependence of the real (ε′) and imaginary (ε″) parts of dielectric permittivity in HN model. The black dotted line shows HN function with $\alpha = 0$ and $\beta = 1$ (Debye), red dotted line denotes HN function with $\alpha = 0.6$ and $\beta = 1$ (Cole-Cole) and blue dotted line denotes HN function with $\alpha = 0$ and $\beta = 0.4$ (Cole-Davidson).

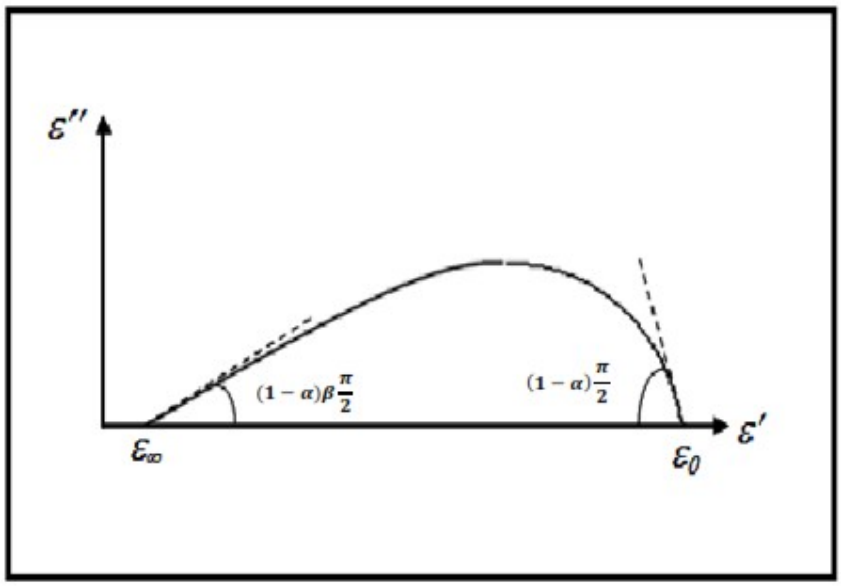

Figure 2.12. Cole-Cole plot for HN relaxation

2.4. Coupling model (CM)

The coupling model was proposed to describe the relaxation phenomena in complex systems, in which intermolecular interactions induce a degree of co-operativity between the molecules. These co-operative interactions arise from the many body anharmonic interactions in the system.[115] Though coupling model is not a full solution for the many body relaxation problems, it can explain the properties of structural relaxations originating from many body interactions.[116] K. L. Ngai in 1979 introduced the many body effects in relaxation and diffusion of complex systems. One of the significant accomplishments of CM is the realization of the correspondence between the primitive relaxation time and the special kind JG secondary relaxation time.

The properties of structural relaxations originating from many body relaxations and its relation to its precursor, namely Johari Goldstein relaxation can be explained using CM predictions.[117] The corresponding correlation function of the model is the Kohlrausch-William-Watts (KWW) stretched exponential function which holds only for $t >> t_c$.

$$\varphi(t) = exp\left[-(\frac{t}{\tau_\alpha})^{1-n}\right] \tag{2.11}$$

where $n = (1- \beta_{KWW})$ is the coupling parameter of the CM and $0 < n < 1$, and the cross over at

t_c leads to a relation between the structural relaxation time, τ_α and the primitive relaxation time, τ_0 which is given by

$$\tau_\alpha = [t_c^{-n}\tau_0]^{\frac{1}{1-n}} \tag{2.12}$$

Larger the value of the coupling parameter, stronger is the slowing effect of the many-molecular dynamics. When the intermolecular interactions are absent in the system *i.e.,* $n = 0$, then the primitive relaxation time τ_0 coincides with the structural relaxation time τ_α. There are experimental evidences [118,119] that the cross-over from the primitive relaxation to Kohlrausch relaxation is at $t_c \approx 2$ps for molecular systems. The correspondence between the independent primitive relaxation time of the coupling model (CM), τ_0 , and the Johari-Goldstein (JG) β-relaxation time, τ_β, was predicted and verified by K.L Ngai.[120] The primitive relaxation and the Johari-Goldstein relaxation are not identical, but they are strongly related and are in good agreement for many molecular and polymeric glass formers[121,122] and for many APIs also.[123]

2.5. Crystallization kinetics

Crystallization of amorphous solids is a complex phenomenon involving nucleation and growth of crystallites.[124] Nucleation may happen spontaneously or can be induced artificially. Nucleation may either occur homogenously, *i.e.,* without the involvement of foreign materials in the interior of the parent system and referred as primary nucleation. Or it may occur heterogeneously, *i.e.,* by the contact of the parent phase with a foreign material which is called as secondary nucleation.[124] Crystal nucleation is followed by crystal growth.

The shelf life of amorphous pharmaceutical is greatly depends on the recrystallization. The conversion of amorphous material into the crystal is influenced by various internal factors like molecular motions and mobility.[125] Primary[81] and secondary relaxations[126,127], density[128], interface energy[58], fragility *etc.,* play a major role in the recrystallization of amorphous systems.[129] External conditions such as defects or cracks[130], surface effects[131], relative humidity, method of amorphization[132,133] *etc.,* also affect crystallization. The tendency of crystallization of organic compounds from undercooled melt is connected to its glass forming ability. Molecules with low molecular weight and rigid structure are more prone to crystallization than complex molecules having more conformational degrees of freedom.[14]

The rate of crystal nucleation reaches maximum at a temperature higher than T_g and the rate of crystal growth attains its maximum value at a temperature much higher than this

temperature. Thus on heating a glass at constant rate crystal nuclei are produced at lower temperature and its size increases at higher temperatures without increase in number.[134] The study of crystallization kinetics is significant as it enables to quantify the crystal nucleation and crystal growth of the crystallites formed. The investigation of crystallization kinetics of amorphous materials can be carried out either isothermally or non-isothermally using various techniques such as BDS and DSC.

During isothermal crystallization experiment using BDS, above T_g, the dielectric strength $\Delta\varepsilon$ of the structural relaxation process falls down, which in turn indicates the declination of amorphous fraction of the samples. This is a typical characteristic of crystallization as the number of relaxing molecules participating in the structural process decreases.[82] On studying crystallization kinetics using various models and by analyzing various parameters such as the crystallization rate k, the characteristic crystallization time τ_{cr} and the kinetic exponent n *etc.,* one can infer about the nucleation and crystal growth mechanisms.[135–138] The isothermal crystallization kinetics can be analyzed using various models, including Avrami and Avramov model.

2.5.1. Avrami model

The Avrami equation usually used to describe the solid-state transformation can be specifically used to describe the isothermal crystallization kinetics of amorphous materials. At constant temperature, crystallization obeys the phenomenological Avrami equation given below

$$\alpha = 1 - exp(-kt^n) \tag{2.13}$$

where α is the fraction of the material crystallized after time t, n is Avrami exponent, a constant depending on the details of nucleation and growth mechanisms and k is defined as the effective overall crystallization rate which depends on the rates of nucleation and growth rate. The parameters n and k can be determined by monitoring x as a function of t at various fixed temperatures.[139] The above equation is also known as Johnson-Mehl-Avrami-Kolomogorov (JMAK) equation.

The transformation from one state to another usually follows characteristic sigmoidal or S-shaped curve. The rate of transformation is low at the beginning and end while rapid in between it. At the beginning, some initial time is required for a significant number of nuclei to form and grow. Then the transformation becomes rapid and on approaching completion,

the production of new particles begins to slow as there remains only few untransformed material for further nucleation.

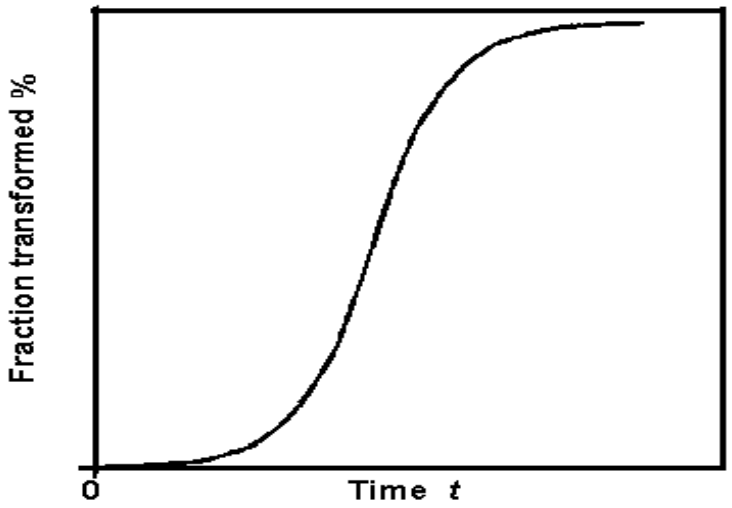

Figure 2.13. Typical isothermal transformation plot

Table 2.1. Values of the Avrami exponent *n* for various crystallization and phase transformation processes.[140]

Polymorphic changes, discontinuous precipitation, eutectoid reactions, interface-controlled growth etc.	
Conditions	*n*
Increasing nucleation rate	> 4
Constant nucleation rate	4
Decreasing nucleation rate	3-4
Zero nucleation rate (site saturation)	3
Grain-edge nucleation after saturation	2
Grain-boundary nucleation after saturation	1
Diffusion-controlled growth	
Conditions	*n*
Increasing nucleation rate (all shapes growing from small dimensions)	2.5
Constant nucleation rate (all shapes growing from small dimensions)	2.5
Decreasing nucleation rate(all shapes growing from small dimensions)	1.5-2.5
Zero nucleation rate (all shapes growing from small dimensions)	1.5
Growth of particles of appreciable initial volume	1-1.5
Needles and plates of finite long dimensions	1
Thickening of long cylinders (needles)	1
Thickening of very large plates	0.5

During BDS experiment, as the crystalline fractional volume increases, the number of reorienting dipoles, which contributes to the structural relaxation, decreases. The rise in the degree of crystallization can be analyzed by the equation,

$$\varepsilon_n^{'}(t) = \frac{\varepsilon^{'}(0)-\varepsilon^{'}(t)}{\varepsilon^{'}(0)-\varepsilon^{'}(\infty)} \tag{2.14}$$

where ε_n' is the normalized real permittivity, $\varepsilon'(0)$ is the static dielectric permittivity at the beginning of the crystallization, $\varepsilon'(t)$ is the value at a given time of crystallization and $\varepsilon'(\infty)$ is the long-time limiting value. The transformation from the chaotic amorphous state to more structured crystalline phase at a particular temperature can be analyzed using the Avrami model.[135,141] According to this model

$$\varepsilon_n^{'}(t) = 1 - exp(-Kt^n) \tag{2.15}$$

where $K = k^n$ is crystalliztion rate constant, n is the Avrami exponent or parameter. The values of Avrami parameters is obtained from the supposed Avrami plot, *log(-ln(1- ε_n')) vs. logt*, which is based on the equation,

$$log(-ln(1-\varepsilon_n')) = logK + n\, logt \tag{2.16}$$

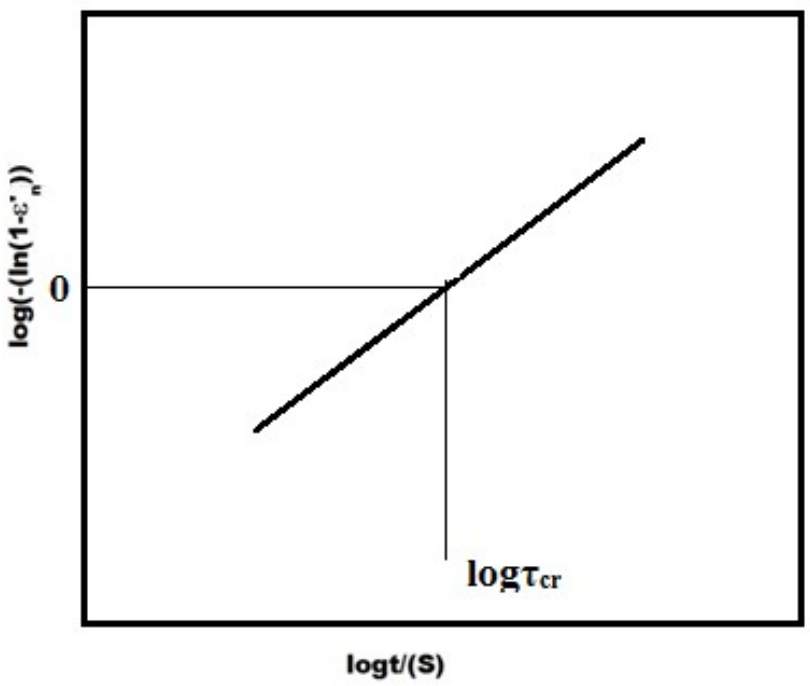

Figure 2.14. Plot of *log (-ln (1- $\boldsymbol{\varepsilon_n'}$)) vs. logt.*

The dependence of $log\ (-ln\ (1-\varepsilon_n'))$ on *logt* is linear and the value of *logK* and *n* can be obtained from the intercept and slope. The isothermal crystallization time τ_{cr} is graphically determined at $log(-ln(1-\varepsilon_n')) = 0$.

2.5.2. Avramov model

Another method used to analyze isothermal crystallization is Avramov model of crystallization.[136] The normalized real permittivity is expressed as

$$\varepsilon_n'(t) = 1 - exp\left(\frac{t-t_0}{\tau_{cr}}\right)^n \tag{2.17}$$

where t_0 is the induction time of crystallization, and τ_{cr} is the characteristic time for isothermal overall crystallization, which is related to the Avrami parameter as $\tau_{cr} = K^{-1/n}$. Avrami model exaggerates the role of initial stages and the role of the stages near the end of the process where most crucial experimental errors appears. Unless the Avrami model, this model hold the linear character for entire time range and estimates the value of t_0 more reliably. Also this method avoids measurement errors due to thermal instability, which arises at the starting of the experiment. The first derivative of equation (2.17) with respect to $ln\ (t-t_0)$ is

$$\frac{d\varepsilon_n'(t)}{d(ln(t-t_0))} = n\left(\frac{t-t_0}{\tau_{cr}}\right)^n exp\left(-\left(\frac{t-t_0}{\tau_{cr}}\right)^n\right) \tag{2.18}$$

And the second derivative is

$$\frac{d^2\varepsilon_n'(t)}{d(ln(t-t_0))^2} = n^2\left(\frac{t-t_0}{\tau_{cr}}\right)^n\left(1-\left(\frac{t-t_0}{\tau_{cr}}\right)^n\right) exp\left(-\left(\frac{t-t_0}{\tau_{cr}}\right)^n\right) \tag{2.19}$$

For each crystallization temperature, the Avramov parameters can be determined from the Avrami-Avramov plot which pictures the dependence of the normalized real permittivity ε_n' with *lnt* and the first derivative of normalized real permittivity $d\varepsilon_n'/d(ln\ t)$ with *lnt*. From the above equations, the extremum appears at $t-t_0 = \tau_{cr}$ and at this point ε_n' = 1-1/e = 0.63. Thus assuming t_0=0, the value of $ln\tau_{cr}$ for $(\varepsilon_n')'_{max}$ can be easily determined from the Avrami-Avramov plot. Also the value of the parameter *n* can be calculated from

$$n = \frac{(\varepsilon_n')'_{max}}{0.368} \tag{2.20}$$

The value of n and τ_{cr} are key factors while studying the kinetics of crystallization. The value of n accounts for the dimensionality of crystal growth. It depends on whether the growth rate is constant with time and it also reflects whether a nucleation process takes place continuously or crystallization takes place on a certain number of active places whereas τ_{cr} is the characteristic time of the process accounting for both the nucleation kinetics and growth rates.[136]

Chapter 3

Materials and Methods

3.1. Materials

The APIs and its use along with its physical properties[14] are listed in table 3.1. The samples with analytical standard grade were purchased from Sigma Aldrich and used as received without further purification.

Table 3.1. Physical properties[14] of clofoctol, droperidol and probucol.

Samples	**Chemical Name**	**Molecular weight (g/mol)**	**Principal Usage**	T_g (K)	T_m (K)
Clofoctol	2-(2,4- dichlorobenzyl)-4-(tetramethyl-l, 1,3,3-butyl)phenol	365.33	bacteriostatic antibiotic	269	361
Droperidol	1-{1-[4-(4-fluorophenyl)-4-oxobutyl]-1,2,3,6-tetrahydro-4-pyridyl}-1,3-dihydro-2H-benzimidazol-2-one	379.42	antidopaminergic drug	302	416
Probucol	4,4′-[(1-methylethylidene) bis(thio)]-bis[2,6bis(1,1-dimethylethyl)]phenol.	516.84	anti-hyper lipidemic drug	300	400

3.2. Methods

3.2.1. Powder X-ray Diffraction (PXRD)

In Powder X-ray diffraction (PXRD), the diffraction pattern of crystalline material is measured. In a crystal the atoms are arranged in a periodic array and hence can diffract light. The wavelength of X-rays are in accordance to the distance between atoms. Diffraction patterns are produced due to the scattering of X-rays from atoms and contain information about the atomic arrangement within the crystal. One of the characteristic features of the crystalline material is the long-range orderly periodic arrangements of atoms. Amorphous materials like glass do not produce a diffraction pattern as they lack the long-range order periodic array. PXRD can be used as a qualitative and sometime quantitative assessment of the degree of crystallinity of the samples.

The distance between parallel planes of atoms determines the position of the diffraction peaks. Bragg's law states the essential conditions required for diffraction. According to Bragg's condition,

$$n\lambda = 2d_{hkl}\, sin\theta \tag{3.1}$$

where λ is the wavelength of the incident wave (X-ray), θ is the scattering angle, d is the interplanar distance between lattice planes and h, k, and ℓ are the Miller indices of the Bragg plane. The constructive interference from X-rays scattered by parallel planes of atoms will produce a diffraction peak and Bragg's law estimates the angle at which the diffraction peak occurs. In most of the diffractometers, X-ray wavelength λ is kept fixed. Thus a family of planes generates a diffraction peak only at a particular angle 2θ. PXRD measurements were carried out using Bruker D8 Diffractometer. The analysis of XRD peaks is out of the scope of this work as our aim is only to ascertain the crystalline nature of the samples before converting it into the amorphous state.

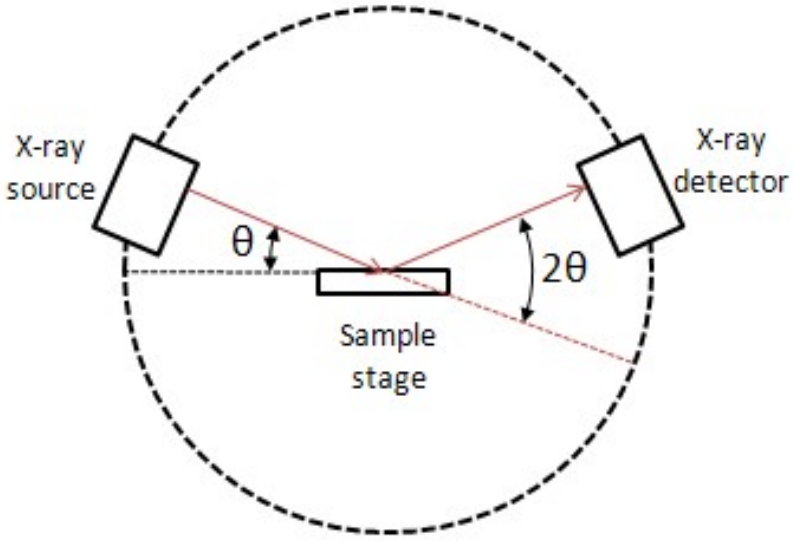

Figure 3.1. Diffractometer beam path

3.2.2. Thermogravimetric Analysis (TGA)

Thermogravimetric Analysis (TGA) measures the change in the mass of a substance, continuously scrutinized as a function of temperature or time, when it is heated or cooled at a predetermined rate. It provides information on the thermal stability of the sample at different

temperatures and pressures of the environmental gases. Measurements are used primarily to determine the composition of materials and to predict their thermal stability at temperatures up to 1200°C. The technique can characterize materials that exhibit weight loss or gain due to decomposition, oxidation, or dehydration. The apparatus used for obtaining TG (thermograms) curves is referred to as a thermobalance. It consists of a continuously recording balance, furnace, temperature, programmer and a recorder. TGA measurements were carried out using STA 8000 PerkinElmer supported with PyrisTM software.

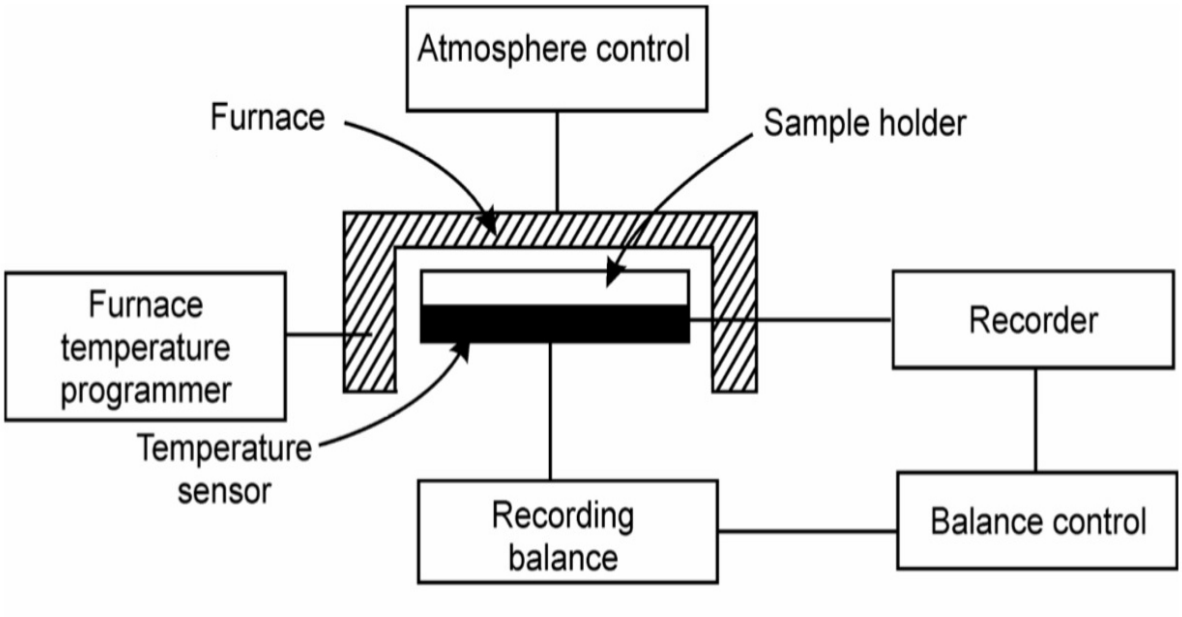

Figure 3.2. Block diagram of thermobalance

3.2.3. Differential Scanning Calorimetry (DSC)

Differential Scanning Calorimetry (DSC) measures the heat flow, *i.e.,* heat absorbed or liberated during heating or cooling as a function of temperature in a controlled atmosphere. DSC provides quantitative and qualitative information about physical and chemical changes, which involves endothermic or exothermic process or changes in heat capacity. In DSC, heat flow to the sample from the furnace is measured in relative to the heat flow to the reference material. Sample and reference crucible are identical except that reference is empty, both crucibles are maintained at the same temperature and are kept in direct contact with sensors. Output is measured as the difference in the heat flow between reference and sample.

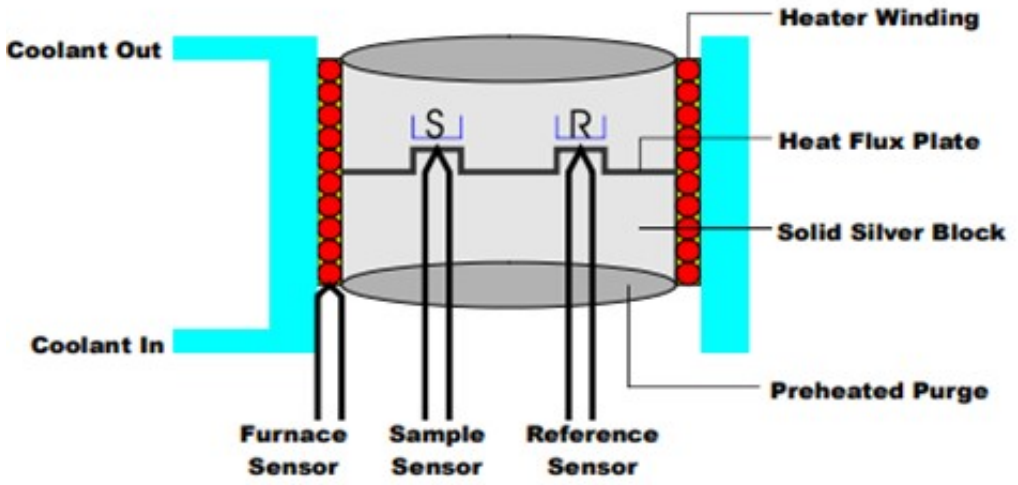

Figure 3.3. DSC Measuring cell

DSC measurements were done using 821^e DSC (Mettler-Toledo, Switzerland) operating with STAR^e software version 9.1. The instrument was calibrated using high purity indium and zinc as standards. The sample weighing 3-5 mg was sealed into a pin-holed aluminum pan and placed inside the calorimeter. The instrument was purged with dry nitrogen at the rate of 40 ml/min. The measurement was performed at a heating rate of 10 K/min. The sample was first heated to a few degrees above the melting point and kept for a while. It was rapidly cooled at a rate of 20 K/min to ensure the smooth passage of the sample without any chance of crystallization to a deep glassy state. The glassy sample was further heated at 10 K/min to get the glass transition temperature and other thermodynamic parameters.

3.2.4. Broadband Dielectric Spectroscopy (BDS)

Dielectric spectroscopy measures the dielectric and electric properties of a medium as a function of frequency or time. It is founded on the interaction of an external applied field with the electric dipole moment and charges of the medium. BDS covers wide frequency range from 10^{-2}-10^{7} Hz with the options to extend both the lower and higher frequency limits. With the help of this technique, one can analyze the molecular dynamics on a large time scale under varying temperature. By measuring the variation of the dielectric constant with frequency and temperature, one can infer about the dipolar reorientational motions and electric conduction that arises from translational motions of charge carriers. BDS measures

the conductivity, complex dielectric and impedance functions of materials versus frequency with high precision.

When a dielectric material is subjected to an electric field, polarization can be induced by different mechanisms such as electronic, atomic and orientational. On applying the electric field, the electron undergoes displacement with respect to the nucleus which leads to electronic polarization. Atomic polarization is observed due to the rearrangement of the relative positioning of atomic nuclei inside the molecule or in an atomic network as a result of the application of the external field. Orientational polarization is caused by the orientation of the permanent dipole moments in the direction of the electric field in polar materials.

Dielectric relaxation spectroscopy apparatuses measure the loss of polarization (*i.e.,* dielectric relaxation) after the step removal of an external electric field at a certain temperature or pressure. The mode of these dipoles relaxations are rationalized in terms of molecular mobility existing in the material. Alternatively, a field sinusoidally changing with time is applied and the gain and phase displacement of the polarization response at different frequencies are acquired, taking to the so-called dielectric spectra. When a relaxation occurs, it can be either detected as a peak in the imaginary part of the spectra or as an inflexion in the curve of the decrease of real part of susceptibility (and thus permittivity).

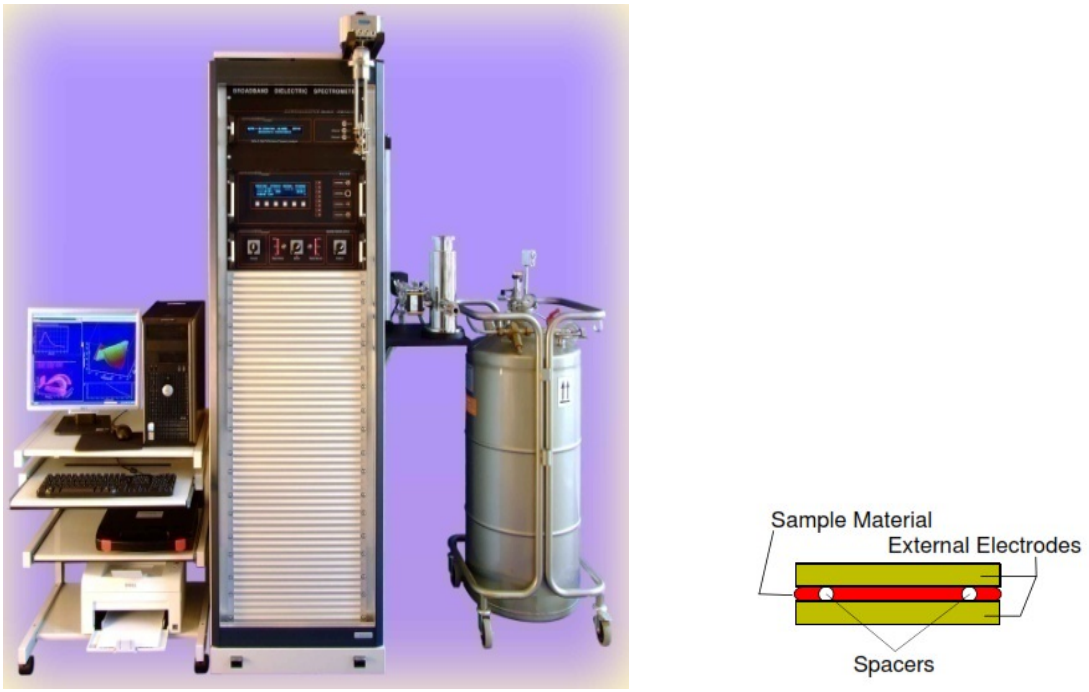

Figure 3.4. Broadband Dielectric Spectrometer and sample cell

The sample material to be examined is mounted in a sample cell between two electrodes forming a sample capacitor. A sinusoidal voltage $U_1(t) = U^* exp(i\omega t)$ with a predetermined frequency $\omega/2\pi$ is applied to the sample capacitor and the current across it $I_S(t) = I^* \exp(i\omega t+\varphi)$ is measured. The angle φ is the phase shift in the current with respect to the applied voltage and it depends on the properties of the sample and on the frequency. The ratio between U_1 and I_s and the phase angle φ are determined by the electrical properties such as permittivity and conductivity as well as the geometry of the sample material.

The voltage U_1 from the digital sine-wave generator is applied to the cell, which generates a current across it and the generated current then converted to the voltage U_2 by a current to voltage converter. This voltage U_2 is amplified, filtered and converted in two digital data streams, and analyzed with discrete Fourier transform technique which in turn gives information about the amplitude and the phase of the voltage U_2. That's why the device is called vector analyzer. From these two voltages, U_1 and U_2, the value of the sample impedance Z_S is calculated using the equation,

$$Z_s = \frac{U_1}{I_s} = -\frac{U_1}{U_2} Z_x \tag{3.2}$$

where $Zx = (R_x^{-1} + i\omega C_x)^{-1}$ is the feedback impedance of the inverting amplifier used in the current to voltage converter. The complex permittivity $\varepsilon^* = \varepsilon' - i\varepsilon''$ is obtained by impedance measurement through the relation $\varepsilon^*(\omega) = (i\omega C_0 Z(\omega))^{-1}$.

Dielectric measurements for different temperatures were carried out using a broadband dielectric spectrometer (Novocontrol GmbH, Germany) for a frequency range of 10 mHz – 10 MHz. The sample capacitor was made by keeping the sample between two stainless steel electrodes of 30 mm effective diameter and keeping two narrow Teflon spacers of 50 micron thickness to get an empty cell capacitance of approximately 100 pF. The temperature was controlled with the use of dry nitrogen-flow by the Novocontrol Quatro cryosystem achieving temperature stability better than ± 0.1 K. As done for DSC, the pharmaceutical was kept in the melt state for a while, and cooled fast across the melting region to deep glassy state to ensure complete vitrification. Then, the dielectric spectra were measured isothermally, after stabilizing the temperature for about 600 seconds. The real and imaginary parts of the dielectric susceptibility were further analyzed with non-linear curve fitting routine of Levenberg Marquadit algorithm using WINFIT software Version 3.2 provided by Novocontrol.

Chapter 4
Thermal and Spectroscopic Studies on Probucol

4.1. Introduction

Probucol is an antihyperlipidemic drug, mainly used for the treatment of type II hyperlipoproteinaemia. Recent studies suggest that this drug can also be used as an antidiabetic agent as it can be used for the prevention of type-2 diabetes.[142] It is reported that probucol can be used for the treatment of common Alzheimer's disease as it has the cholesterol lowering effect.[143] It acts as a potent antioxidant and can be used to protect and amend heart and vascular disorders and it also shows some effects on neural and synaptic plasticity in brain aging.[144] Probucol has low aqueous solubility and high permeability through the gastrointestinal membrane, and thus belongs to biopharmaceutical classification system (BCS) Class II.[145] Probucol has aqueous solubility of around 2-5 ng/mL at 25 ºC and its logP is 11. Probucol is slightly absorbed in the gastrointestinal tract due to its poor solubility in water.[146]

As the solubility and hence the absorption rate of probucol is very low, several techniques have been employed to enhance the solubility and bioavailability of probucol. Benmore *et al.* prepared the amorphous form of probucol by acoustic levitation by dissolving in acetone and reported the melt quenched product as brittle solid with clear flakes.[147] According to J. J. Gerber *et al.*, the saturated solution of probucol in ethanol or acetone rapidly crystallizes into one of its polymorphic form.[148] P. Thybo *et al.* in 2008 reported that amorphous form of the drug can be prepared by mixing it with a hydrophilic polymer and spray drying.[149] Yagi *et al.* formulated the solid dispersion of probucol with polyvinylpyrrolidone (PVP)[146] and Broman et al. formulated probucol into solid dispersion with polyacrylic acid (PAA) and polyoxyethylene (POE) and verified that the release of probucol depends mostly on the properties of the polymer, than the drug in the solid dispersion.[150] Zaghloul *et al.* determined the solubility of probucol in different oils, surfactants co-surfactants using saturation solubility method and prepared a self-emulsified drug delivery system of probucol having enhanced dissolution and oral absorption.[151] This chapter discusses thermal, spectroscopic and dielectric relaxation studies of poorly water soluble, antihyperlipidemic drug probucol using various techniques. A comprehensive study of the drug's molecular mobility employing the broadband dielectric spectroscopy might

be appropriate for deciding the formulation technique, storage conditions and handling precautions.[152]

Probucol chemically described as 4,4′-[(1-methylethylidene)bis(thio)]-bis[2,6bis(1,1-dimethylethyl)]phenol was purchased from Sigma Aldrich. The empirical formula of probucol is $C_{31}H_{48}O_2S_2$ and molecular weight is 516.84 g/mol. The chemical structure[153] is shown in figure 4.1. The sample was used as received without any further purification.

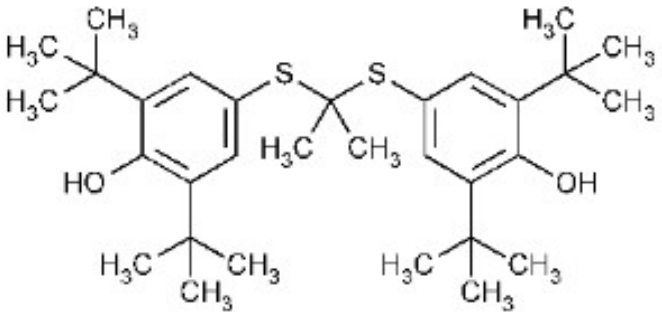

Figure 4.1. Chemical structure of probucol

4.2. Powder X-Ray Diffraction (PXRD)

The analytical technique, PXRD is used to verify the crystalline nature of the sample probucol. The sharp Bragg peaks in the figure show the crystalline nature of probucol.

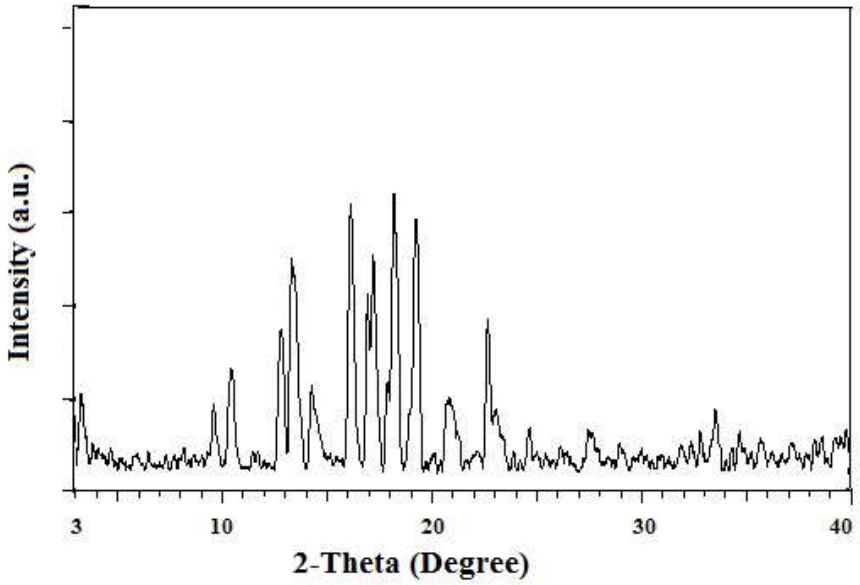

Figure 4.2. PXRD pattern of probucol

4.3. Thermogravimetric Analysis (TGA)

Thermogravimetric analysis was carried out to investigate the possibility of thermal degradation. To study the molecular dynamics, it is needed to assure that the sample does not undergo thermal degradation during heating while doing BDS experiment. From the TGA thermogram, it is clear that the onset of thermal degradation is at 260.7^0 C and thus the sample did not undergo thermal degradation during BDS experiment.

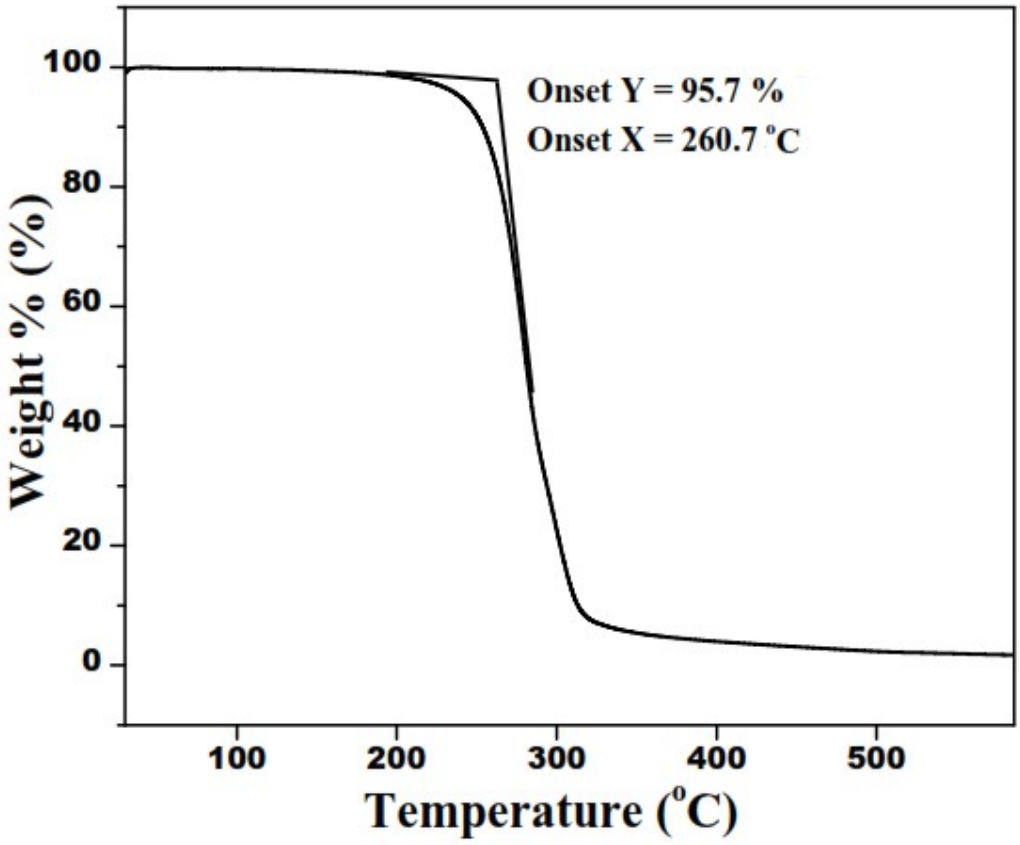

Figure 4.3. TGA thermogram of probucol

4.4. Differential Scanning Calorimetry (DSC)

From the DSC measurements, it was observed that the sample did not crystallize during the cooling and second heating cycle and this is in good agreement with the earlier report by Baird *et al.* (2010).[14] Thus probucol belongs to class (III) molecules with high Glass Forming Ability (GFA) upon cooling as well as high ‘‘glass stability’’ upon reheating above T_g. So probucol can be taken as a non-crystallizing compound. The glass transition temperature, T_g of the amorphous sample was observed to be at 301.6 K which is the peak maximum of glass transition endotherm, the onset of melting endotherm appears at 399.5 K

and is taken as the melting point of crystalline probucol. Both these values are in close agreement with the earlier reports.[14,113] The melting enthalpy was found to be 65.7 J/g.

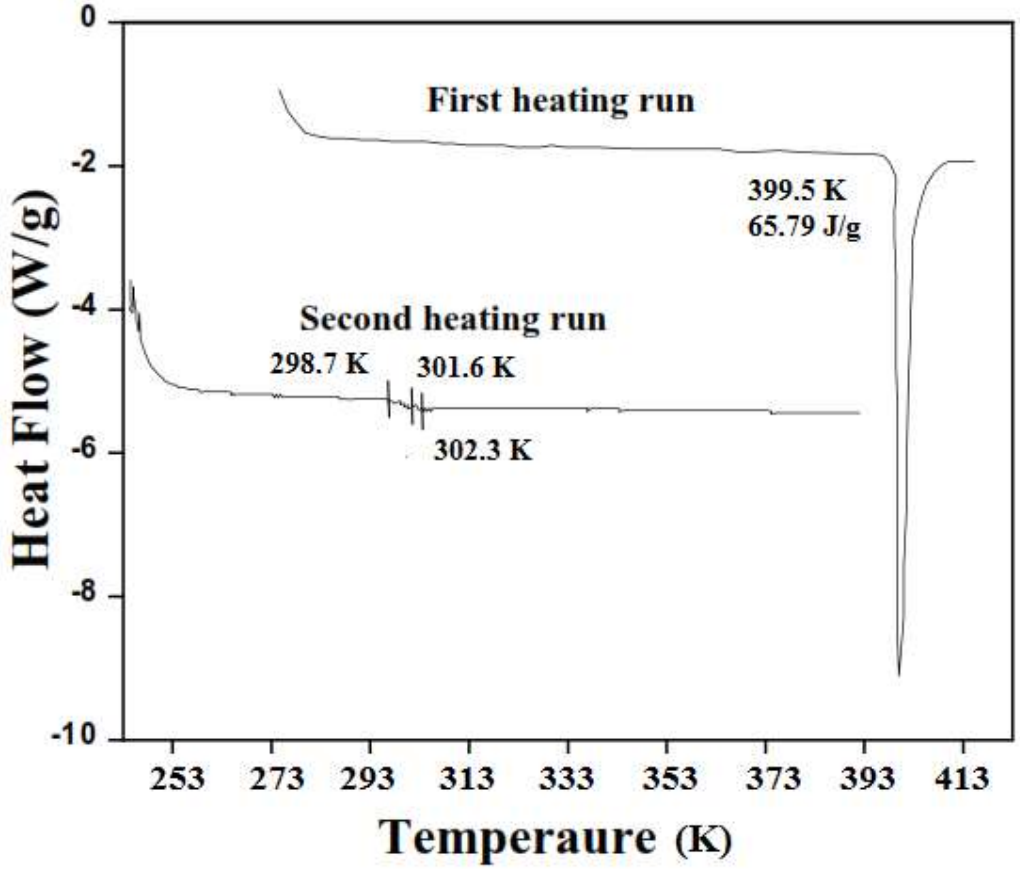

Figure 4.4. DSC thermogram of probucol. The curves are vertically shifted for clarification.

Probucol is known to having at least two conformational polymorphs. Both polymorphic forms have monoclinic space groups and the packing is determined by Van der Waals interactions.[148] The onset melting point of Form I is at 399.15 K and is thermodynamically stable, whereas for Form II, the onset melting point is at 389.15 K. From the DSC experiment, the sample exhibited a melting point at 399.5 K and therefore is Form I.

4.5. Broadband Dielectric Spectroscopy

The complex dielectric function $\varepsilon^*(f) = \varepsilon'(f)-i\varepsilon''(f)$ was measured during the heating of the amorphous probucol from 183.15 K to 353.15 K, where f is the frequency, ε' is the real part of dielectric permittivity and ε'' is the imaginary part of dielectric permittivity. The dielectric loss spectra of probucol, imaginary part ε'' plotted against frequency is shown in the figures below. Figure 4.5 shows the relaxation above T_g, which is known as the structural α-

relaxation and arises because of the cooperative motion of the molecules and became kinetically frozen while cooling the liquid to form a glass. The α-relaxation peak shifts towards lower frequencies as the temperature is decreased. The rise of the signal at low frequencies is due to the presence of dc conductivity. The dc conductivity usually arises from the diffusion of ionic impurities in a material. The real part of the dielectric spectra of probucol plotted against frequency is shown in figure 4.7.

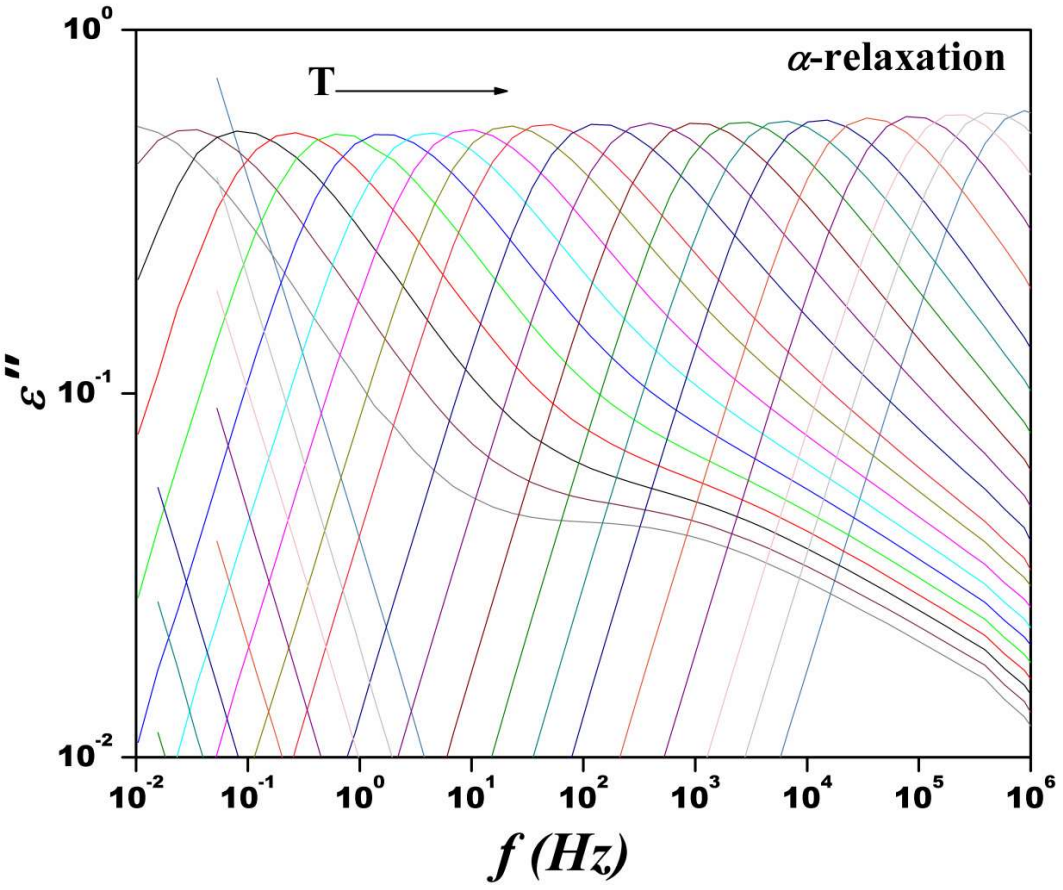

Figure 4.5. Dielectric loss curves of probucol for temperatures above T_g (297.15 K-315.15 K, ΔT=2 K; 318.15 K-333.15 K, ΔT=3 K and 337.15 K-353.15 K, ΔT=4 K).

Below T_g (figure 4.6), the α-relaxation process is too slow to be measured and it moves out of the window. As the temperature lowers, the secondary relaxation process moves towards the lower frequencies. The real and imaginary parts of the dielectric permittivity were further analyzed with the non-linear curve fitting routine of Levenberg Marquadit algorithm using WINFIT software Version 3.2 provided by Novocontrol. The equation used for the analysis of dielectric spectra is Havriliak-Negami equation[113] given by equation (2.9).

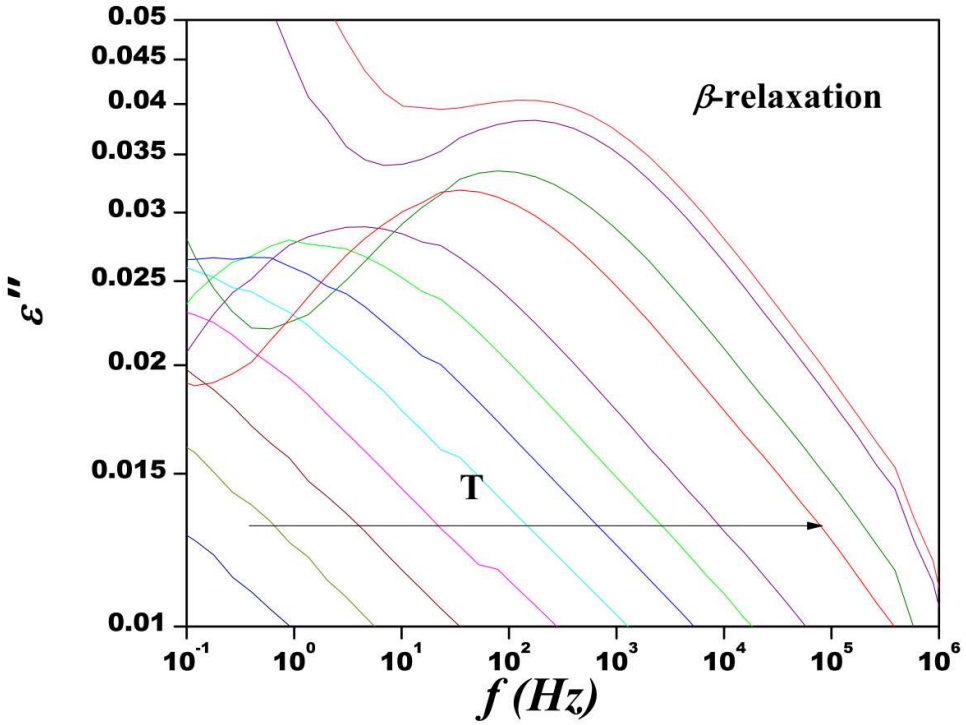

Figure 4.6. Dielectric loss spectra of probucol for temperatures below T_g (295.15 K-293.15 K, ΔT=2 K and 283.15 K-183.15 K, ΔT=10 K).

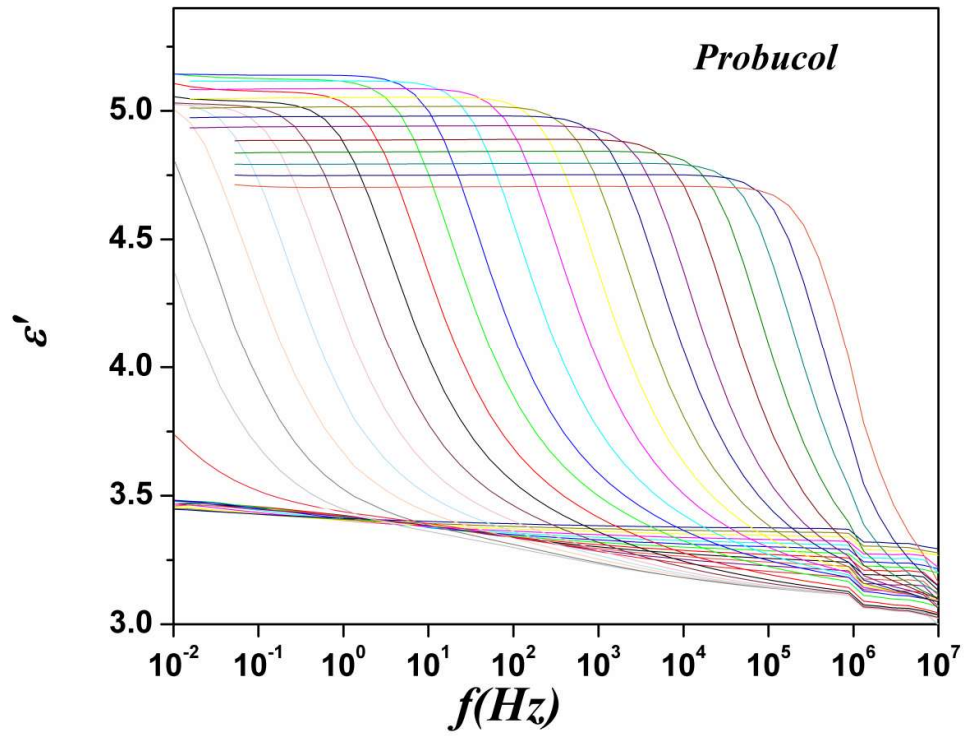

Figure 4.7. Real part of the complex permittivity of probucol for various temperatures ranging from 353.15 K-183.15 K.

Debye-Stokes-Einstein (DSE) equation represents the relation between dc conductivity and structural relaxation times in glass forming liquids. This equation describes the relation between the translational motions of ions and rotational motions of molecules.

$$\tau_\alpha \sigma_{dc} \approx \text{ constant.} \tag{4.1}$$

As approaching the glass transition temperature, this equation fails for most of the molecular liquids while the modified form of this equation known as fractional Debye-Stokes-Einstein (FDSE) equation succeeds in overcoming this limitation.[55]

$$\tau_\alpha^s \sigma_{dc} \approx \text{constant} \tag{4.2}$$

where s is the fractional exponent and its value is less than 1. The value of s obtained for probucol was 0.89 and hence the enhancement of translational motion over rotational motion is observed while approaching T_g. The plot of dc conductivity versus structural relaxation time is shown figure 4.8 in log-log scale.

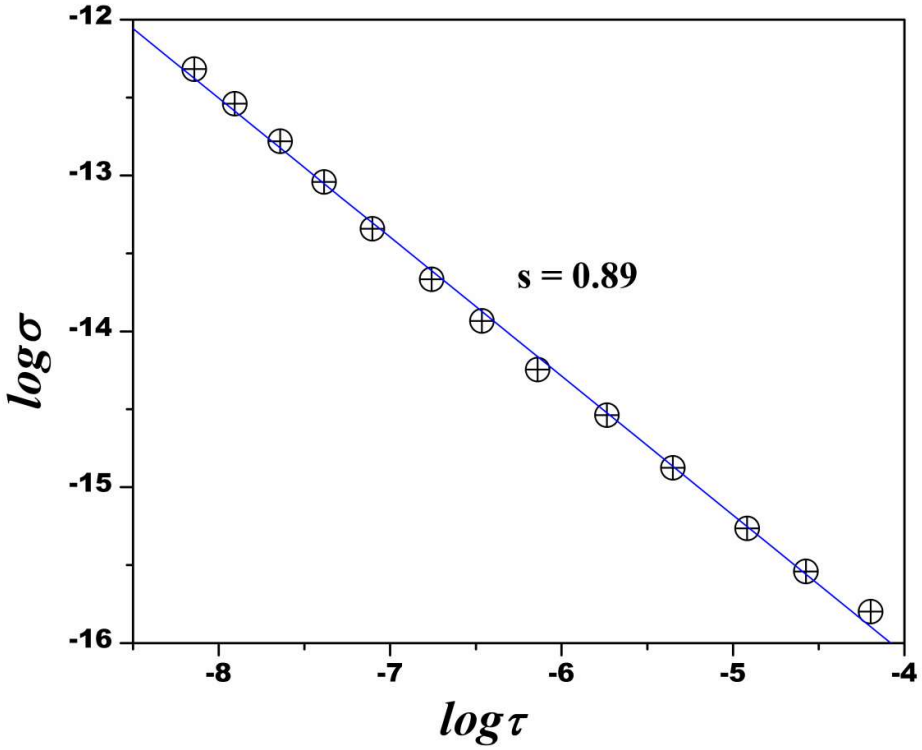

Figure 4.8. dc conductivity *vs.* structural relaxation time in double log scale.

4.5.1. The structural α-relaxation

The dielectric loss spectra of probucol for temperatures above T_g is fitted using the HN function given by equation (2.9) and is shown in figure 4.9. The conductivity is subtracted from the fitted data inorder to get clear and distinct α-peaks. The temperature dependence of the relaxation time of α-process is non-Arrhenius in nature and can be well described by the Vogel-Fulchers-Tammanns equation[94,95,97,154] given by equation (2.2). Matlab code is used for obtaining relevant VFT parameters such as T_g, fragility *etc*. For probucol, the fitted parameters are B = 2360.4, and T_g obtained from VFT fit is 294.7 K and the anticipated value of T_0 is equal to 235.8K.[155] Our observations are analogous with the previous reports.[69]

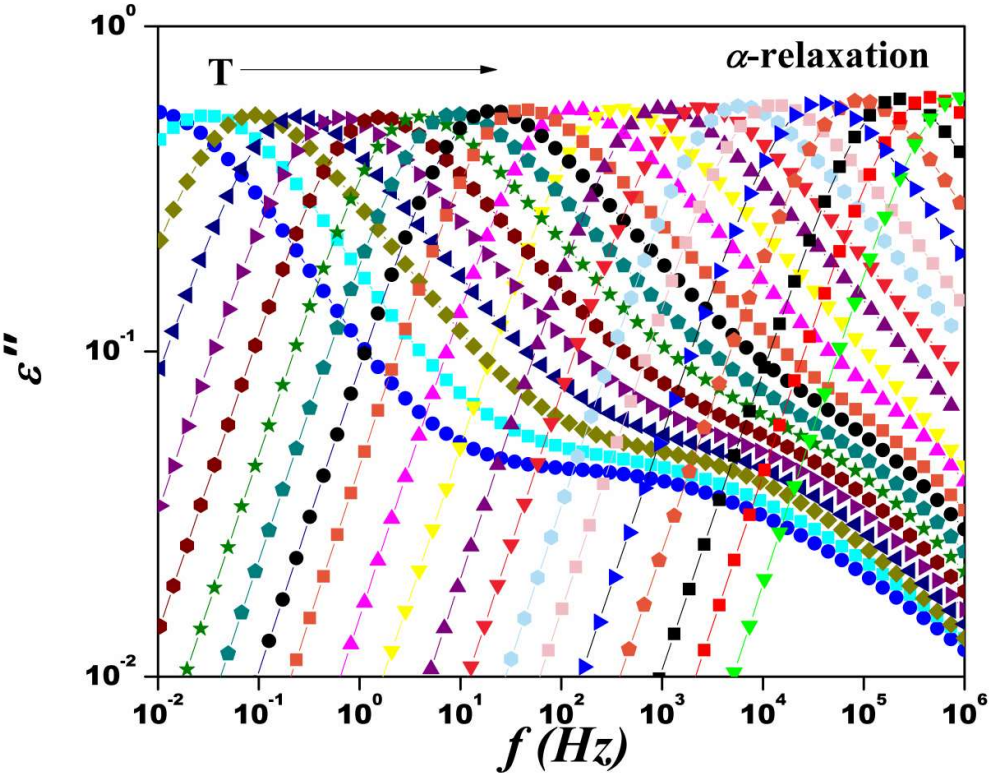

Figure 4.9. HN fitted dielectric loss spectra of probucol for temperatures above T_g (297.15 K-315.15 K, ΔT=2 K; 318.15 K-333.15 K, ΔT=3 K and 337.15 K-353.15 K, ΔT=4 K) after subtracting the conductivity.

This value of T_0 is approximately equal to the Kauzmann temperature, T_K [156], which is the hypothetical temperature at which the molecular motions cease completely and this temperature can be considered as the ideal temperature for the storage and is almost 50 degrees below the T_g. In the vicinity of this temperature, primary structural relaxation

would have the time scale of exceeding years.[152] The translational molecular motions are assumed to be negligible below this temperature. So it is recommended that the storage of this particular API below 235.84 K would provide better shelf-life and stability. The activation energy of α-process is estimated as 19.6 kJ/mol.[155] The values of VFT fitting parameters are tabulated in table 4.1.

In order to verify that the shape of the structural relaxation peak is invariant for various temperatures above T_g, Master plot was created by scaling several spectra for temperatures above T_g between the temperature range 297.15 K to 315.15 K. It shows that it is valid for probucol. Such superposition of spectra is possible due to the temperature independent nature of the shape of the structural peak. The spectra before and after superposition are shown in the figure. 4.10.

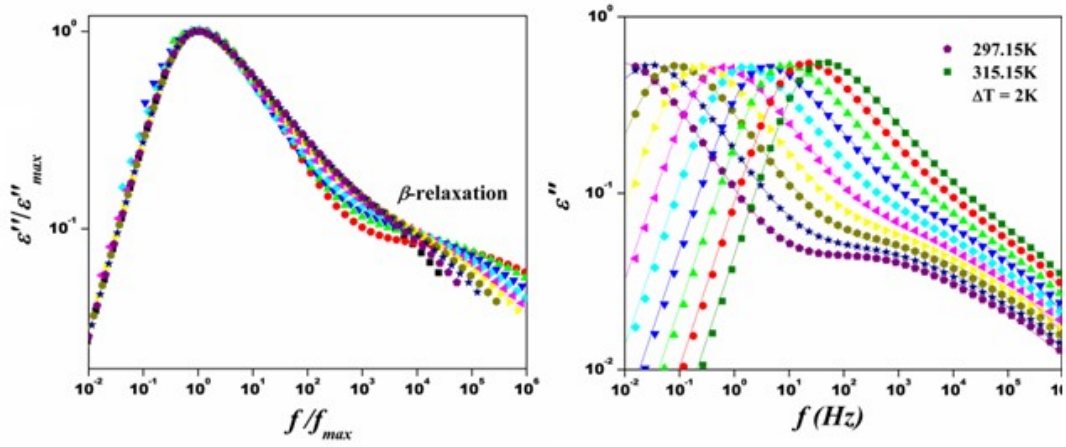

Figure 4.10. Master plot formed by overlapping the spectra between temperatures ranging from 297.15 K- 315.15 K. The plot on the right side picturise the same spectra before superposition.

4.5.2. Fragility

The fragility index or steepness index, m can be calculated from VFT fit using the equation (2.3) and is defined as the slope of the relaxation time curve *vs*. T_g /T at the glass transition temperature T_g in the Oldekop-Laughlin-Uhlmann-Angell (OLUA) plot. If the value of m is less than 45, then such system belongs to strong liquids and if m is greater than 75 such system belongs to fragile liquids.[23] For probucol m = 87 and is a fragile glass former[155] and the plot is shown in figure 4.11. In earlier studies, the fragility index of probucol reported to be 101 by Biard *et al.* (2010).[14]

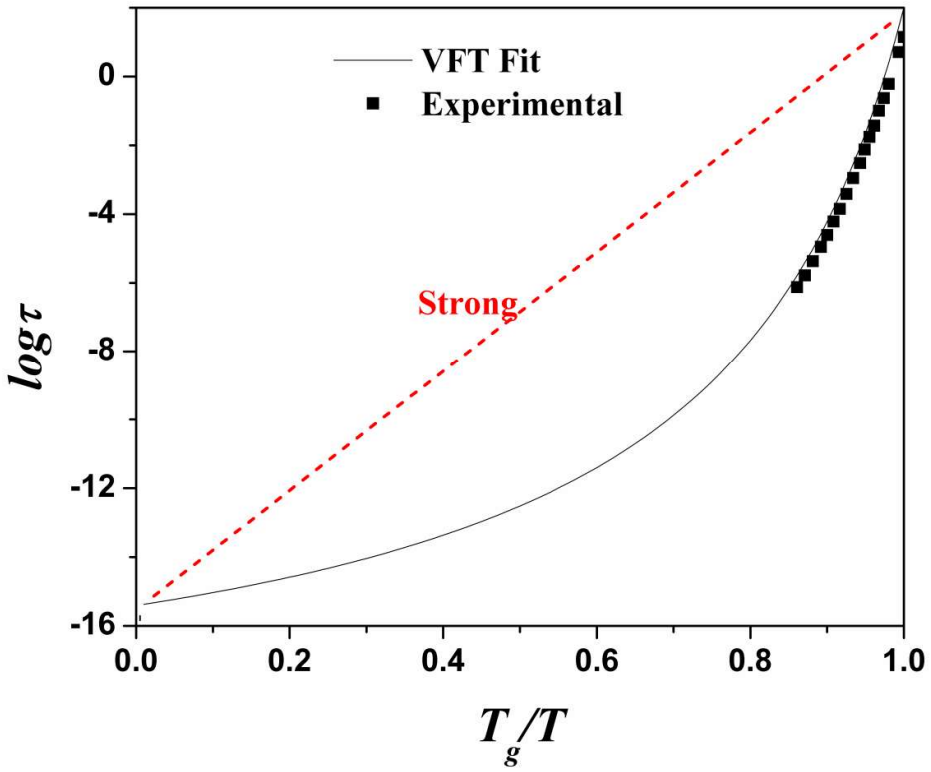

Figure 4.11. Angell plot, here the solid line represents the fitted data and the symbols represent experimental values.

4.5.3. The secondary relaxation

From the dielectric spectra, it is evident that probucol had a well resolved secondary relaxations near and below T_g. The HN fitted dielectric loss curves of probucol below T_g are shown in figure 4.12. From the fit, the value of β_{HN} is obtained as ≈ 1, which indicates that the secondary relaxations obey Cole-Cole behavior. At temperature below the glass transition temperature when the structural relaxation moved out of the frequency interval of the measurement, the temperature dependence of the secondary β-relaxations is usually described by the Arrhenius equation (2.4). The activation energy for β-process was obtained as 67.9 kJ/mol.

Table 4.1. Fitting parameters for the VFT and Arrhenius equations of probucol

α-process				β-process	
VFT				Arrhenius	
$logf_0$ (Hz)	B (K)	T_0 (K)	E_α (kJ/mol)	E_β (kJ/mol)	m
14.61	2360.4	235.8	19.6	67.9	87

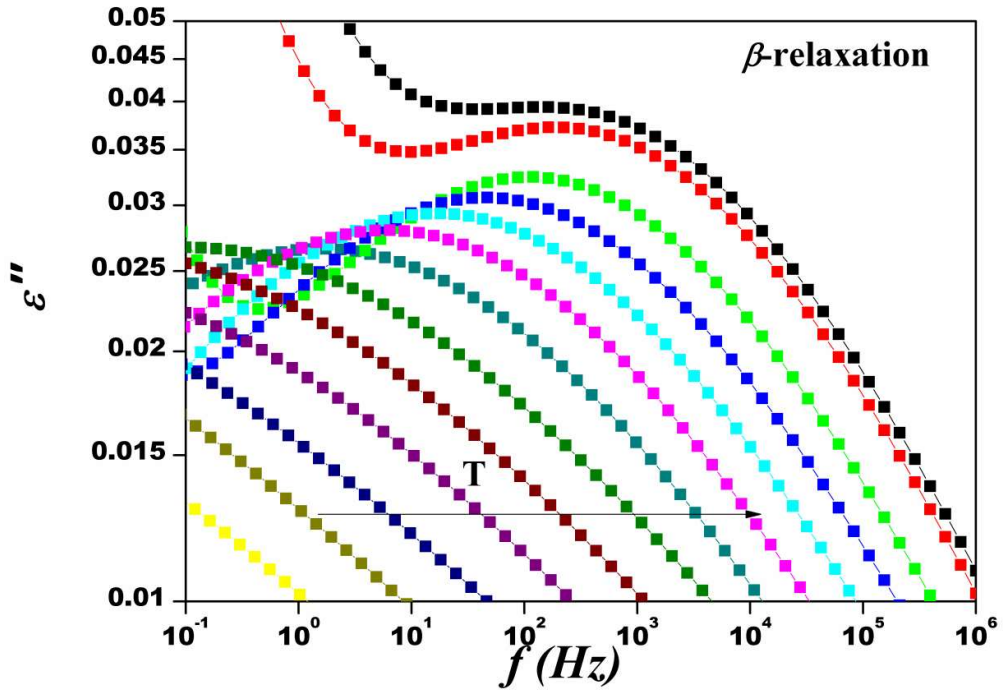

Figure 4.12. HN fitted dielectric loss spectra of probucol for the temperatures below T_g (295.15 K-293.15 K, ΔT=2 K and 283.15 K-183.15 K, ΔT=10 K).

4.6. Coupling Model (CM) Predictions

The properties of structural relaxations originating from many body relaxations and its relation to its precursor, namely Johari Goldstein relaxation can be explained using CM predictions.[117] The dielectric loss spectra for the temperatures 301.15 K, 303.15 K and 305.15 K were fitted using Fourier transform of KWW function. For probucol, all the fitted spectra near to the glass transition temperature T_g exhibits nearly invariant n values of 0.43 (thus $\beta_{KWW} = (1-n) = 0.57$) and a representative spectrum at 303.15 K is shown in figure 4.13. The value of β_{KWW} corresponds to the deviation from the exponential behavior of the relaxation function in the time domain. The knowledge of the distribution function also helps to anticipate the resistance of the amorphous state against the crystallization as well as chemical degradation.

From the figure, the primitive relaxation time is calculated using equation (2.12) and the value of τ_0 for the above temperature is obtained as 7.1167 x 10^{-6} s and the corresponding frequency f_0 is calculated as , $f_0 = (1/2\pi\tau_0) = 22.36$ kHz. It was found that the estimated value of f_0 agrees well with the maximum of the secondary relaxation peak and thus it is considered as JG secondary relaxation from the CM predictions. In view of that, the secondary relaxation observed in this system was supposed to be intermolecular in origin and is associated to the

local motion of the whole molecule. Similar evidence was also reported by Knapik *et al.* by doing dielectric experiments at ambient and elevated pressure.[69]

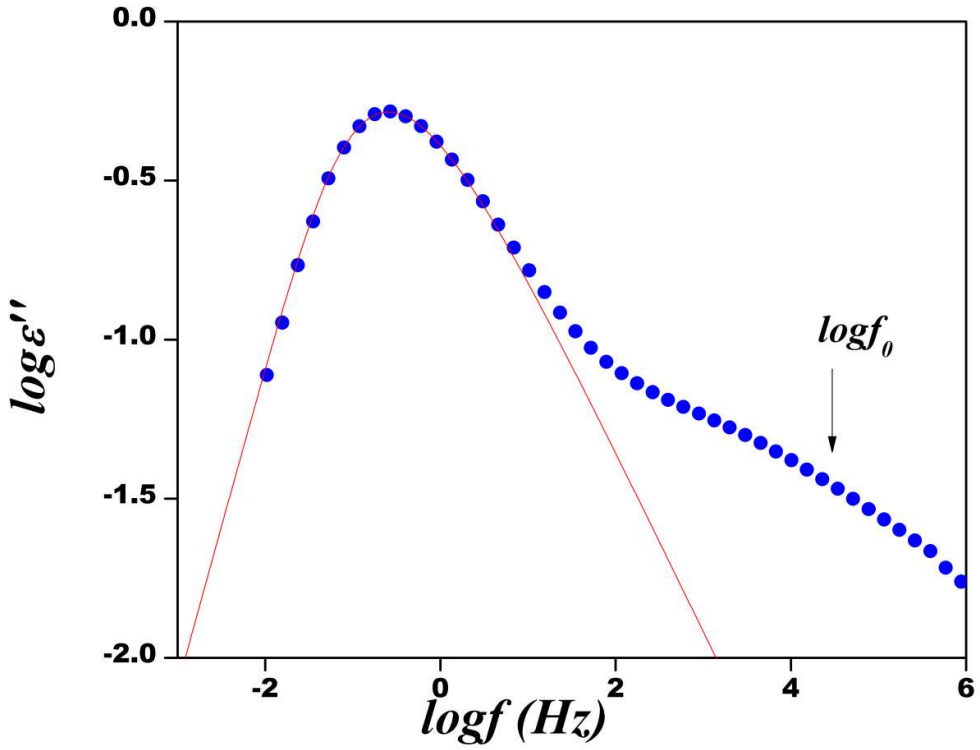

Figure 4.13. KWW fit for the temperature 303.15 K. The red line denotes the fitted data and the arrow indicates the position of primitive relaxation frequency.

For glass forming substances of all kinds, Ngai and Capaccioli[157] predicted the ratio E_β/RT_g quantitatively from the coupling model and arrived at the relation,

$$E_\beta/RT_g = 2.303(2 - 13.7n - log_{10}\tau_\alpha) \quad (4.3)$$

The ratio E_β/RT_g depends on the exponent n of α-relaxation and the pre-factor τ_α of the JG β-relaxation and the ratio fall within a broad neighborhood about 24 for most glass formers. Interestingly, the ratio E_β/RT_g for probucol was obtained as 27.3 from the experimental data and that calculated from equation (4.3) is 26.53 are matching nicely. This is further verification that the secondary relaxation obtained for probucol is JG β-relaxation.

The relaxation map of probucol for both the processes is presented in figure 4.14. From the figure, it is clear that CM predictions are in agreement with the experimental secondary relaxations which emphasize that the secondary relaxations obtained in probucol are of intermolecular origin and belongs to JG-relaxation.

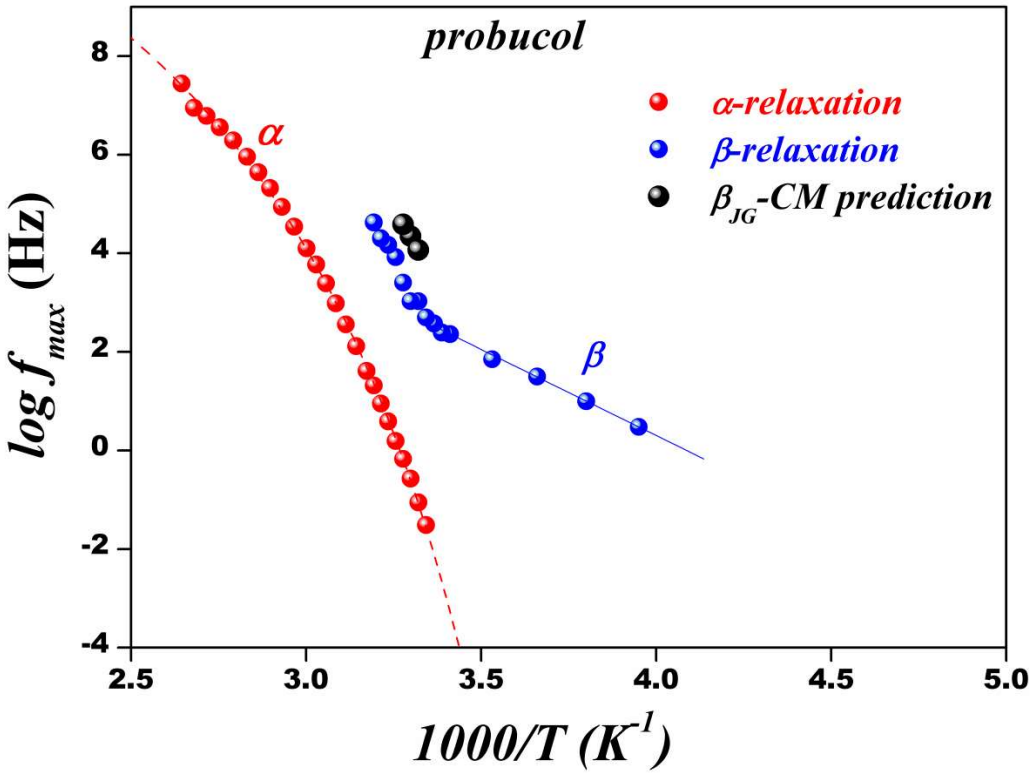

Figure 4.14. Relaxation map of probucol. Red circles denote α-relaxation, blue circles for β-relaxation and black circle indicate the CM prediction for JG β-relaxation. Dotted red line represents the VFT fit for α-relaxation and solid blue line represent the Arrhenius fit for β-relaxation.

4.7. Conclusions

From the DSC study, it was proved that probucol is a noncrystallizing compound and has good glass forming ability. It was also revealed that out of the two conformational polymorphs, the supplied sample belonged to Form I. From the TGA experiment, the onset of thermal degradation for probucol is obtained at 260.7^0 C and thus it is verified that the sample did not undergo thermal degradation during BDS experiment.

Dielectric studies of probucol revealed two types of relaxation process, namely the structural α- relaxation and more local β-relaxation. This β-relaxation is revealed to be as JG β-relaxation from the KWW fit of CM prediction. Thus the secondary relaxation in probucol is proved to be intermolecular in origin. The α-relaxation shows non-Arrhenius behavior and the temperature dependence of this process was described by the VFT equation while β-relaxation shows Arrhenius temperature dependence. The presence of conductivity was

also observed for temperatures above T_g. As the fragility index is 87, probucol is considered as a fragile glass former.

In probucol molecule, internal rotation around the CO bond may be possible since it has dielectrically active internal degrees of freedom. This rotation will lead to conformational changes to the OH bond relative to the aromatic ring. Another possible rotation is of the C-S-C dipole, which may arise from the rotation of the whole molecule in its cage or from the fluctuation of the C-S-C angles. Hence it is reasonable to suppose that this rotation may belong to the Johari-Goldstein relaxation.[158]

Chapter 5

Thermal, Spectroscopic Studies and Crystallization Kinetics of Clofoctol

5.1. Introduction

Clofoctol is a bacteriostatic antibiotic and used for the treatment of upper and lower respiratory tract infections both in adults and children.[159] It was reported that clofoctol could serve as a potential anticancer drug as it inhibits protein translation in mammalian cells. Wang *et al.* identified clofoctol as a novel inhibitor of prostate cancer cell proliferation.[160] Benmore *et al.* prepared the amorphous form of clofoctol by acoustic levitation by dissolving in pure anhydrous ethanol.[147] Clofoctol has aqueous solubility of 3.62e-05 mg/mL and its logP is 7.62.

Clofoctol chemically described as [2-(2,4- dichlorobenzyl)-4-(tetramethyl-l, 1,3,3-butyl)phenol] was purchased from Sigma Aldrich. The empirical formula of clofoctol is $C_{21}H_{26}Cl_2O$ and the molecular weight is 365.33 g/mol. The chemical structure[161] is shown in figure 5.1. The sample was used as received without any further purification

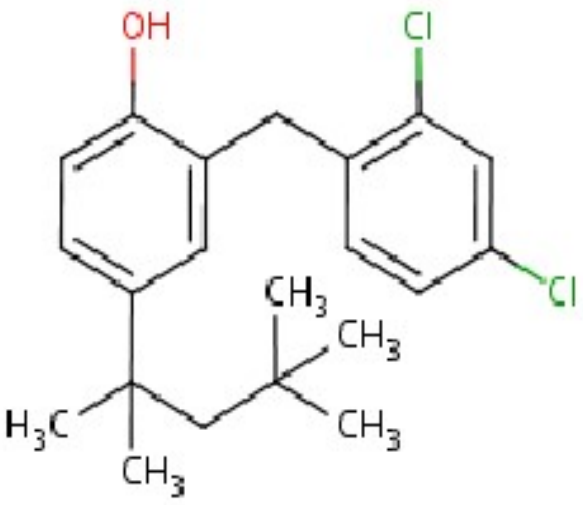

Figure 5.1. Chemical structure of clofoctol

5.2. Powder X-Ray Diffraction (PXRD)

The crystalline nature of clofoctol is verified using PXRD. The sharp Bragg peaks show the crystalline nature of clofoctol.

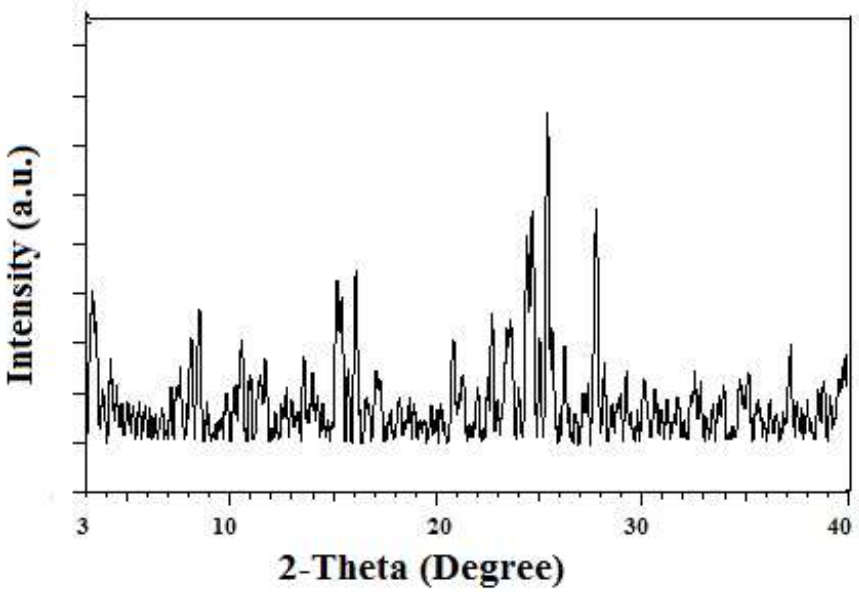

Figure 5.2. PXRD pattern of clofoctol

5.3. Thermogravimetric Analysis (TGA)

Thermogravimetric analysis was carried out to find the possibility of thermal degradation. The onset of thermal degradation is at 256^0 C. Thus, it is evident that the sample did not undergo thermal degradation while conducting BDS experiments.

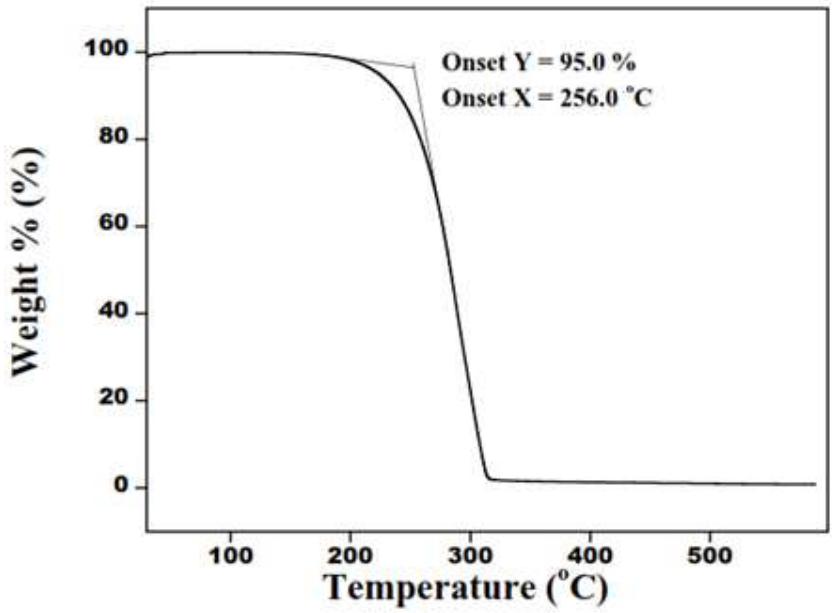

Figure 5.3. TGA thermogram of clofoctol

5.4. Differential Scanning Calorimetry

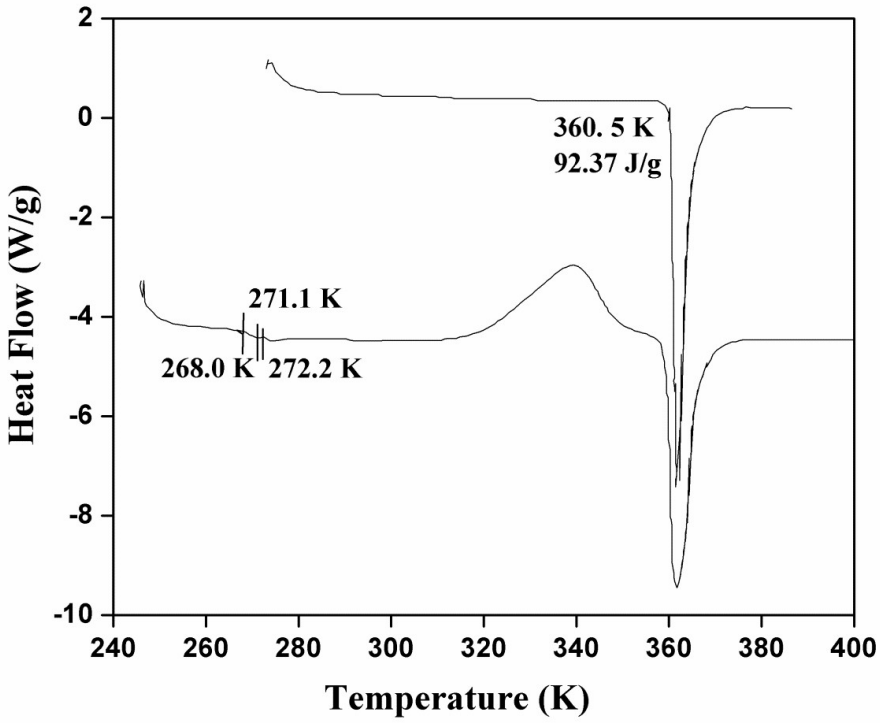

Figure 5.4. DSC thermogram of clofoctol. The curves are vertically shifted for clarification

From the DSC measurements, it was observed that clofoctol shows no crystallization during cooling from the under-cooled melt to below T_g , but shows crystallization during reheating above T_g and thus belongs to class (II) molecules according to Baird *et al.* (2010).[14] The glass transition temperature, T_g of the amorphous sample was observed to be at 271 K and the melting point of crystalline clofoctol was 360.5 K. Both these values are in agreement with the earlier report. The melting enthalpy was found to be 92.4 J/g.

5.5. Broadband Dielectric Spectroscopy

The complex dielectric function $\varepsilon^*(f) = \varepsilon'(f)-i\varepsilon''(f)$ was measured during the heating of the amorphous clofoctol from temperature 163.15 K to 294.15 K. Relaxation dynamics of amorphous material are characterized by motions occurring on different length and time scales. Two kinds of relaxation behavior are observed in the dielectric spectra of clofoctol. Dielectric spectra are obtained by plotting real and imaginary parts of the complex dielectric permittivity data for different temperatures over a wide frequency range. The α-relaxation shows the signatures of typical glass forming systems and as the temperature is increased, the

loss peaks shift towards higher frequencies. Further, the rise in loss peaks at low frequencies is due to the presence of dc conductivity, and the magnitude of it increases in an Arrhenius manner on increasing the temperature. Secondary relaxations are observed below T_g. The dielectric loss spectra of clofoctol for temperatures above and below T_g are shown figure 5.5 and 5.6, respectively whereas the real part of dielectric spectra is shown in figure 5.7.

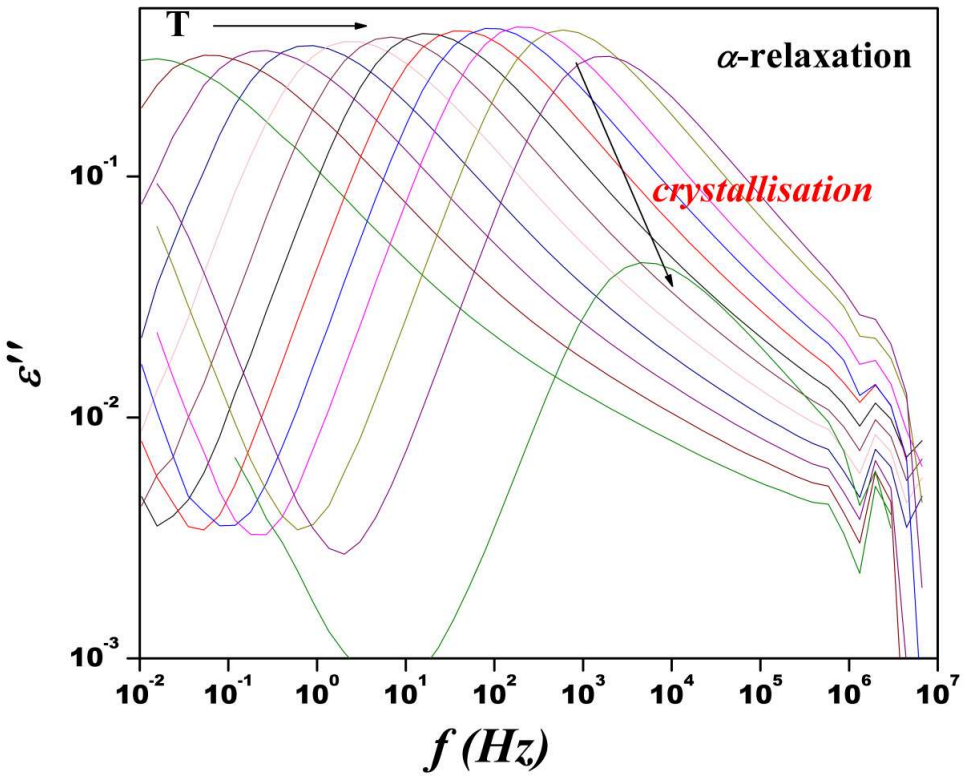

Figure 5.5. The dielectric loss spectra of clofoctol for temperatures above T_g (267.15 K-285.15 K, ΔT=2 K and 288.15 K-294.15 K, ΔT=3 K).

The fall in dielectric strength at high temperature region are due to the onset of crystallization. . We were unable to get the dielectric spectra at higher temperatures beyond the onset of crystallization during heating. We overcome this issue by melting the samples and repeating the measurements during subsequent cooling. We could get the information about the peak loss frequency to fill the relaxation map up to 10^7 Hz for clofoctol. The real and imaginary parts of the dielectric permittivity were further analyzed with non-linear curve fitting routine of Levenberg Marquadit algorithm using WINFIT software Version 3.2 provided by Novocontrol. The dielectric spectra were fitted using HN equation.

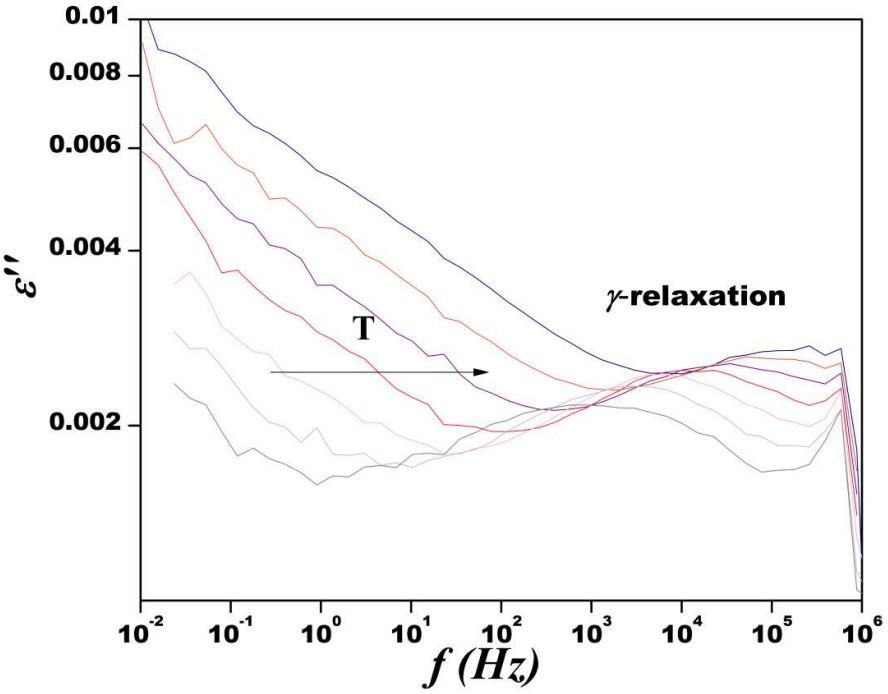

Figure 5.6. The dielectric loss spectra of clofoctol for temperatures below T_g (223.15 K-163.15 K, ΔT=10 K)

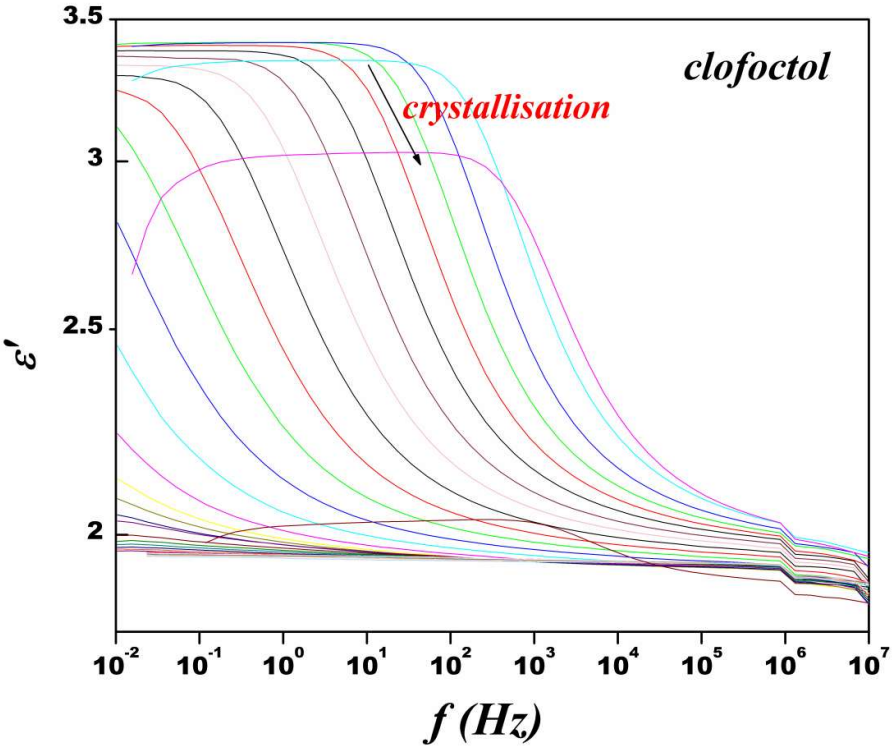

Figure 5.7. Real part of the complex permittivity of clofoctol for various temperatures ranging from 294.15 K-163.15 K.

The relation between dc conductivity and structural relaxation times is plotted in figure 5.8, which is a straight line and follows the fractional Debye-Stokes-Einstein (FDSE) equation (4.2). The value of the fractional exponent *s* is obtained as 0.94.

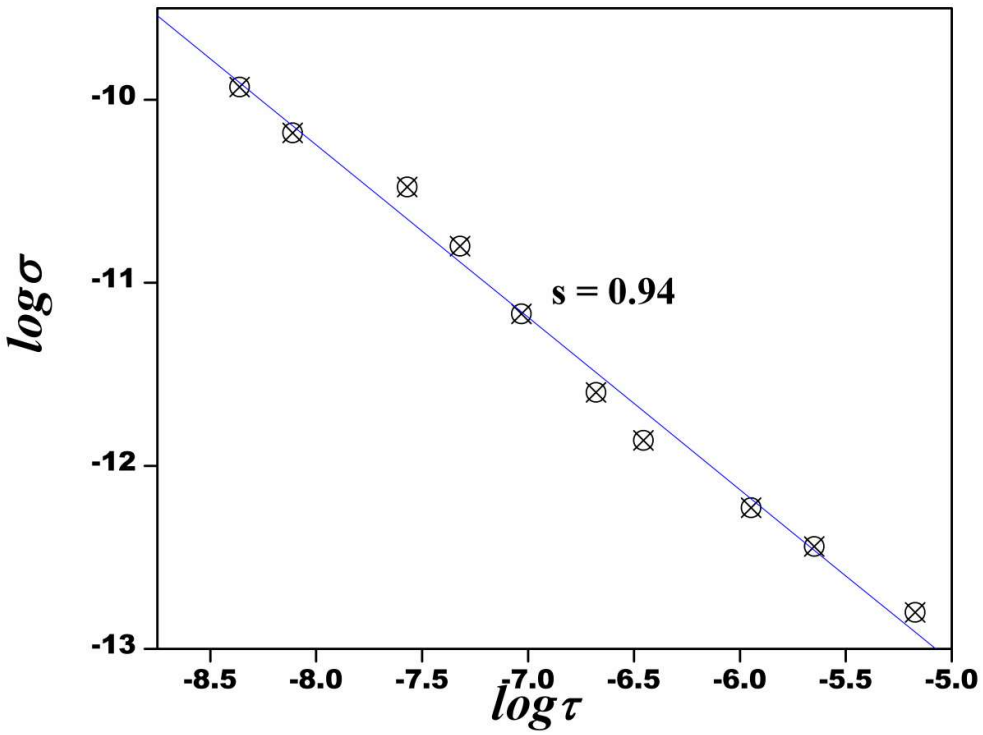

Figure 5.8. dc conductivity *vs*. structural relaxation time on a log-log scale.

5.5.1. The structural α-relaxation

This process involves the cooperative motion of molecules which slow down dramatically on approaching the glass transition by decreasing temperature. The falling of peak in dielectric spectra indicates crystallization. The dielectric spectra are fitted using HN equation and conductivity is subtracted from the fitted data to get a clear picture of the α-relaxation peaks. The HN fitted curves are shown in figure 5.9. The structural relaxation process shows non-Arrhenius temperature dependence and can be well described by VFT equation. For clofoctol, the fitted VFT parameters are B = 1596.2, and the estimated value of T_g is 264.3 K and the value of T_0 obtained from VFT fit is equal to 220.6 K.[155] So it is suggested that the storage of this particular API clofoctol below 220.6 K would provide better shelf-life and stability. The activation energy of α-process is estimated as 13.2 kJ/mol. The VFT parameters are tabulated in table 5.1.

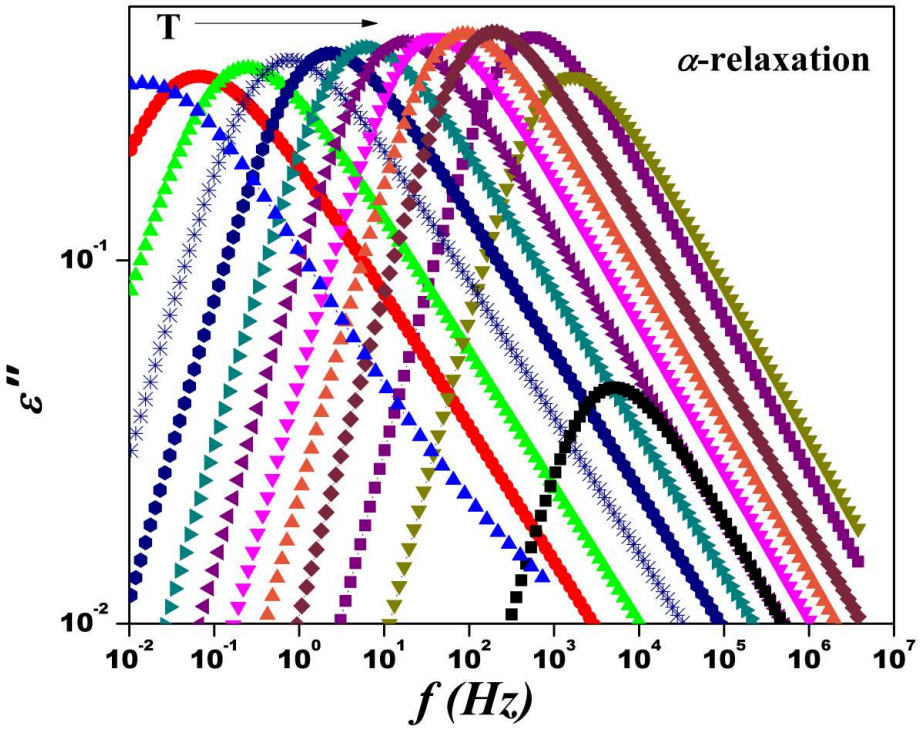

Figure 5.9. HN fitted curves for the dielectric loss spectra of clofoctol for temperature above T_g (267.15 K-285.15 K, ΔT=2 K and 288.15 K-294.15 K, ΔT=3 K) after subtracting conductivity.

Master plot was drawn by normalizing the imaginary part of dielectric data by its maximum value plotted against frequency/maximum frequency of the loss. The result indicates that the dielectric response of structural relaxation is temperature independent.

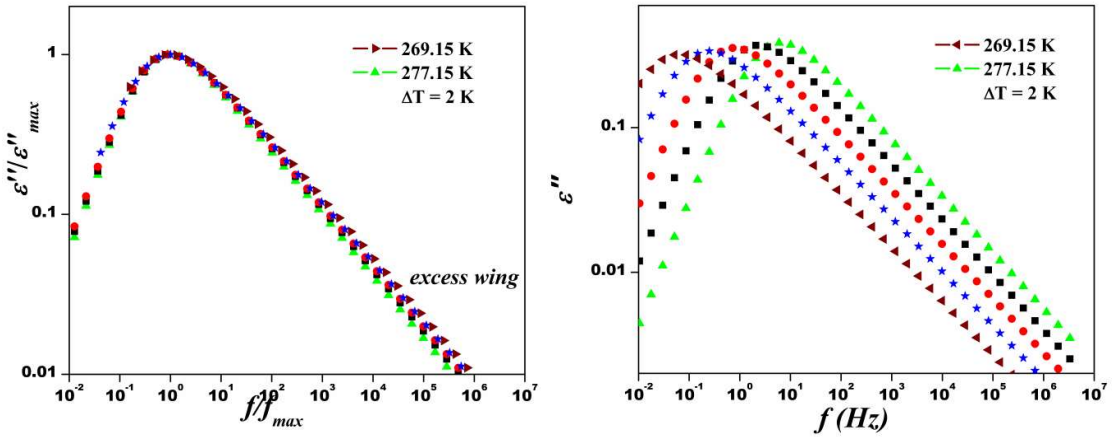

Figure 5.10. Master plot formed by overlapping the spectra between temperatures ranging from 269.15 K- 277.15 K. The plot on the right side picturise the same spectra before superposition.

5.5.2. Fragility

The fragility index represents the temperature sensitivity of the relaxation time of the primary process. Fragility index is a measure of rapidity with which ordering happens in the amorphous glassy phase. It represents the rate at which molecular motion is arrested when the amorphous glassy state is reached. The fragility index calculated for clofoctol is, m = 95. This value indicates that clofoctol is a fragile glass former. In earlier studies, the fragility index of clofoctol reported to be 70 by Biard *et al.* (2010).[14] The Angell plot for the pharmaceutical clofoctol is shown below, in figure 5.11.

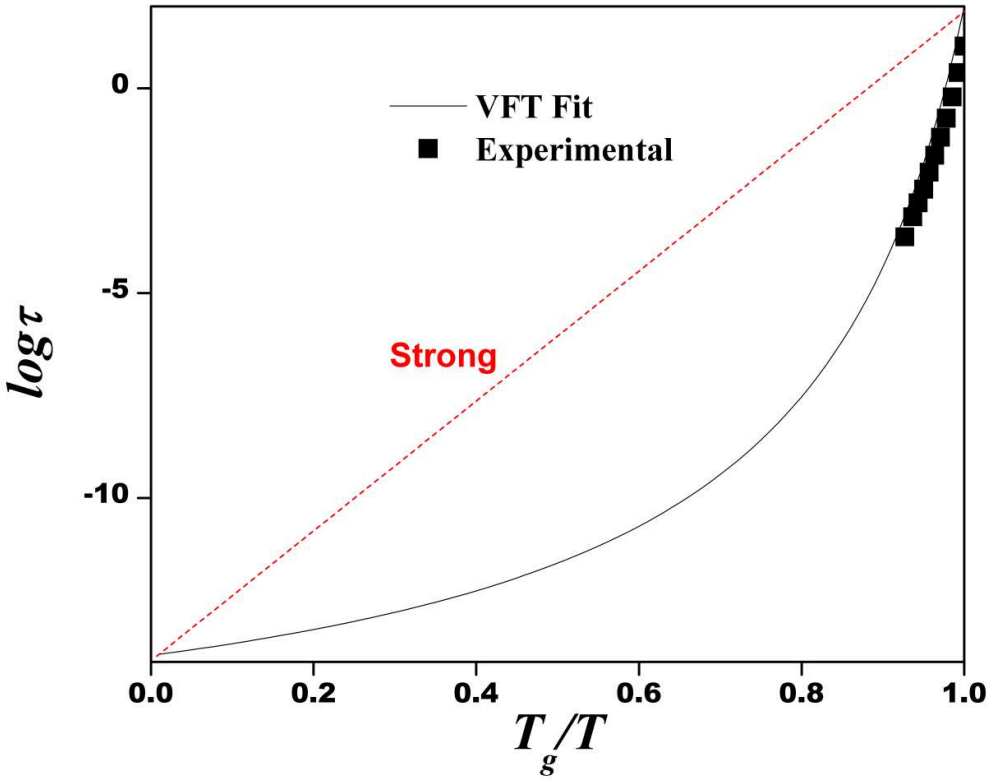

Figure 5.11. Angell plot, here the solid line represents the fitted data and the symbols represent experimental values.

5.5.3. The secondary relaxation

The secondary relaxations are originating from either the small angle rotations of the whole molecule or rotation of parts of the molecule such as side chain rotation. The HN fitted dielectric loss curves of clofoctol below T_g are shown in figure 5.12. Secondary relaxations obey Arrhenius temperature dependence and the activation energy for γ-process was obtained as 25.6 kJ/mol.

Table 5.1. Fitting parameters for the VFT and Arrhenius equations of clofoctol

α-process				γ-process	
VFT				Arrhenius	
$logf_0$ (Hz)	B (K)	T_0 (K)	E_α (kJ/mol)	E_γ (kJ/mol)	m
13.04	1596.2	220.6	13.2	25.6	95

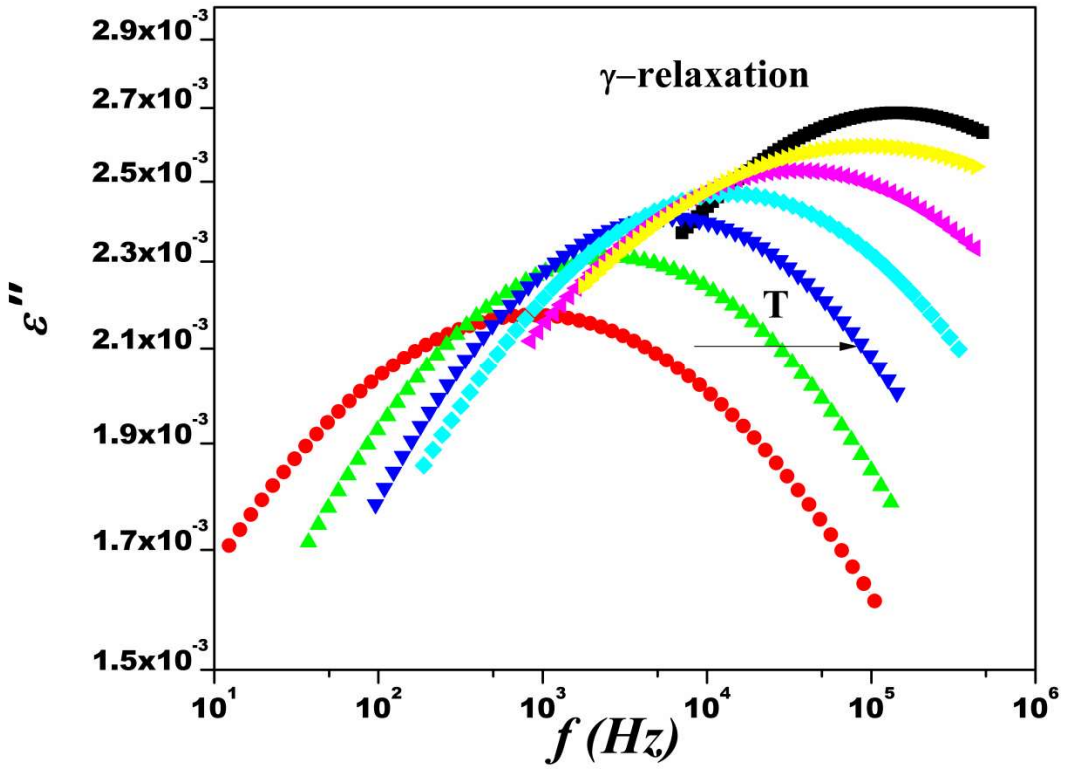

Figure 5.12. HN fitted curves for the dielectric loss spectra of clofoctol for temperatures below T_g (223.15 K-163.15 K, ΔT=10 K)

5.6. Coupling Model (CM) Predictions

The dielectric loss spectra of the sample clofoctol were fitted using the Fourier transform of the KWW function for the temperatures near to the glass transition temperature T_g. As shown in figure 5.13, for clofoctol, we could only observe a deviation of loss at higher frequencies from the KWW fits in the vicinity of T_g. It also points out that the resolved secondary relaxation (γ) is non JG.

From the figure, it is evident that n is time dependent in the case of clofoctol. Also the calculated $logf_0$ is located at several orders of magnitude lower than that of the resolved secondary relaxation depending on the temperature. This difference is additional evidence that the resolved secondary relaxation is not the JG beta relaxation. In order to examine the validity of equation (4.3), the value of E_γ/RT_g is calculated and is obtained as 11.6, too small for JG beta. This result also provides an additional evidence that the JG β-relaxation is not resolved in the isothermal loss spectra.[155] Thus the secondary relaxation observed in this system was supposed to be intramolecular in origin.

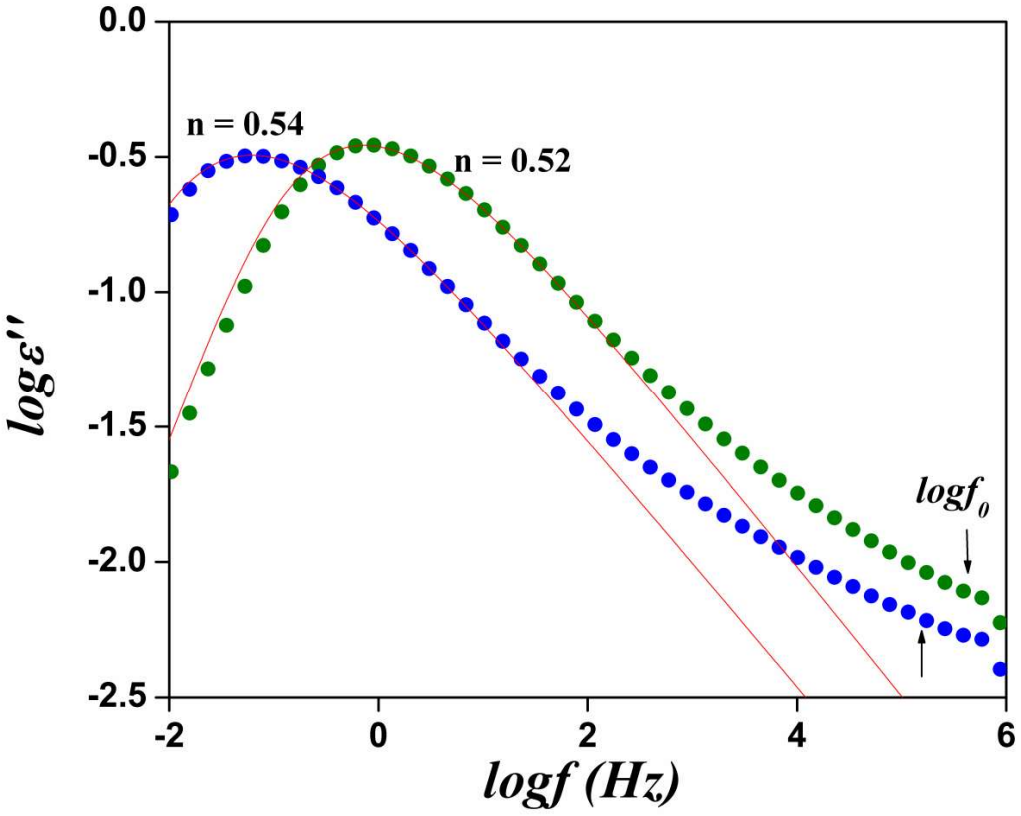

Figure 5.13. KWW fit of clofoctol for temperatures 269.15 K and 273.15 K. The red line denotes the fitted data and the arrow indicates the position of primitive relaxation frequency as predicted by equation (2.12).

The relaxation map of clofoctol for both the processes is presented in figure 5. 14. From the figure, it is clear that CM predictions are not in agreement with the experimental secondary relaxations which underline that the secondary relaxations obtained in clofoctol are non JG-relaxation.

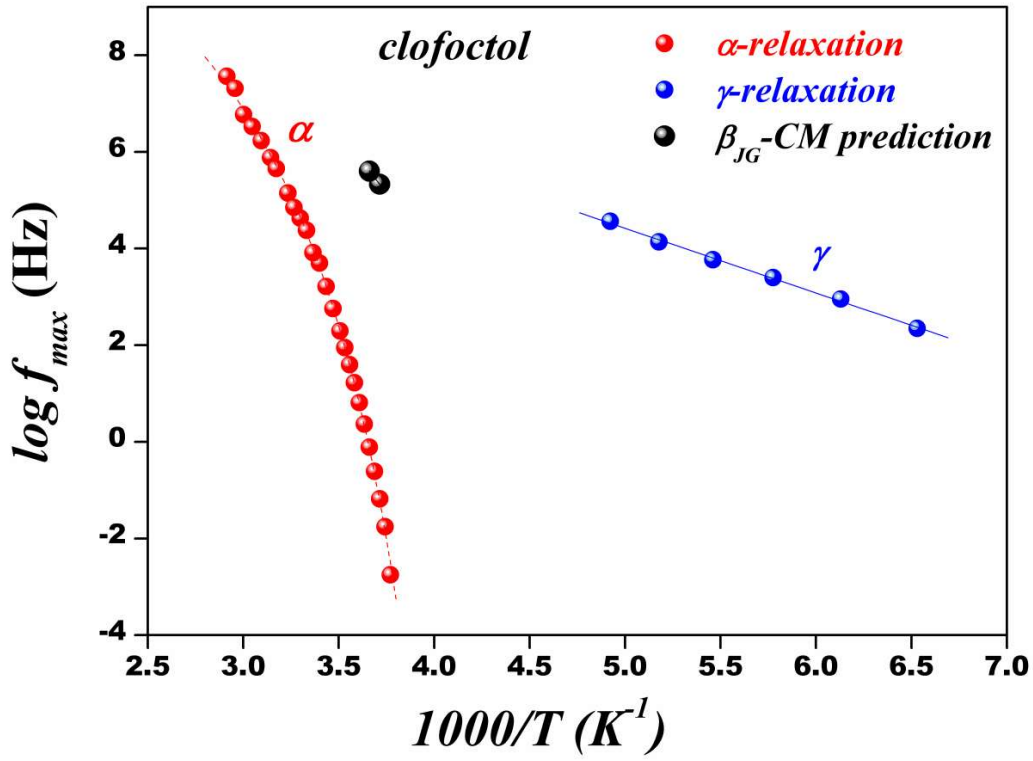

Figure 5.14. . Relaxation map : Red circles denote α-relaxation, blue circles for γ-relaxation and black circle indicate the CM prediction for JG β-relaxation. Dotted red line represents the VFT fit for α-relaxation and solid blue line represent the Arrhenius fit for γ-relaxation.

5.7. Isothermal crystallization kinetics

Isothermal cold crystallization kinetics of clofoctol was investigated for selected crystallization temperatures - 285.15K and 288.15K. The frequency range of each measurement was adjusted to measure the dielectric loss of structural relaxation at the particular temperature. A new amorphous sample was prepared for each measurement. The real and imaginary parts of dielectric permittivity with respect to frequency, recorded during isothermal crystallization at 285.15K and 288.15 K are presented in figure 5.15 and figure 5.16 respectively. From the figure, it is evident that the amplitude of structural relaxation loss peaks and the static dielectric permittivity notably decrease with time after an induction time of crystallization. Such remarkable change in dielectric strength $\Delta\varepsilon$ is a characteristic of the crystallization process. The isothermal crystallization kinetics is analyzed using Avrami and Avramov model.

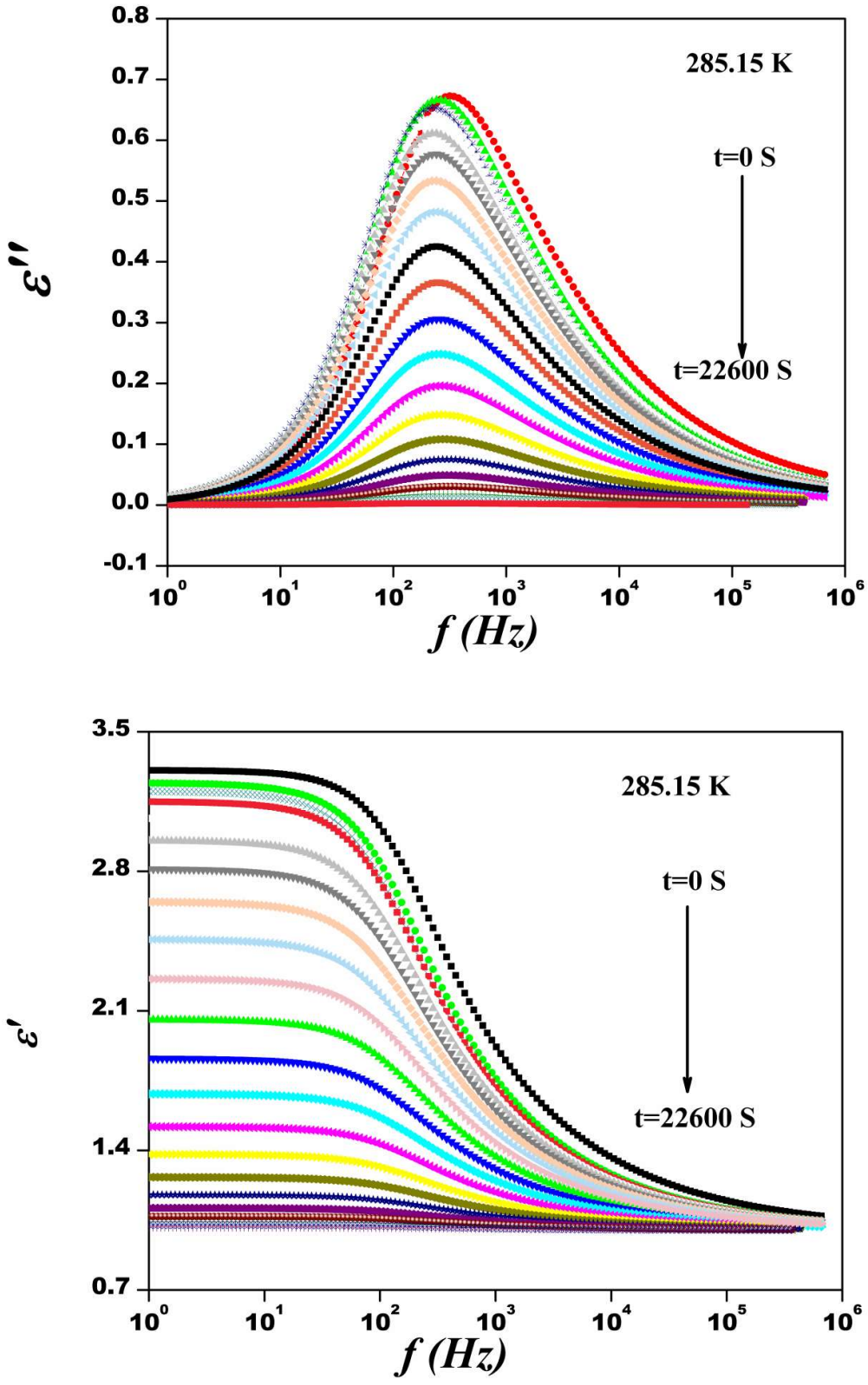

Figure 5.15. Imaginary and real part of dielectric spectra of clofoctol at crystallization temperature T = 285.15 K

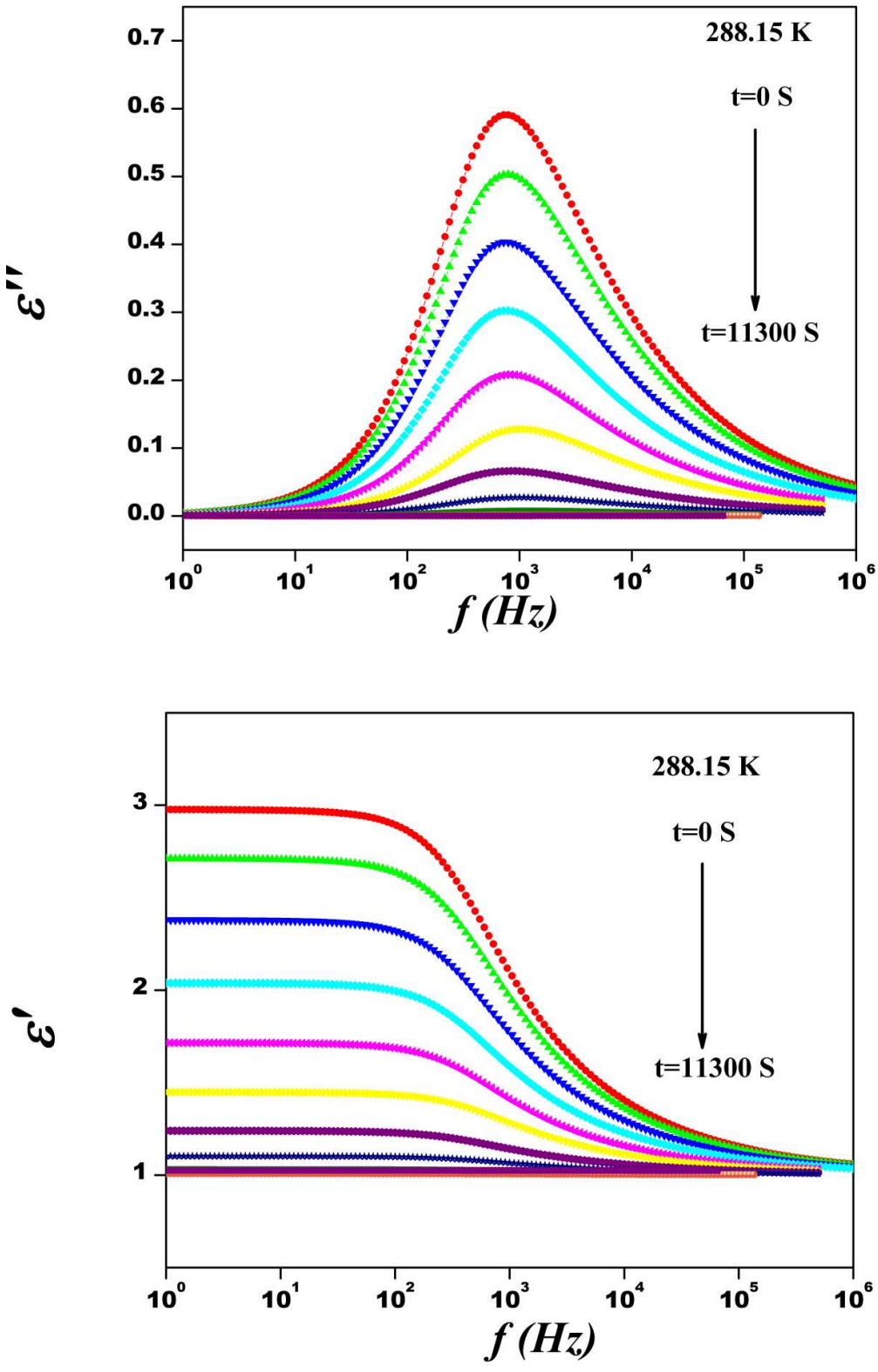

Figure 5.16. Imaginary and real part of dielectric spectra of clofoctol at crystallization temperature $T = 288.15$ K

5.7.1. Avrami model

According to the Avrami model, the time dependences of the crystallization rate to the nucleation and growth mechanisms can be explained in terms of the normalized real permittivity using the equation given in (2.14). The graph of ε_n' as a function of time during each crystallization temperature is plotted in figure 5.17. The graph follows a sigmoidal shape as the rate of transformation is low at the beginning and end while the transformation is fast in between it. The parameters obtained by fitting the Avrami equation (2.15) are given in table 5.2.

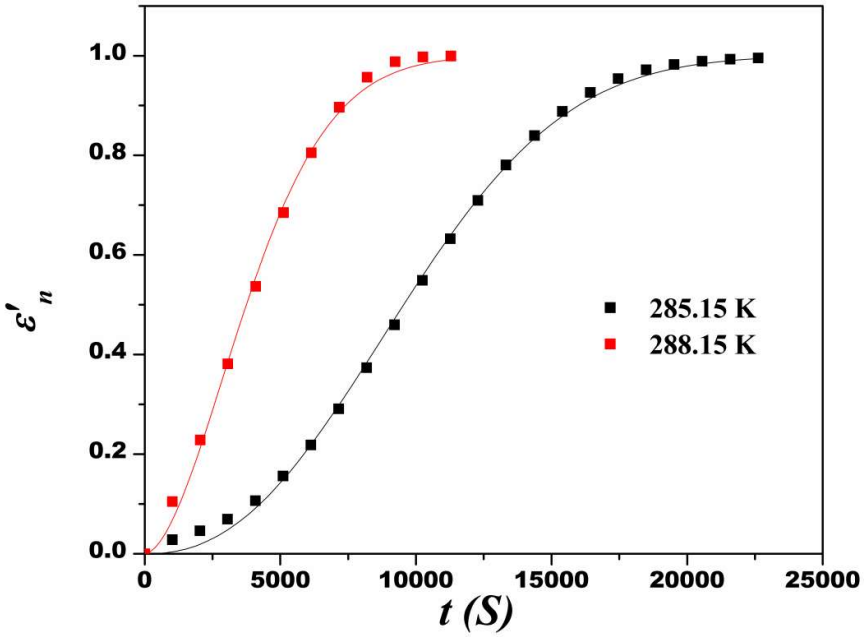

Figure 5.17. Time dependence of normalized real permittivity for crystallization temperatures 285.15 K and 288.15 K Solid line represents fits for Avrami equation.

The values of Avrami parameters are calculated from the Avrami plot, *log(-ln(1- ε_n'))* *vs. logt*. The value of *logK* and *n* are obtained from the intercept and slope of the plot. The isothermal crystallization times τ_{cr} graphically determined at *log(-ln(1-ε_n'))* = 0.

Table 5.2. Parameters calculated from Avrami model for clofoctol

	From Avrami equation fit			From Avrami plot, *log(-ln(1-ε_n')) vs. logt*		
Crystallization temperature [K]	*N*	*log(K*[S^{-n}]*)*	τ_{cr} [min]$_{= K^{-1/n}}$	*n*	*log(K*[S^{-n}]*)*	τ_{cr} [min]
285.15	2.33±0.06	-9.4±0.2	184	2.35±0.03	-9.5±0.10	183
288.15	1.76±0.07	-6.5±0.3	75	1.89±0.06	-6.9±0.21	76

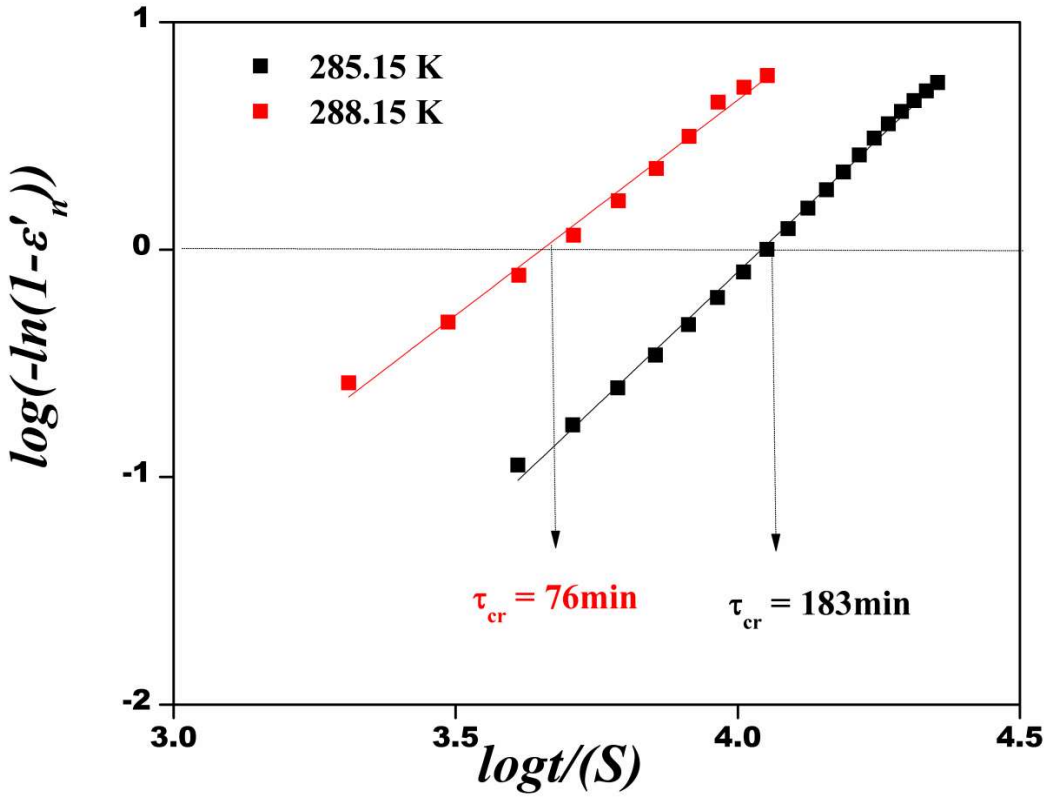

Figure 5.18. Avrami plots of clofoctol for each crystallization temperature.

The value of *n* and *logK* are recorded in table 5.2. The value of Avrami parameter *n* changes from 2.35 to 1.89 with increasing crystallization temperature. As the nucleation rate is changing with temperature, the nucleation processes considered to be continuous nucleation, which means that the rate of nucleation is monotonically increasing with time. The nucleation rate is determined by the number of critical nuclei present and the rate of jump of atoms across the interface from parent to the critical nuclei of the product phase. The important characteristic of continuous nucleation is that at $t = 0$ the number of nuclei of supercritical size will be zero. Moreover, the growth processes could be either diffusion controlled, or interface controlled depending on whether overall kinetics is being determined by diffusion or interface mobility.[135,140,141,162–166] It is observed that the crystallization rate constant increases with crystallization temperature, which in turn indicates that the process of crystallization is dominated by the diffusion of molecules and not by the nucleation of crystallites for which the temperature dependence of *K* is a decreasing function.[167] Also the crystallization time calculated from the Avrami parameters $\tau_{cr} = K^{-1/n}$ are in accordance with those determined graphically.

5.7.2. Avramov model

The isothermal crystallization kinetics is also analyzed using Avramov model of crystallization.[136] The graph of ε_n' as a function of time during each crystallization temperature is shown in figure 5.19. The fitting parameters for the Avramov equation (2.17) are given in table 5.3.

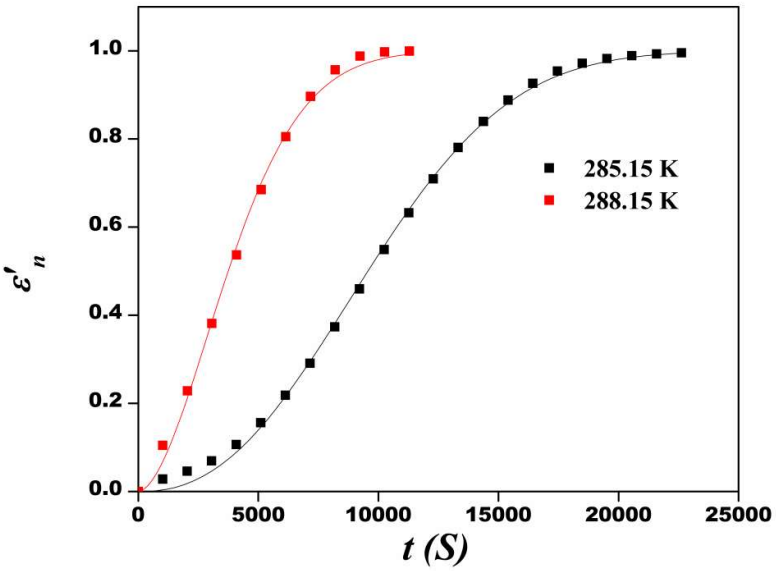

Figure 5.19. Time dependence of normalized real permittivity for crystallization temperatures 285.15 K and 288.15 K Solid line represents fits for Avramov equation.

The normalized real permittivity and its derivative with respect to *lnt* are plotted against *lnt*, which is known as Avrami-Avramov plot. The values of the parameters *n* and τ_{cr} can be calculated from this plot. The value of τ_{cr} can be estimated from $(\varepsilon_n')'_{max}$ whereas value of *n* is calculated using the equation (2.20). It has to be noted that from equation (2.19), $\varepsilon_n'(\tau_{cr}) = 0.63$. But usually we obtain the value of $\varepsilon_n'(\tau_{cr})$ as less than 0.63 from the experimental values which means that the induction time t_0 is greater than zero. Although for clofoctol, from the figure 5.20, we obtain that at the inflection point, the value of $\varepsilon_n' \approx 0.63$, which is an indication of no induction time.[136] Thus for clofoctol, $t_0 = 0$.

Table 5.3. Parameters calculated from Avramov model for clofoctol

	From Avramov equation fit		From Avrami-Avramov plot	
Crystallization temperature [K]	*n*	τ_{cr} [min]	*n*	τ_{cr} [min] at $(\varepsilon_n')'_{max}$
285.15	2.36±0.04	186±1	2.42	186
288.15	1.76±0.06	77±1	1.81	76

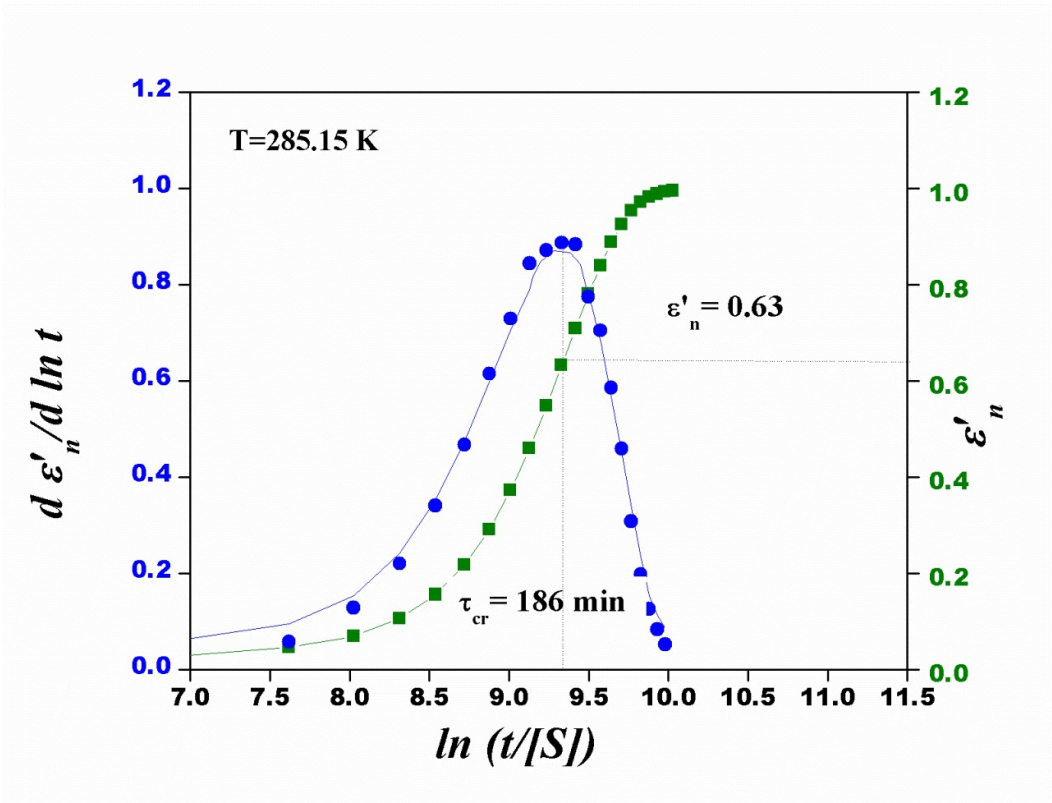

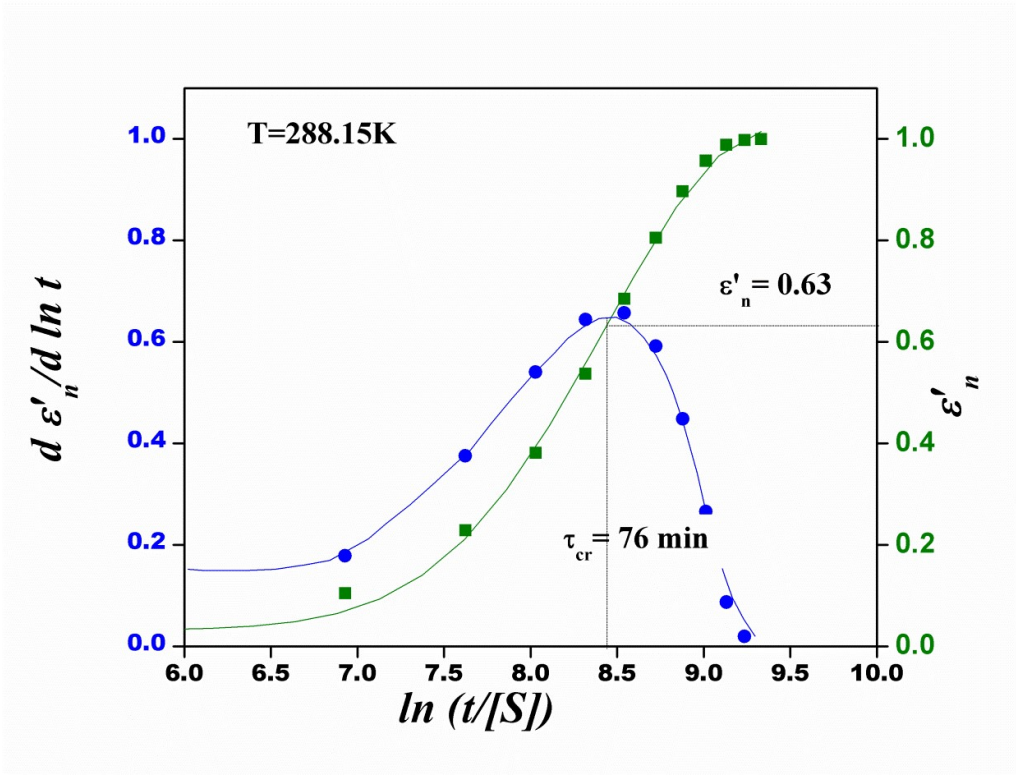

Figure 5.20. Avrami-Avramov plots for temperatures 285.15 K and 288.15 K : normalized real permittivity *vs. lnt* (green) and its first derivative with respect to *lnt* (blue).

According to the growth mechanism and nucleation, the Avrami exponent *n* should be an integer value. But the values of *n* reported in the literature varies ranging from 1.8 to 4[168]. For clofoctol, the value of *n* estimated from both Avrami and Avramov model is ≈ 2, can be attributed to homogeneous nucleation with two-dimensional growth.[168]

5.8. Conclusions

DSC study of clofoctol showed crystallization during reheating above T_g, indicating its poor glass forming ability.

It has been verified from the BDS experiments that the amorphous clofoctol prepared from the crystalline counterpart by quench cooling its melt is physically unstable and hence easily recrystallizes. The presence of conductivity was also observed for temperatures above T_g. Dielectric studies of clofoctol revealed two types of relaxation process, namely the structural α-relaxation and γ-relaxation. This γ-relaxation is revealed to be as non JG β-relaxation from the KWW fit of CM prediction. The α-relaxation shows non-Arrhenius behavior and the temperature dependence of this process was described by the VFT equation while γ-relaxation shows Arrhenius temperature dependence. The dynamic fragility index calculated from VFT fit for clofoctol is 95, which indicate the fragile nature of this drug. Isothermal crystallization studies of amorphous clofoctol were carried out for temperatures above T_g using dielectric measurements. The isothermal kinetics of clofoctol was studied using Avrami and Avramov model to extract the characteristics crystallization time, τ_{cr}. The value of *n* indicates homogeneous nucleation with two-dimensional crystal growth.

Chapter 6

Thermal, Spectroscopic Studies and Crystallization Kinetics of Droperidol

6.1. Introduction

Droperidol is an antidopaminergic drug and is used to produce tranquilization and to reduce postoperative nausea and vomiting in surgical and diagnostic procedures.[169] Droperidol reduced motor activity, anxiety, and causes sedation; also possesses adrenergic-blocking, antifibrillatory, antihistaminic, & anticonvulsive properties. According to Richards. J *et al.* droperidol produce a more rapid and better sedation than lorazepam in agitated patients requiring chemical restraint.[170] Droperidol has aqueous solubility of 0.0966 mg/mL and its logP is 3.93.

Droperidol chemically described as 1-{1-[4-(4-fluorophenyl)-4-oxobutyl]-1,2,3,6-tetrahydro-4-pyridyl}-1,3-dihydro-2H-benzimidazol-2-one] was purchased from Sigma Aldrich. The empirical formula of droperidol is $C_{22}H_{22}FN_3O_2$ and molecular weight is 379.42 g/mol. The chemical structure[171] is shown in figure 6.1. The sample was used as received without any further purification

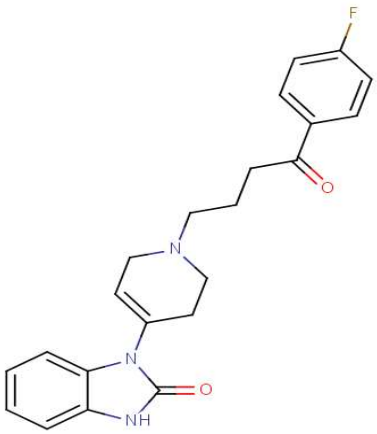

Figure 6.1. Chemical structure of droperidol

6.2. Powder X-Ray Diffraction (PXRD)

In order to verify the crystalline nature of droperidol, X-ray diffraction measurement was carried out. The sharp Bragg peaks show the crystalline nature of droperidol.

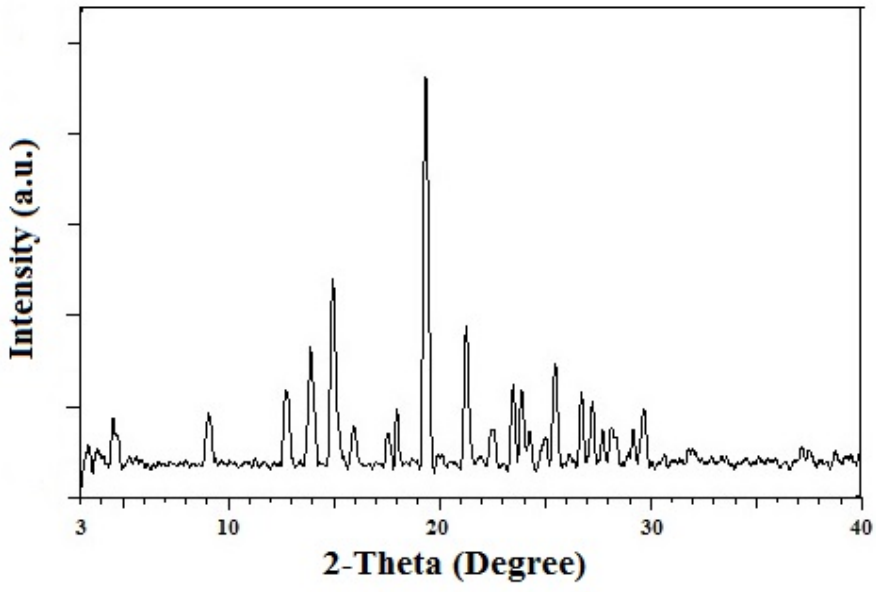

Figure 6.2. PXRD pattern of droperidol

6.3. Thermogravimetric Analysis (TGA)

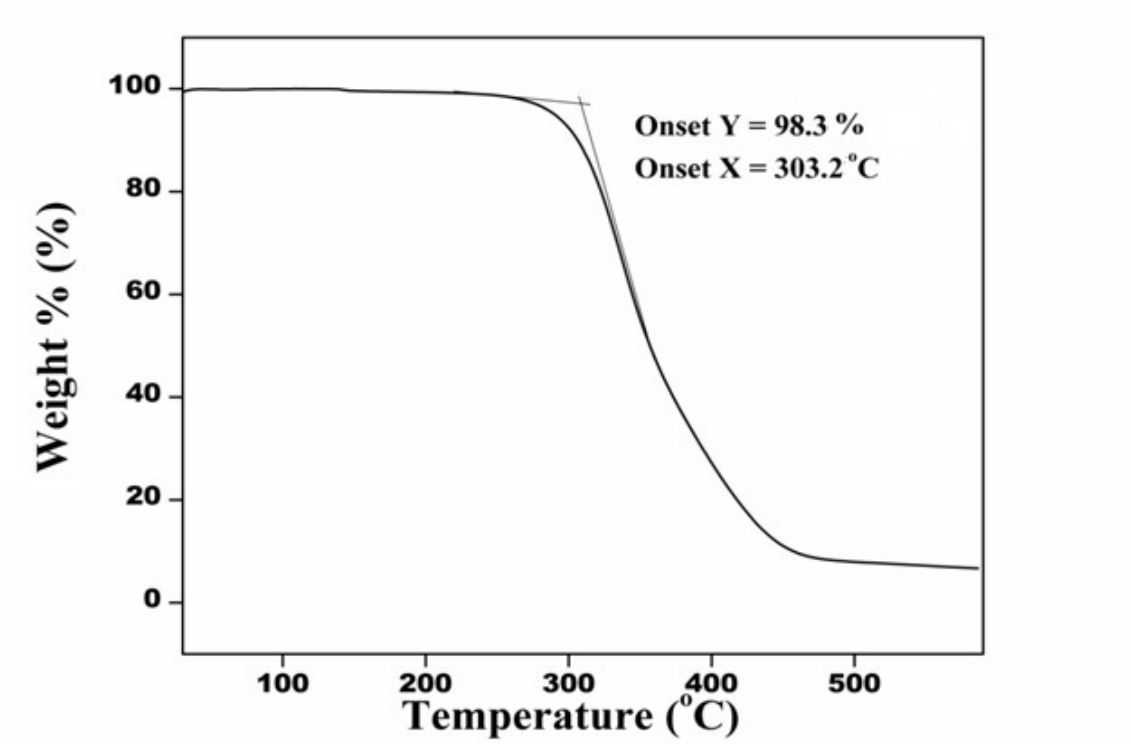

Figure 6.3. TGA thermogram of droperidol

The possibility of thermal degradation is investigated using thermogravimetric analysis and the onset of thermal degradation is obtained at temperature 303^0 C. Hence there will be no thermal degradation during BDS experiment.

6.4. Differential Scanning Calorimetry

From the DSC measurements, it was observed that droperidol crystallizes during reheating above T_g and thus belongs to class (II) molecules according to Baird *et al.* (2010).[14] The glass transition temperature, T_g of the amorphous sample was observed to be at 307.9 K and the melting point of crystalline droperidol was 422.4 K. Both these values are in agreement with the earlier report. The melting enthalpy was found to be 57.6 J/g.

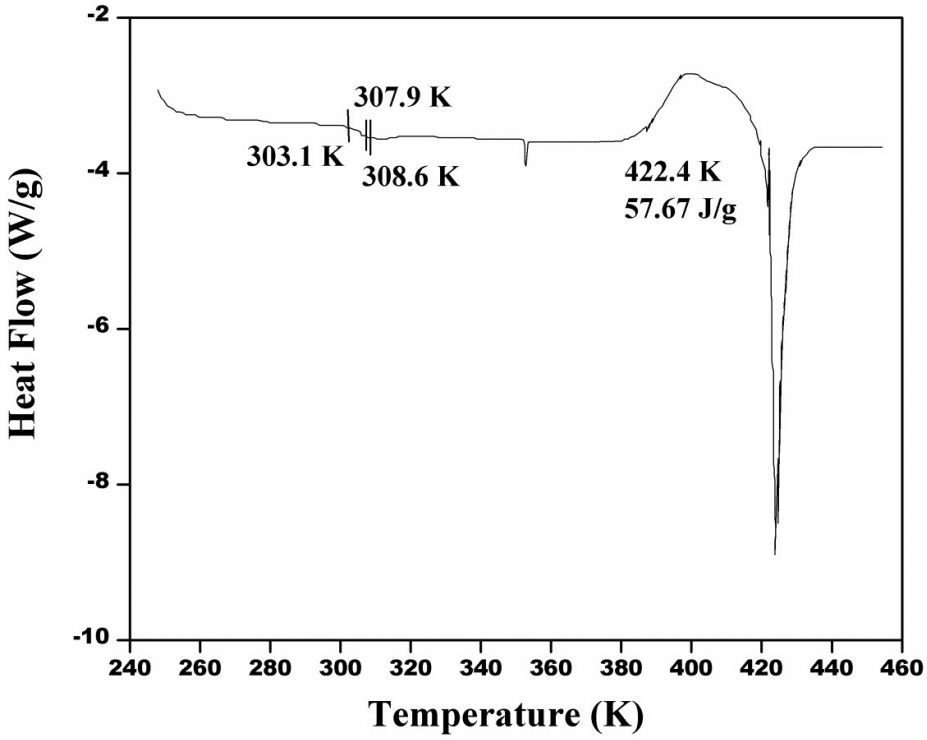

Figure 6.4. DSC thermogram of droperidol

6.5. Broadband Dielectric Spectroscopy

The dielectric measurements were carried out for temperatures ranging from 133.15 K to 339.15 K. Multiple relaxations were observed in droperidol. The typical α-relaxation was observed above T_g while two relaxations were observed below T_g. The dielectric loss spectra

of droperidol for temperatures above and below glass transition temperature are shown figure 6.5 and 6.6 respectively and the real part of dielectric spectra is shown in figure 6.7.

The rise of the signal at low frequencies is due to the presence of dc conductivity. The decrease in dielectric strength at high temperature side is due to the onset of crystallization. We were unable to get the dielectric spectra at higher temperatures beyond the onset of crystallization during heating. We overcome this issue up to a limit, by melting the samples and repeating the measurements during subsequent cooling. We had difficulty in measuring the loss peaks for frequencies higher than 10^5 Hz for droperidol due to the interference of crystallization even during cooling.

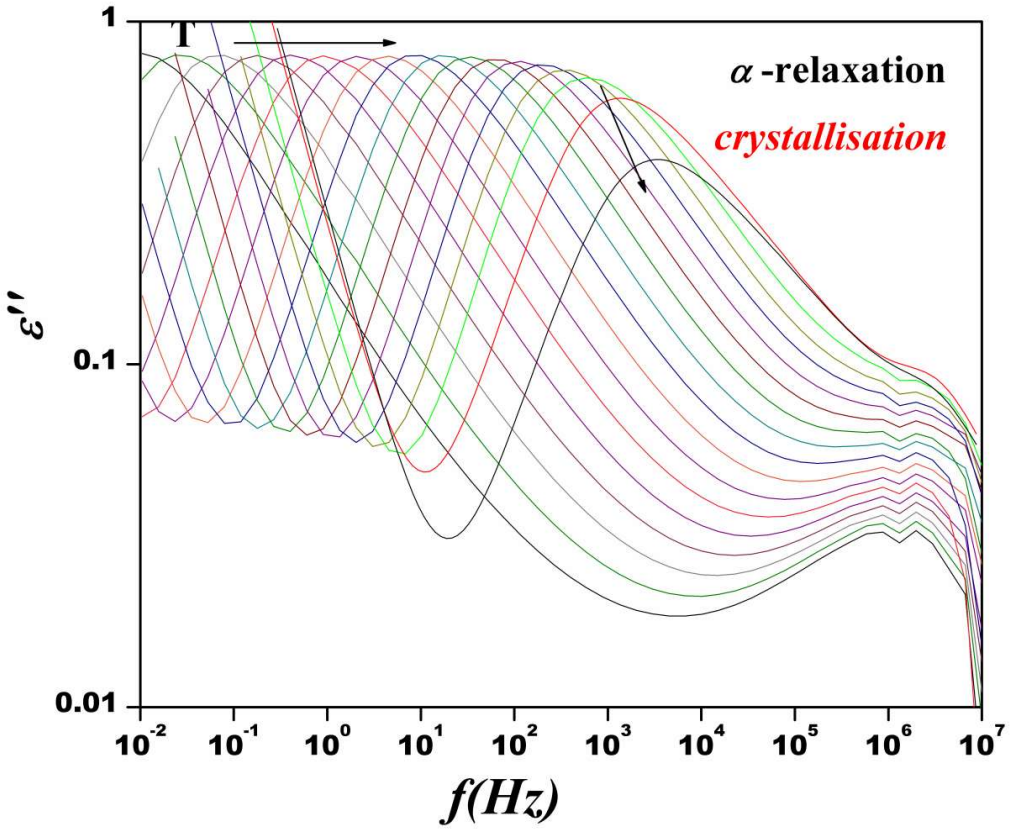

Figure 6.5. Dielectric loss spectra of droperidol for temperatures above T_g (303.15 K-333.15 K, ΔT=2K and 336.15 K-339.15 K, ΔT=3 K).

The real and imaginary parts of the dielectric susceptibility were further analyzed with non-linear curve fitting routine of Levenberg Marquadit algorithm using WINFIT software Version 3.2 provided by Novocontrol. The dielectric spectra were fitted using HN equation.

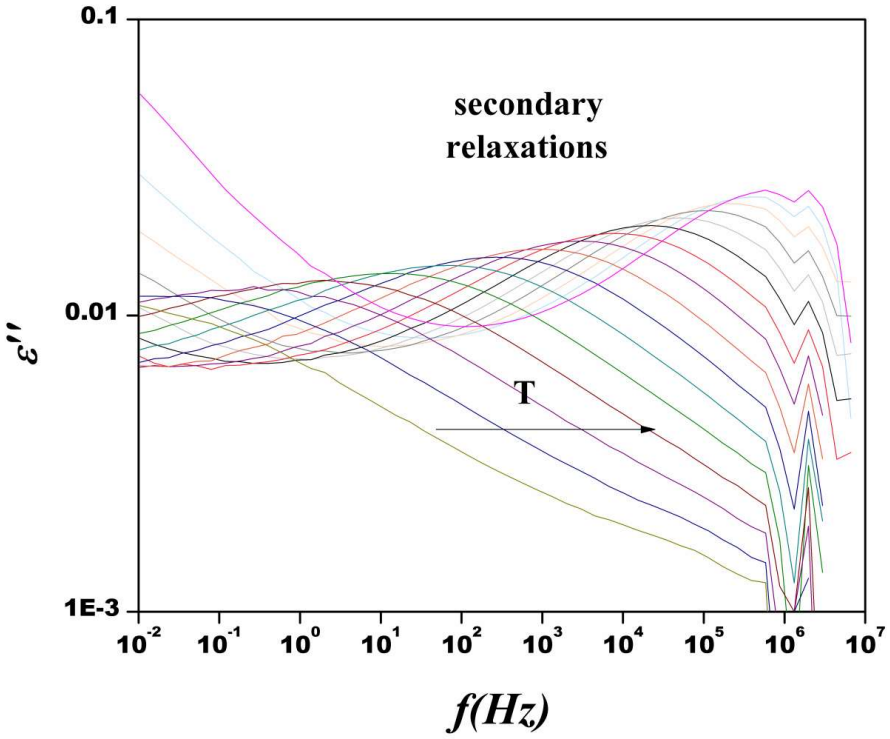

Figure 6.6. Dielectric loss spectra of droperidol for temperatures below T_g (283.15 K-133.15 K, ΔT=10 K)

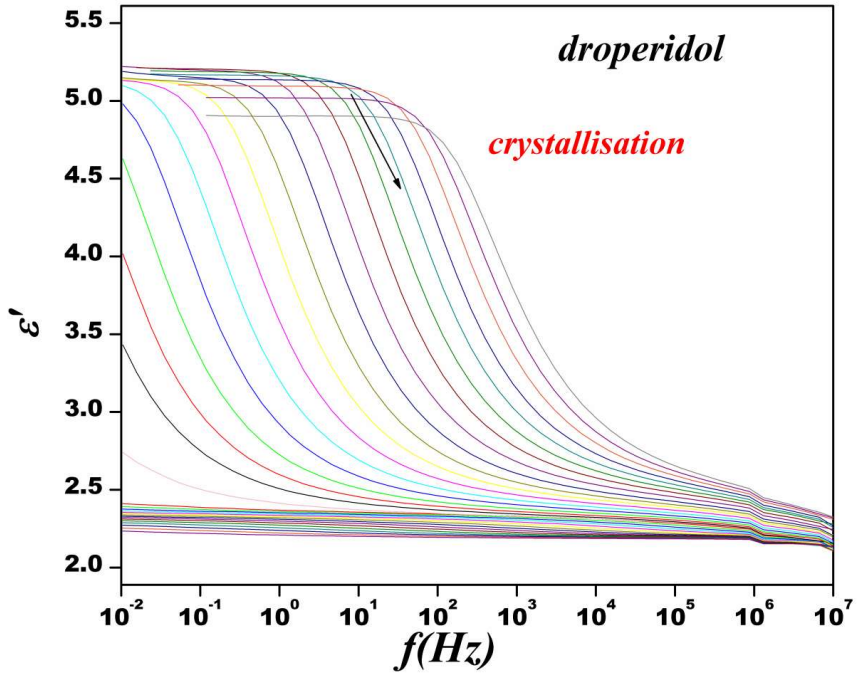

Figure 6.7. Real part of the complex permittivity for droperidol for various temperatures ranging from 339.15 K-133.15 K.

As like in the case of probucol and clofoctol, droperidol also obeys fractional Debye-Stokes-Einstein FDSE equation (4.2). The relation between dc conductivity and structural relaxation times is plotted in figure 6.8, which is a straight line. The value of the fractional exponent *s* is obtained as 0.93.

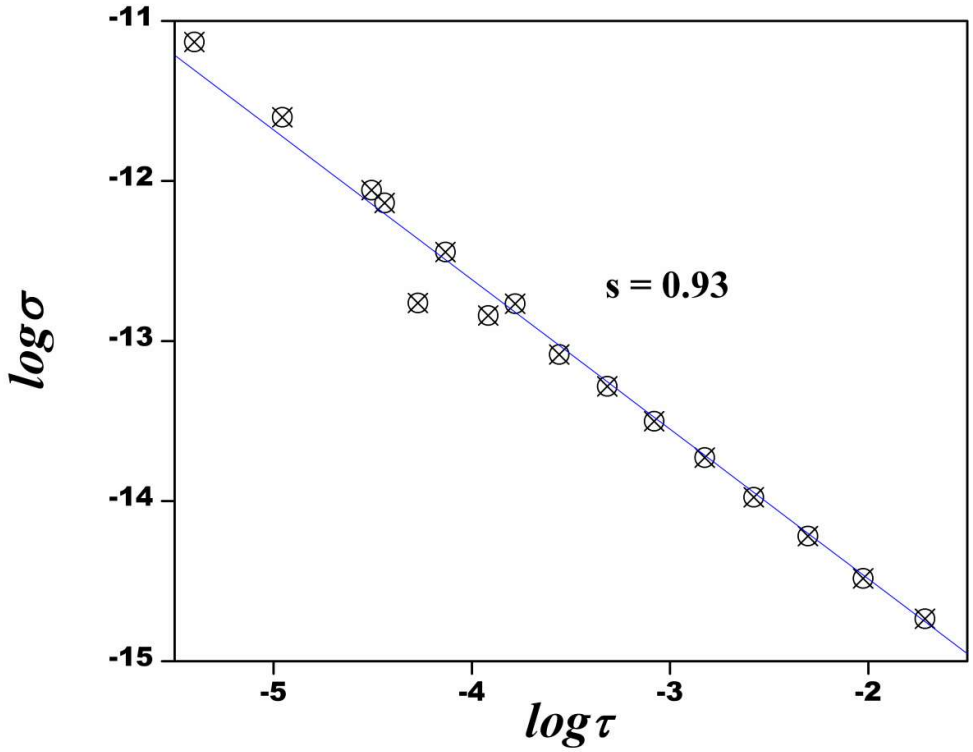

Figure 6.8. dc conductivity *vs.* structural relaxation time on a log-log scale.

6.5.1. The structural *α*-relaxation

This structural relaxation is due to the cooperative motion of molecules and becomes kinetically freezes on reaching T_g. The decrease in amplitude of dielectric spectra indicates crystallization. The dielectric spectra are fitted using HN equation and conductivity is subtracted from the fitted data to get a clear picture of the *α*-relaxation peaks. The HN fitted curves for temperature above T_g are shown in figure 6.9. The non-Arrhenius temperature dependence of structural relaxation process can be well described by the VFT equation. For droperidol, B = 1651.7, and T_g obtained from VFT fit is 300.8 K and the estimated value of T_0 is equal to 250.5 K. Thus to achieve better shelf life, amorphous droperidol should be kept at a temperature below 250.5 K. The activation energy of *α*-process is estimated as E_α = 13.7 kJ/mol. The values of VFT parameters are tabulated in table 6.1.

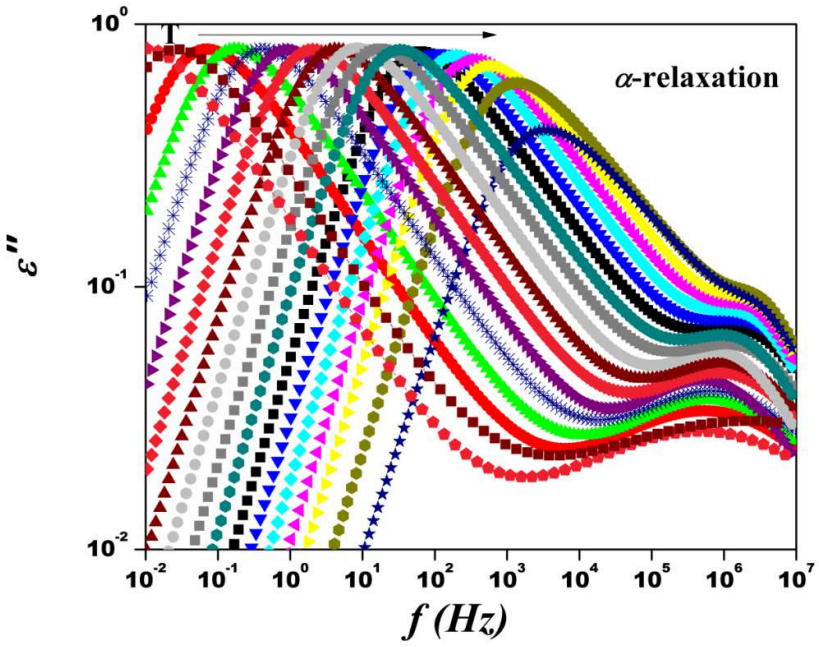

Figure 6.9. HN fitted curves for the dielectric loss spectra of droperidol for temperatures above T_g (303.15 K-333.15 K, ΔT=2K and 336.15 K-339.15 K, ΔT=3 K) after subtracting conductivity

The normalized plot (master plot) for various temperatures is shown in figure 6.10. From the figure, it is evident that all curves have coalesced into a single one, which in turn indicates the temperature independent nature of structural relaxation.

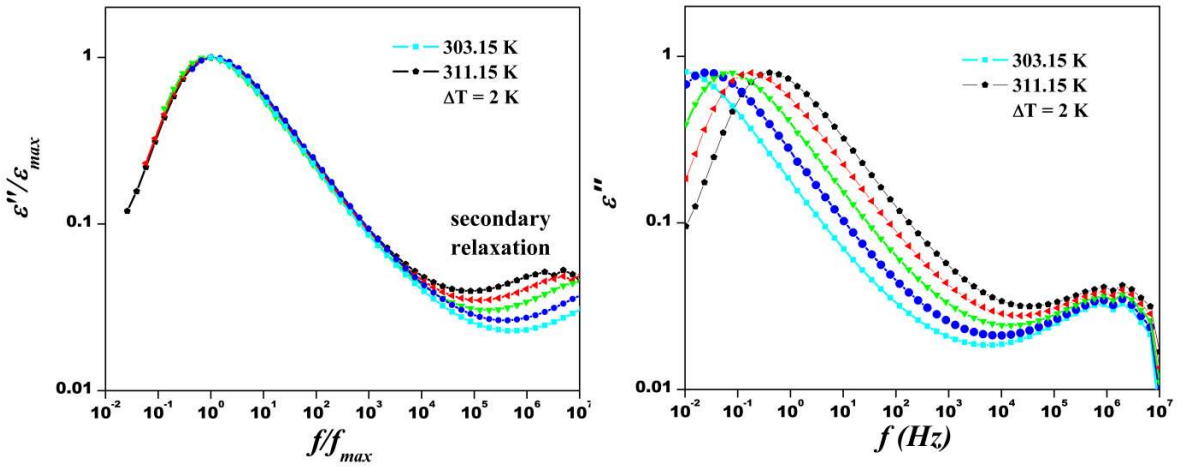

Figure 6.10. Master plot formed by overlapping the spectra between temperatures ranging from 303.15 K- 311.15 K. The plot on the right side picturise the same spectra before superposition.

6.5.2. Fragility

The fragility index represents the temperature sensitivity of the relaxation time of the primary process. Fragility index is a measure of rapidity with which ordering happens in the amorphous glassy phase. It represents the rate at which molecular motion is arrested when the amorphous glassy state is reached. The fragility index for droperidol is calculated as, m = 85, which means that droperidol is a fragile glass former. In earlier studies, the fragility index of droperidol reported to be 108 by Biard *et al.* (2010).[14] The Angell plot for droperidol is shown in figure 6.11.

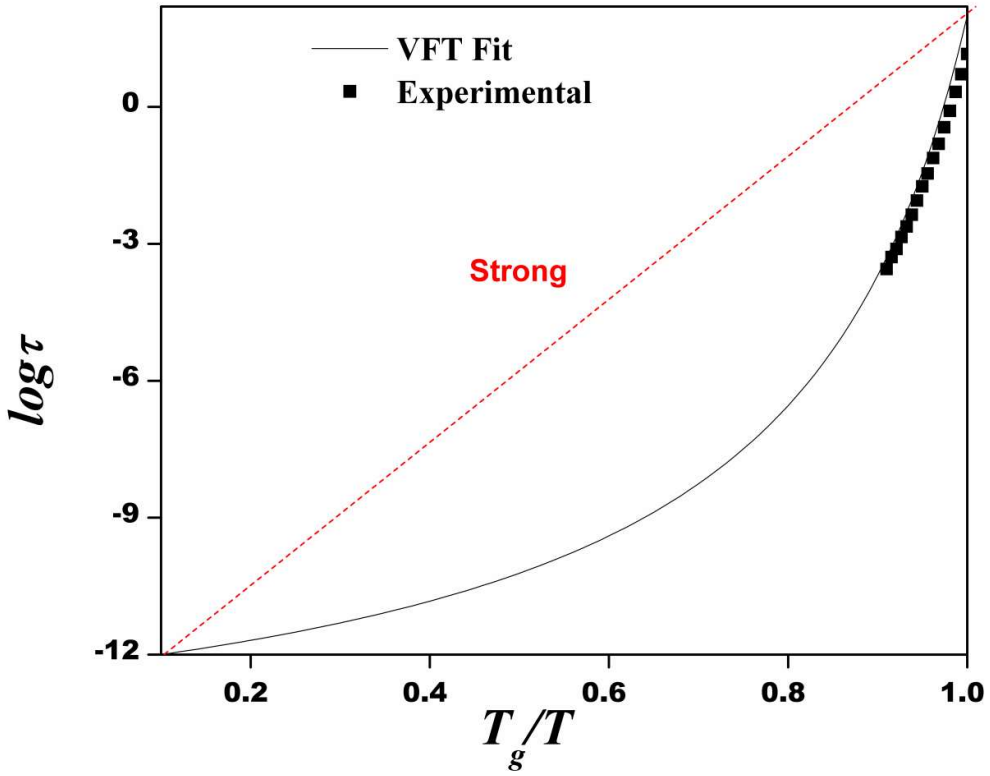

Figure 6.11. Angell plot, here the solid line represents the fitted data and the symbols represent experimental values.

6.5.3. The secondary relaxations

Two well resolved secondary relaxations were observed in the dielectric loss spectra of droperidol, below T_g. Arrhenius temperature dependence of secondary relaxation was verified using the equation (2.4). The activation energies for the two relaxations are calculated as

E_γ = 41.5 kJ/mol and E_δ = 11.6 kJ/mol. The HN fitted dielectric loss curves of droperidol for temperatures below T_g are shown in figure 6.12.

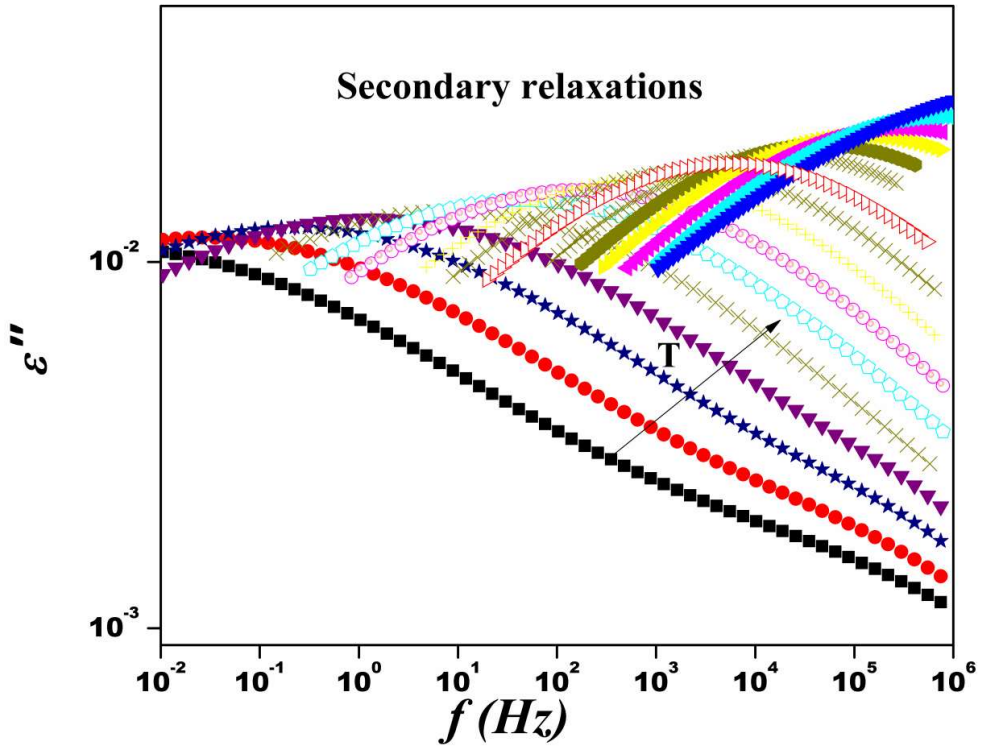

Figure 6.12. HN fitted curves for the dielectric loss spectra of droperidol for temperatures below T_g (283.15 K-133.15 K, ΔT=10 K)

Table 6.1. Fitting parameters for the VFT and Arrhenius equations of droperidol

α-process				γ and δ-process		
VFT				Arrhenius		
$logf_0$ (Hz)	B (K)	T_0 (K)	E_α (kJ/mol)	E_γ (kJ/mol)	E_δ(kJ/mol)	m
11.46	1651.7	250.5	13.7	41.5	11.6	85

6.6. Coupling Model Predictions

The dielectric loss spectra of the samples were fitted using the Fourier transform of the KWW function for the temperatures near to the T_g. In the case of droperidol, as shown in figure 6.13, the well resolved secondary relaxation was found which does not shift much with

the temperature. Also the calculated $logf_0$ is located three-four orders lower to the resolved secondary relaxation. Further, there is a clear deviation of the loss spectra around T_g from the fits of the α-relaxation process to the KWW fits, indicating that there could be an unresolved slower secondary relaxation process beneath the intense α-peaks. All these evidence points out that the resolved secondary relaxation is not the JG-relaxation. In addition to the above, there is another faster relaxation (δ-process) which was resolved at much lower temperatures.

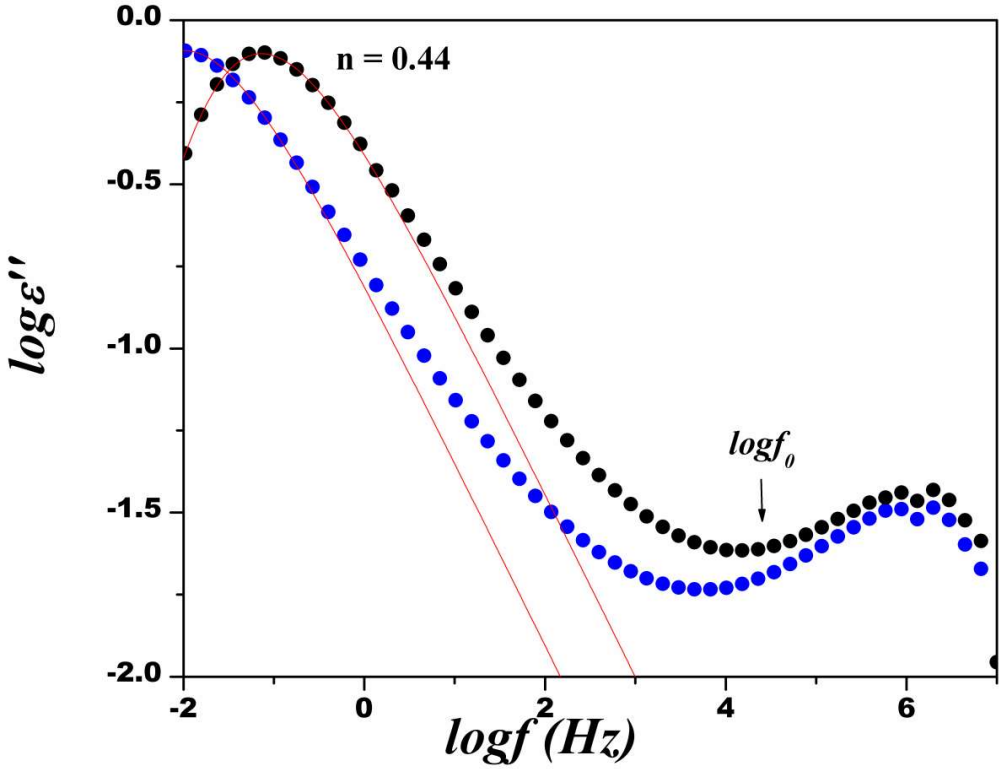

Figure 6.13. KWW fit of droperidol for temperatures 303.15 K and 307.15 K. The red line denotes the fitted data and the arrow indicates the position of the primitive relaxation frequency

The values of E_β/RT_g were calculated to check whether the ratio falls within a broad neighborhood about 24 as in the case of the majority of glass formers. But for droperidol, the small values of the ratios, E_γ/RT_g = 16.6 and E_δ/RT_g = 4.64 also indicates that none of the resolved secondary relaxations are JG.

The relaxation map of droperidol for all the relaxations are presented in the figure. 6.14. From the figure, it is clear that CM predictions are not in agreement with the experimental secondary relaxations which underline that both the secondary relaxations obtained in clofoctol are non JG-relaxation.

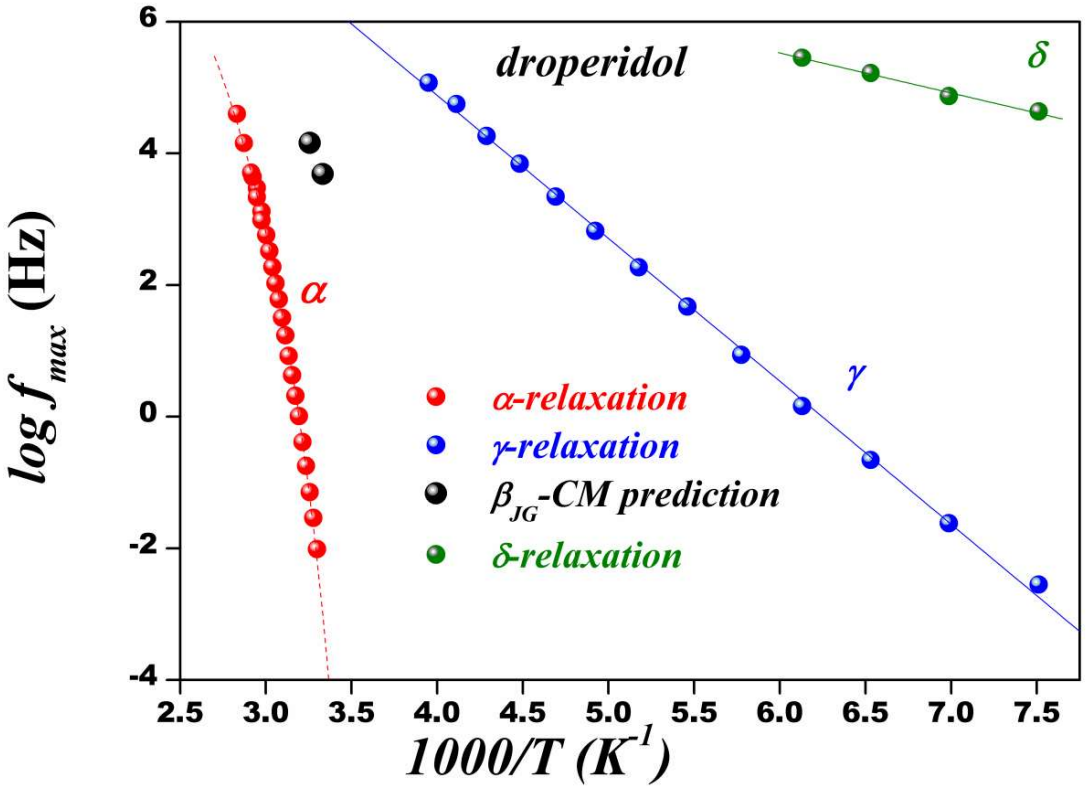

Figure 6.14. Relaxation map of droperidol. Red circles denote α-relaxation, blue circles for γ-relaxation, green circle for δ-relaxation and the black circle indicates the CM prediction for JG β-relaxation. Dotted red line represents the VFT fit for α-relaxation and solid blue and green line represents the Arrhenius fit for γ and δ-relaxations respectively.

In addition to the experimental investigations, we have pursued computational investigations of droperidol, using density functional theory calculation with the help of Gaussian 09 software. Here, we have checked the occurrence of intra-molecular secondary relaxations by incorporating all possible side-chain rotations about various dihedral angles. Among them, the rotation of droperidol shows a correlation with that of experimental results. The rotation around the oxygen atom labeled 3O of droperidol, as shown in figure 6.15. has comparable barrier opposing energy of 11.14 kJ/mol with an experimental activation energy 11.6 ± 0.05 kJ/mol for the δ-process.[155] The calculated value of activation energy may be slightly lower than that of observed experimental values since we considered only one single molecule for the simulation. Even though, the obtained results are quite comparable within a tolerance limit of few kJ/mol.[172]

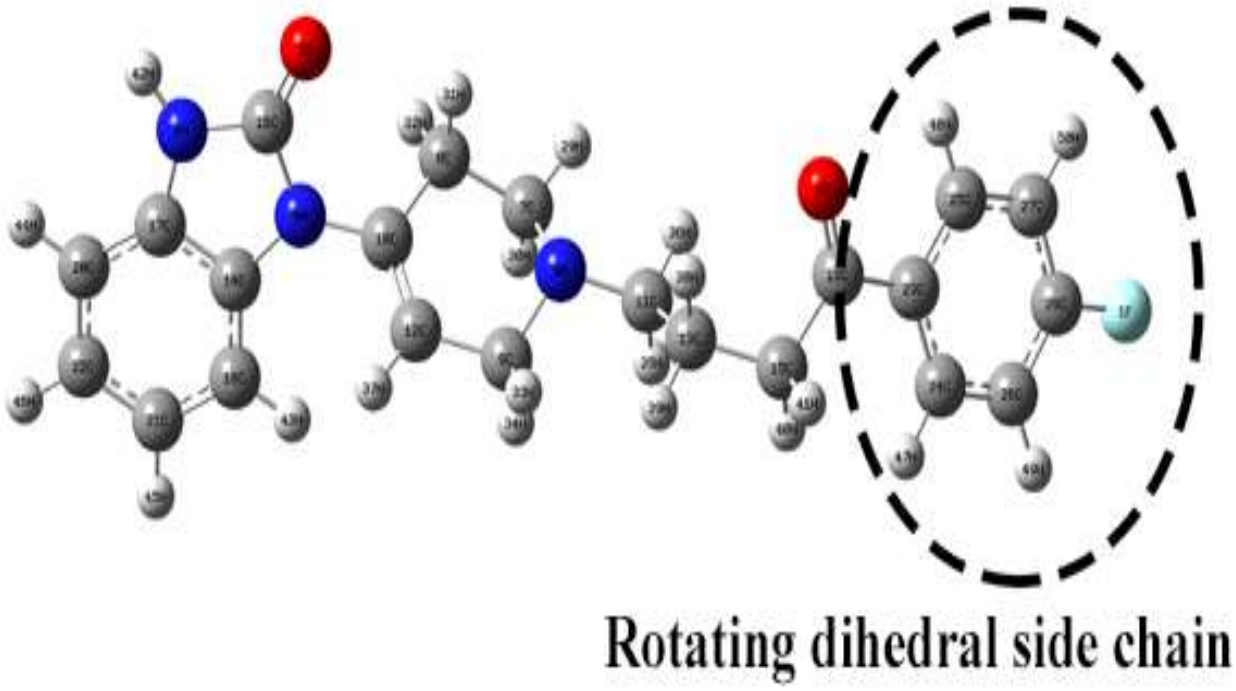

Figure 6.15. Atomic arrangement of the droperidol structure, the rotated group is marked.

6.7. Isothermal crystallization kinetics

Isothermal cold crystallization kinetics of droperidol was investigated for selected crystallization temperatures - 330.15 K and 333.15 K. The frequency range of each measurement was adjusted to measure the dielectric loss of structural relaxation at the particular temperature. A new amorphous sample was prepared for each measurement. The real and imaginary parts of dielectric permittivity with respect to frequency, recorded during isothermal crystallization at 330.15 K and 333.15 K are presented in figures 6.16 and 6.17 respectively. From the figure, it is evident that the amplitude of structural relaxation loss peaks and the static dielectric permittivity notably decrease with time after an induction time of crystallization. Such a remarkable change in dielectric strength $\Delta\varepsilon$ is a characteristic of the crystallization process. As the crystalline fractional volume increases, the number of reorienting dipoles which contributes to the structural relaxation decreases. The rise in the degree of crystallization can be analyzed using the normalized permittivity given by equation (2.14).

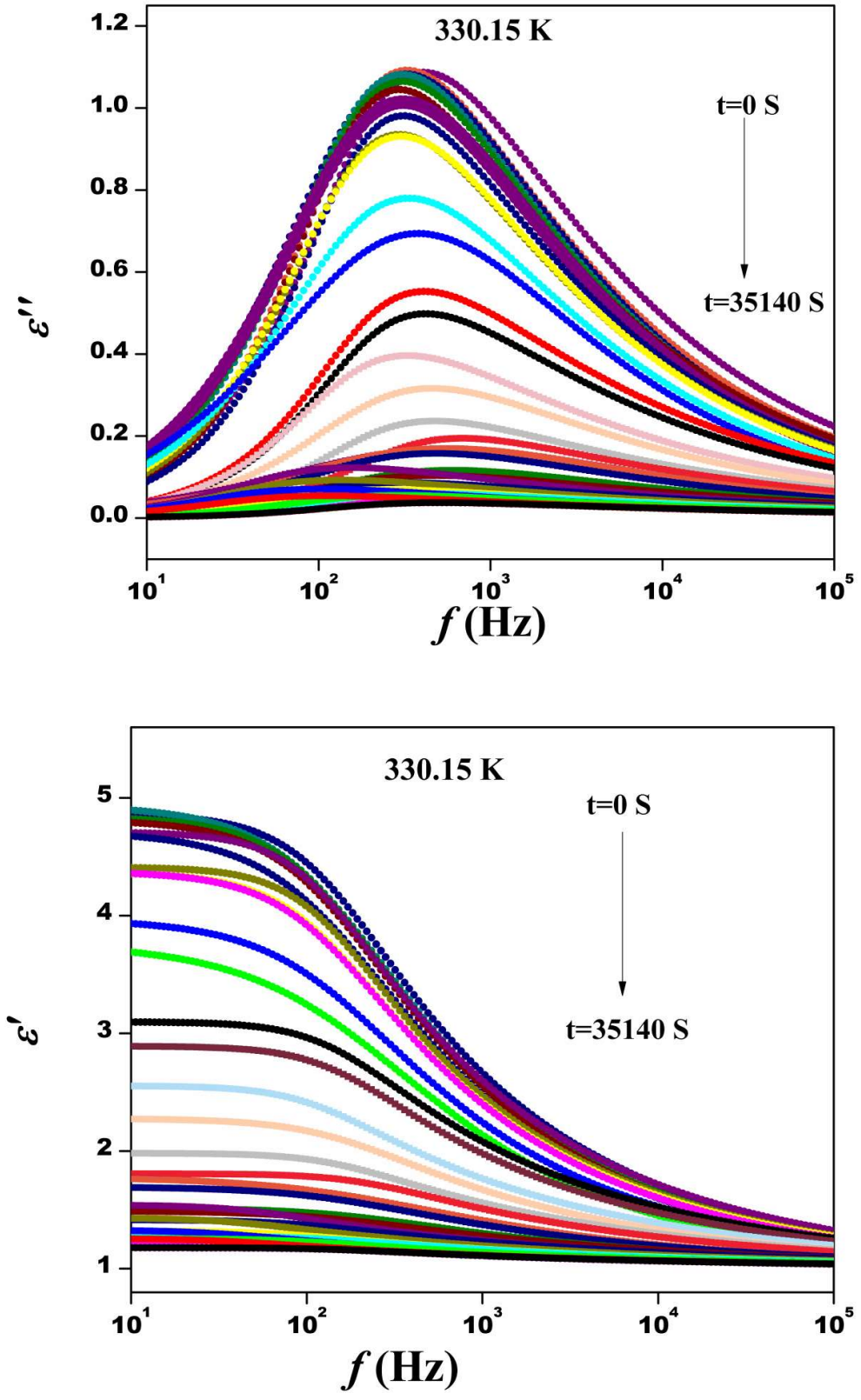

Figure 6.16. Imaginary and real part of dielectric spectra of droperidol at crystallization temperature $T = 330.15$ K

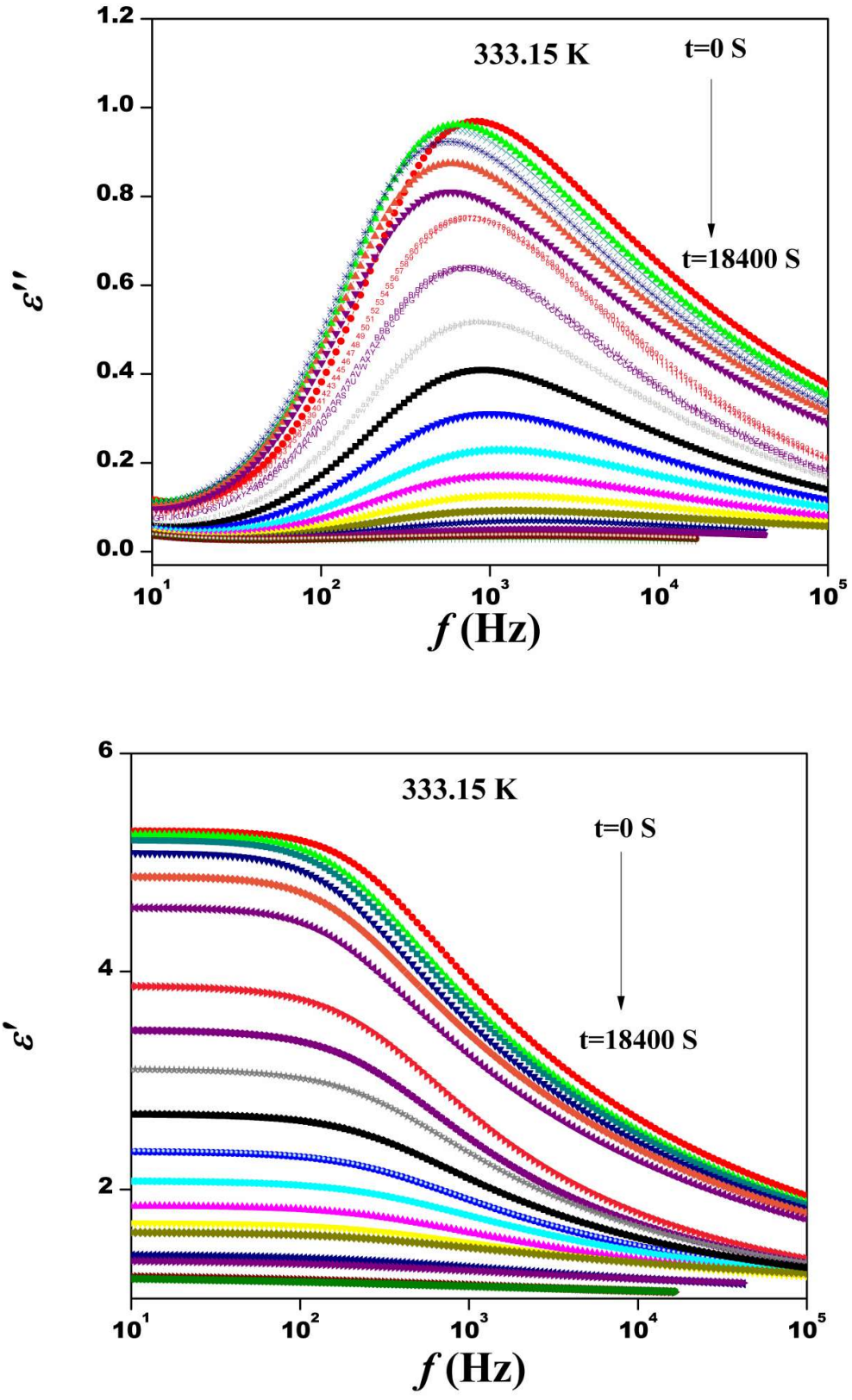

Figure 6.17. Imaginary and real part of dielectric spectra of droperidol at crystallization temperature T = 333.15 K

6.7.1. Avrami model

According to the Avrami model of isothermal crystallization, the time dependence of normalized permittivity often observed to follow a characteristic S-shaped, or sigmoidal profile. The graph of ε_n' as a function of time during each crystallization temperature is plotted in figure 6.18. The fitting parameters of the Avrami equation (2.15) are given in table 6.2.

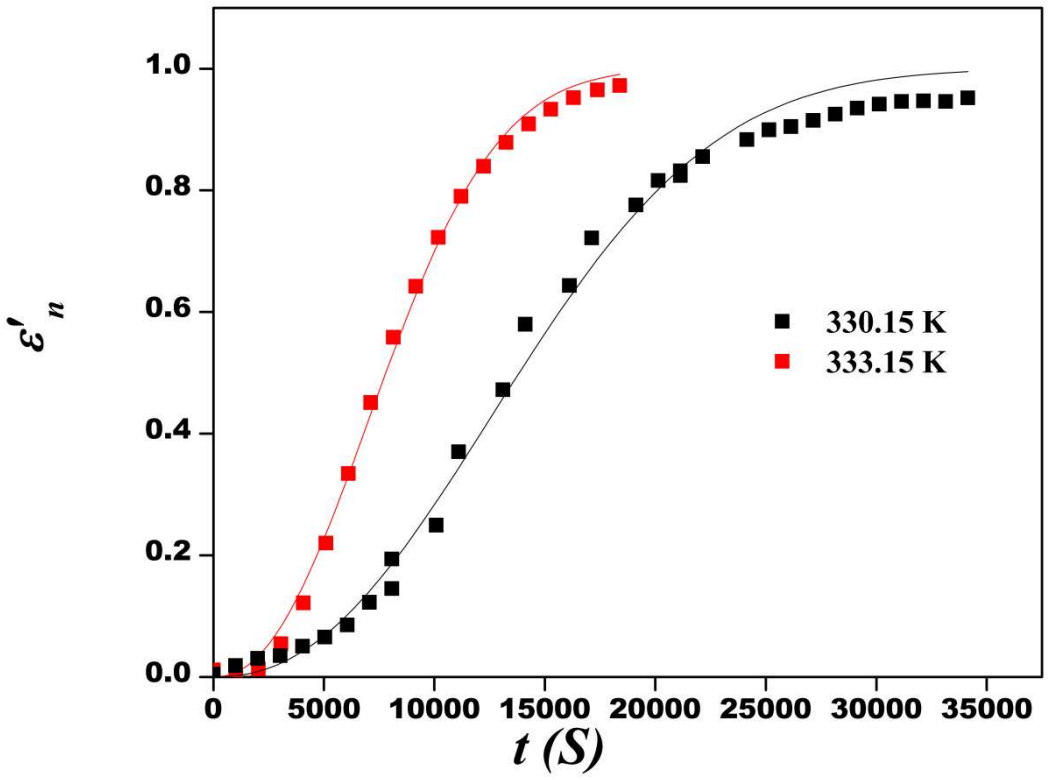

Figure 6.18. Time dependence of normalized real permittivity for crystallization temperatures 330.15 K and 333.15 K Solid line represents fits for Avrami equation.

The values of Avrami parameters are obtained from the supposed Avrami plot, *log(-ln(1- ε_n')) vs. logt* which is shown in figure 6.19. The dependence of *log (-ln (1- ε_n'))* on *logt* is linear and the value of *logK* and *n* can be obtained from intercept and slope. The isothermal crystallization times τ_{cr} graphically determined at *log(-ln(1-ε_n'))* = 0. The value of *n* and *logK* are recorded in table 6.2. The value of Avrami parameter *n* changes from 2.30 to 2.22 with increasing crystallization temperature.

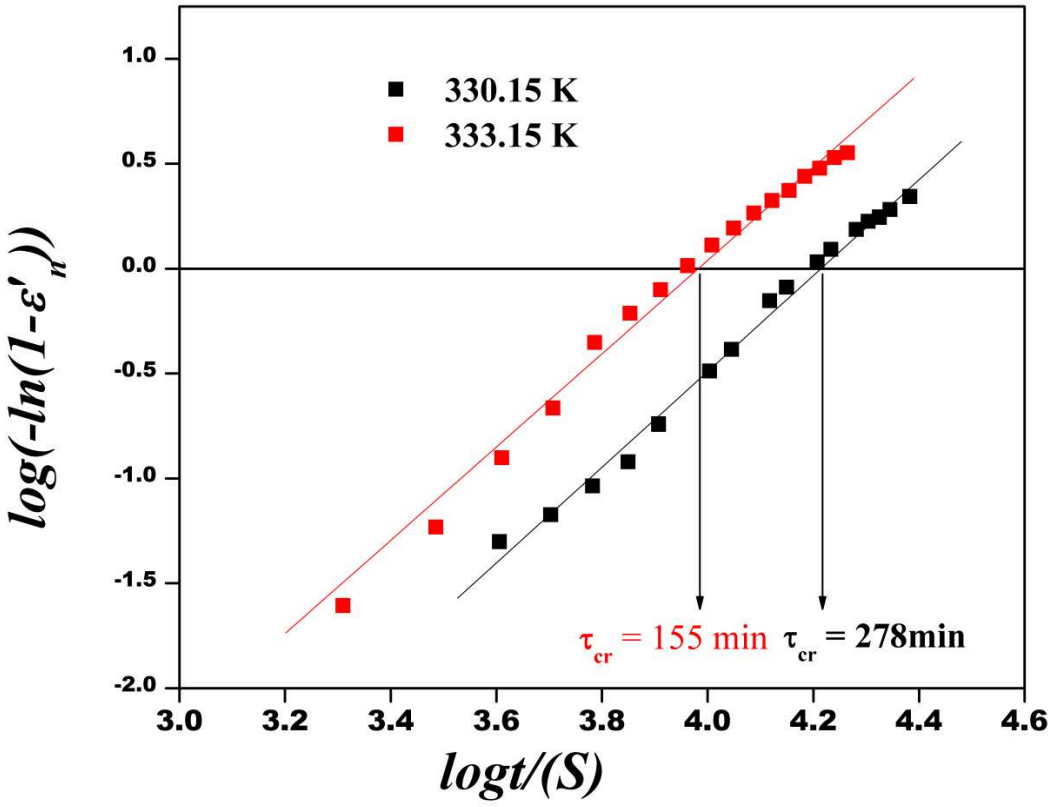

Figure 6.19. Avrami plots for each crystallization temperature.

Table 6.2. Parameters calculated from Avrami model for droperidol

	From Avrami equation fit			From Avrami plot, *log(-ln(1-ε'_n)) vs. logt*		
Crystallization temperature [K]	*n*	*log(K*[S^{-n}]*)*	τ_{cr} [min]$_{1/n}$ $_{= K^-}$	*n*	*log(K*[S^{-n}]*)*	τ_{cr} [min]
330.15	2.25±0.14	-9.5±0.3	281	2.30±0.05	-9.7±0.19	278
333.15	2.22±0.13	-8.8±0.4	152	2.22±0.05	-8.8±0.19	155

The value of Avrami exponent *n* should be an integer value according to the growth mechanism and nucleation. But in reported literatures *n* always shows non-integer values which may be due to factors such as secondary crystallization process, mixed nucleation modes, and the change in material density *etc.*[168] Also experimental factors such as error introduced in the determination of zero points of crystallization and the melting residence time can lead to non-integer values of *n*.[168,173]

6.7.2. Avramov model

The isothermal crystallization kinetics of droperidol is further analyzed using Avramov equation. Time dependence of normalized real permittivity for crystallization temperatures 285.15K and 288.15K are shown in figure 6.20. The fitting parameters for Avramov equation (2.17) are tabulated in table 6.3. For each crystallization temperature, the Avramov parameters can be determined from the Avrami-Avramov plot which pictures the dependence of the normalized real permittivity ε_n' with *lnt* and the first derivative of normalized real permittivity $d\varepsilon_n'/d(lnt)$ with *lnt*. The parameters obtained from Avrami-Avramov plot are recorded in table 6.3.

Table 6.3. Parameters calculated from Avramov model for droperidol

	From Avramov equation fit		From Avrami-Avramov plot	
Crystallization temperature [K]	N	τ_{cr} [min]	n	τ_{cr} [min] at $(\varepsilon_n')'_{max}$
330.15	2.31±0.07	272±3	2.63±0.04	277
333.15	2.21±0.06	154±2	2.06±0.03	155

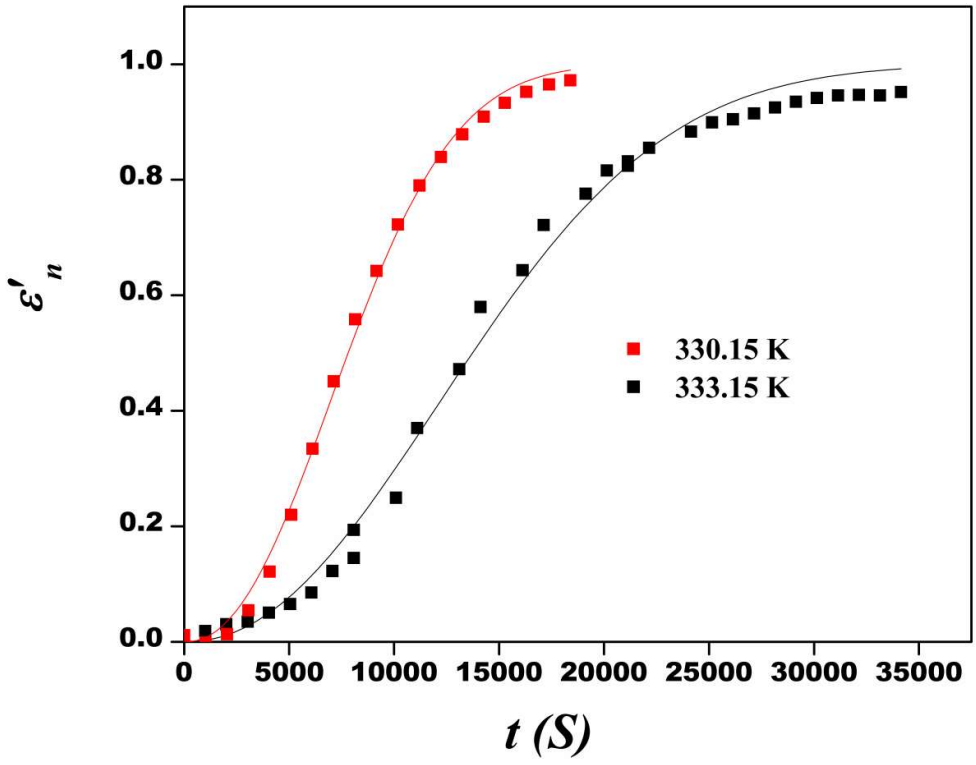

Figure 6.20. Time dependence of normalized real permittivity for crystallization temperatures 330.15 K and 333.15 K Solid line represents fits for Avramov equation.

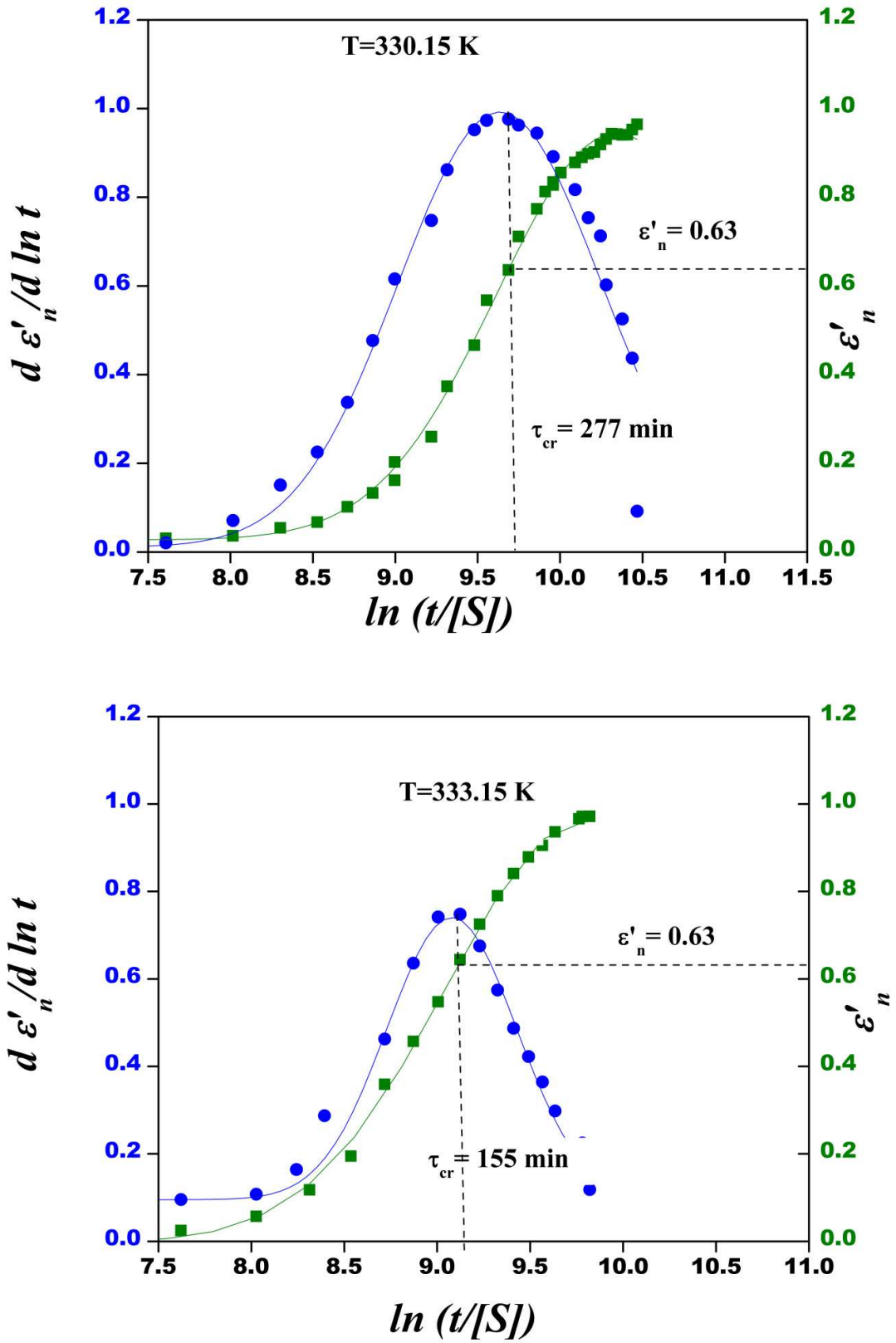

Figure 6.21. Avrami-Avramov plot for temperatures 330.15 K and 333.15 K: normalized real permittivity *vs. lnt* (green) and its first derivative with respect to *lnt* (blue).

From the figure 6.21, we obtain that at the inflection point the value of ε_n' is ≈ 0.63, which means that the induction time[136] is zero. Thus for droperidol, $t_0 = 0$. For droperidol, from both the models-Avrami and Avramov-the value of n is obtained as ≈ 2 which is attributed to homogeneous nucleation with two-dimensional growth.[168]

6.8. Conclusions

DSC study of droperidol showed crystallization during reheating above T_g indicating its poor glass forming ability.

It has been verified from the BDS experiments that the amorphous droperidol prepared from the crystalline counterpart by quench cooling its melt is physically unstable and hence easily recrystallizes. The presence of conductivity was also observed for temperatures above T_g. Dielectric studies of droperidol revealed three types of relaxation process, namely the structural α-relaxation and γ-relaxation and δ- relaxation. Both of the secondary relaxations are revealed to be as non JG β-relaxation from the KWW fit of CM prediction. The α-relaxation shows non-Arrhenius behavior and the temperature dependence of this process was described by the VFT equation while γ and δ-relaxation show Arrhenius temperature dependence. The dynamic fragility index calculated from VFT fit for droperidol is 85, which indicate the fragile nature of this drug. Isothermal crystallization studies of amorphous droperidol were carried out for temperatures above T_g using dielectric measurements. The isothermal kinetics of droperidol was studied using Avrami and Avramov model to extract the characteristics crystallization time, τ_{cr}. The value of n points that the nucleation in droperidol is homogeneous with two-dimensional growth.

Chapter 7

Test of Correlation between β_{KWW} and $\Delta\varepsilon(T_g)$, Stability Prediction using β_{KWW} and Fragility Comparison.

7.1. Test of correlation between β_{KWW} and $\Delta\varepsilon(T_g)$

The pharmaceuticals, chosen for study have significantly broader structural dispersion than the majority of the drugs investigated so far and thus we have carried out the anti-correlation study between the width of the structural loss peak at T_g to the polarity of the drugs [83,84] in the light of dipole-dipole interaction to the attractive part of the intermolecular potential. They are instrumental in testing the anti-correlation within the family of molecular pharmaceuticals as part of the totality of molecular glassformers studied by dielectric spectroscopy.

Paluch and co-workers[83] examined the characteristics of structural α-relaxation in practically all Van der Waals molecular glass-formers reported so far by dielectric spectroscopy. They found that the width of the dielectric loss peak at the glass transition temperature T_g is strongly anti-correlated with the polarity of the molecule. The larger the dielectric relaxation strength $\Delta\varepsilon(T_g)$ of the system, the narrower is the α-loss peak. The frequency dispersion of the α-relaxation is obtained by fitting the complex dielectric permittivity data $\varepsilon^*(f)$ by the Fourier transform of the KWW function. Thus, narrower the width of the α-loss peak, larger is the value of β_{KWW}. They explained this remarkable property via the correlation between $\Delta\varepsilon(T_g)$ and β_{KWW} by the contribution from the dipole-dipole interaction potential $V_{dd}(r) = -Dr^{-6}$ to the attractive part of the intermolecular potential, making the resultant potential more harmonic and the frequency dispersion of the α-relaxation narrower. The effect increases rapidly with the dipole moment μ and $\Delta\varepsilon(T_g)$ in view of the relation, $D \propto (\mu^4/kT_g) \propto kT_g[\Delta\varepsilon(T_g)]^2$. This trend is supported by molecular dynamics simulations of binary Lennard-Jones particles as model glass-formers[174]. Modifications of the repulsive part and/or the attractive part of the inter-particle potential resulted in different dynamic properties including non-exponentiality of the structural α-relaxation. The width of the frequency dispersion is a measure of the degrees of non-exponentiality and dynamic heterogeneity of the α-relaxation, and in turn the viscosity and

diffusion coefficient. Therefore the correlation found is not only of fundamental interest but also of practical applications.

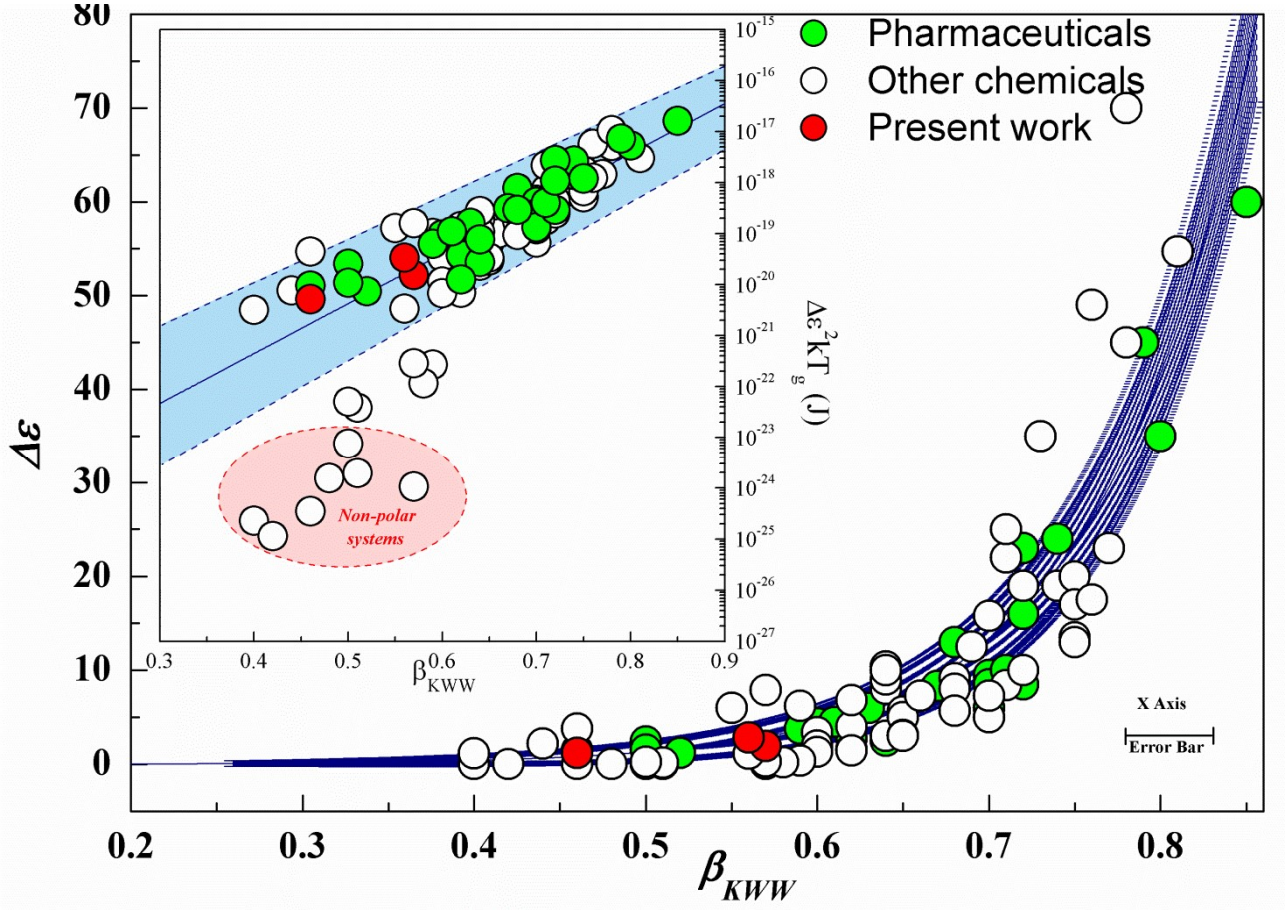

Figure 7.1. β_{Kww} *vs.* $\Delta\varepsilon(T_g)$. The inset pictures β_{Kww} *vs.* $kT_g[\Delta\varepsilon(T_g)]^2$

Among the 88 glass-formers considered by Paluch and co-workers, many are pharmaceuticals and were shown to conform well to the correlation. These pharmaceuticals are picked out in the original figures published in reference 83. by coloring them green in figure 7.1. Most of the pharmaceuticals studied by Paluch and coworkers[83] (green symbols) have larger values of β_{KWW} larger than 0.57. The exceptions are three, namely azithromycin (β_{KWW} = 0.52), itraconazol (β_{KWW} = 0.52), and posaconazone (β_{KWW} = 0.52). The three currently studied pharmaceutical, probucol, droperidol, and clofoctol, have values of β_{KWW} = 0.57, 0.56, and 0.46, respectively. On the lower end of the values of β_{KWW} of pharmaceuticals, these three new members afford a meaningful test of the correlation found by Paluch *et al.*

The data of $\Delta\varepsilon(T_g)$ and $kT_g[\Delta\varepsilon(T_g)]^2$ of the three are plotted against β_{KWW}, and shown by the circles colored red in figure 7.1 and the inset respectively. The results of the three (red) support well the correlation.[155]

7.2. Stability prediction using β_{KWW}

The value of β_{KWW} calculated from KWW function, provides the non-exponential character of the relaxation function in the time domain. In the frequency domain it represents the shape of the relaxation spectra. β_{KWW} = 1 gives symmetric and narrow relaxation. The knowledge of the distribution function also helps to predict the resistance of the amorphous state against the crystallization and chemical degradation. The correlation between the crystal nucleation rate and the KWW parameter has been put forward by Shamblin *et al.*[175] As per this correlation, the amorphous stability at various temperatures but having the similar relaxation time, decreases as the value of β_{KWW} decreases[175,176](Shamblin's criteria). As the value of β_{KWW} decreases, the asymmetric distribution of relaxation times becomes broader and stability would also decrease.

Comparison of the β_{KWW} obtained for the probucol, clofoctol, droperidol and other drugs was made to get some idea about the amorphous stability against crystallization [table. 7.1]. Clofoctol have the lowest value of β_{KWW}, hence the amorphous stability. However, it is reported that there are exceptions from this criteria and correlation between β_{KWW} and tendency to crystallization is not satisfied by all APIs.[82,127,177] For instance, acetaminophen, ezetimibe, sidenafil and celecoxib have the value of β_{KWW} as 0.79, 0.70, 0.68 and 0.67 respectively, indicating narrow structural relaxation spectra. But these pharmaceuticals easily recrystallize from their amorphous form.[177] It is reported that verapamil hydrochloride did not show any crystallization tendency during the measurement although its β_{KWW} = 0.61. Similarly, probucol also exhibits comparatively low value of β_{KWW} = 0.57, but did not show any tendency of crystallization during the experiment over the entire measured temperature range while droperidol with β_{KWW} = 0.56, showed crystallization during the experiment. Thus out of the three pharmaceuticals studied clofoctol and droperidol follow Shamblin's criteria whereas probucol did not obey Shamblin's criteria.

Table 7.1. The value of stretching parameter β_{KWW} o for different pharmaceuticals

Sl.No	**Pharmaceuticals**	β_{KWW}
1	Clofoctol (Present study)	0.46
2	Aspirin (Johari et al. 2007)[30]	0.465
3	Quinidine (Schamme et al. 2016)[127]	0.50
4	Ibuprofen (Bras et al. 2008)[52]	0.52
5	Azithromycin (Adrjanowicz et al. 2012)[59]	0.52
6	Droperidol (Present study)	0.56
7	Probucol (Present study)	0.57
8	Indomethacin (Carpentier et al. 2006)[178] (Wojnarowska et al. 2009)[57]	0.59
9	Telmisartan (Adrjanowicz et al. 2009)[152]	0.61
10	Verapamil hydrochloride (Adrjanowicz et al. 2010)[179]	0.61
11	Clarithromycin (Adrjanowicz et al. 2012)[59]	0.62
12	Roxithromycin (Adrjanowicz et al. 2012)[59]	0.62
13	Vitamin E (Kaminski et al. 2007)[180]	0.65
14	Tramadol hydrochloride (Kaminski et al. 2010)[123]	0.65
15	Celecoxib (Grzybowska et al. 2010)[79]	0.67
16	Sildenafil (Kolodziejczyk *et al.* 2013)[82]	0.68
17	Fenofibrate (Sailaja et al.)[64]	0.70
18	Tramadol monohydrate (Kaminski et al. 2010)[123]	0.70
19	Perphenazine (Sailaja et al.)[63]	0.70
20	Ezitimibe (Knapik et al. 2014)[181]	0.70
21	Ketoprofen (Sailaja et al.)[39]	0.71
22	Indapamide (Wojnarowska et al. 2013)[75]	0.72
23	Glibenclamide (Wojnarowska et al. 2011)[182]	0.74
24	Acetaminophen (Johari et al. 2005)[29]	0.79
25	Nonivamide (Wojnarowska et al. 2011)[183]	0.79
26	Nizatidine (Sailaja et al.)[63]	0.87

7.3. Fragility comparison

The concept of fragility is of great interest in areas such as amorphous drug formulation, food preservation *etc*. fragility is considered as an important factor as it correlates glass forming ability and physical stability of amorphous systems. As proposed by Angell glass formers are now classified by their degree of fragility *i.e.,* by their deviation from Arrhenius behavior. The fragility parameter, m is related to the average degree of molecular mobility reflected in structural relaxation near T_g.[184] In contrast to strong liquids, the molecular mobility of fragile glass formers varies rapidly near T_g. Because of this, strong liquids are considered to be more stable than fragile liquids.

Böhmer *et al.* put forward a linear empirical correlation between isobaric fragility and the stretched exponent β_{KWW} of KWW function given as

$$m = (250 \pm 30) - 320\,\beta_{KWW} \tag{7.1}$$

According to this relation, strong glass formers exhibits narrow relaxation peaks or larger values of β_{KWW} whereas fragile glass formers have broader structural relaxation peaks in the vicinity of T_g. Fragile glass formers are more susceptible to nucleation as faster modes of molecular motions within the spectrum of relaxation times can be responsible for nucleation in the glassy state.[184] However, there are a few materials that do not follow the correlation proposed by Böhmer *et al.* For clofoctol the calculated value of m using the equation (7.1) is 103 ± 30, for droperidol , it is estimated as 71 ± 30 and for probucol, m = 68 ± 30. Thus the three pharmaceuticals studied follow the empirical correlation between m and β_{KWW}, considering the error limit.

We have compared the fragility indices of some of the drugs already investigated by others using broadband dielectric spectroscopy and are given in table 7.2 and from that it is clear that most of the pharmaceuticals are fragile glass formers. The value of the fragility index of our pharmaceutical also indicates that they are fragile glass formers and hence not good glass formers. However, probucol does not show crystallization during DSC and also does not show any indication of crystallization on BDS experiment window, while clofoctol and droperidol showed a tendency of crystallization during both experiments. Thus probucol is comparatively a good glass former than the two others.

Table 7.2. Fragility indices of some pharmaceuticals

Sl. No	Name	Fragility	Reference
1	Nifedipine	33	Biard *et al.* J. Pharm. Sci. 2010[14]
2	Carbamazepine	55.3	K. Kawakami *et al.* J. Pharm. Sci. 2012[185]
3	Indomethacin	67	Natalia. T *et al.* Phar. Res. 2001[186]
4	Procane	69	Biard *et al.* J. Pharm. Sci. 2010[14]
5	Haloperidol	72.8	K. Kawakami *et al.* J. Pharm. Sci. 2012[185]
6	Ketoconazole	78	Biard *et al.* J. Pharm. Sci. 2010[14]
7	Acetaminophen	79.5	Deliang Zhou *et al.* J.Pharm.Sci. 2002[50]
8	Nimesulid	82	Knapik. J *et al.* Mol. Pharm. 2016[187]
9	Fenofibrate	83.4	Deliang Zhou *et al.* J.Pharm.Sci. 2002[50]
10	Captopril	84	Sailaja *et al.* IOSR J. Pharm. 2012[65]
11	Sildenafil	85	K. Kolodziejczyk *et al.* Mol. Pharm. 2013[82]
12	Droperidol	85	Present study
13	Quinidine	86	B. Schamme et al. J. Phy. Chem. 2016[127]
14	Ketoprofen	86.57	Sailaja *et al.* Euro. J. Pharm. Sci. 2013[39]
15	Probucol	87	Present study
16	Telmisartan	87	K. Adrjanowicz *et al. Eur. J. Pharm. Sci. 2009*[152]
17	Verapamil hydrochloride	88	K. Adrjanowicz *et al. J. Pharm. Sci.2010*[179]
18	Ibuprofen	93	Bras A. R *et al.* J. Phy. Chem. B 2008[52]
19	Clofoctol	95	Present study
20	Sucrose	95.3	Deliang Zhou *et al.* J.Pharm.Sci. 2002[50]
21	Tolbutamide	101	K. Kawakami *et al.* J. Pharm. Sci. 2012[185]
22	Ritonavir	107.3	Deliang Zhou *et al.* J.Pharm.Sci. 2002[50]
23	Celecoxib	110	Grzybowska *et al.* J. Phy. Chem. B 2010[79]
24	Flurbiprofen	113	A. C. Rodrigues *et al.* Mol. Pharm. 2014[55]
25	Azithromycin	117	K. Adrjanowicz *et al.*, Mol. Pharm. 2012[59]
26	Clarithromycin	118	”
27	ABT-229	119.4	Deliang Zhou *et al.* J.Pharm.Sci. 2002[50]
28	Roxithromycin	121	K. Adrjanowicz *et al.*, Mol. Pharm. 2012[59]

Chapter 8

Conclusions

8.1. Conclusions

Three pharmaceutically important drugs, namely probucol, clofoctol and droperidol were studied to get an idea about the glass forming abilities of these pharmaceuticals and also the molecular dynamics of these APIs were probed to study the molecular relaxations, crystallization tendency and stability of amorphous formulations.

Crystalline nature of the three pharmaceuticals was verified using Powder X-ray Diffraction and the existence of sharp Bragg peaks during the experiment proved the long-range order and the crystalline nature of the pharmaceuticals studied.

Thermal studies of the pharmaceuticals, namely probucol, clofoctol, droperidol were carried out using experimental techniques-Differential Scanning Calorimetry and Thermogravimetric Analysis. Glass transition temperature and the melting point of these samples were calculated using DSC.

Possibility of thermal degradation during heating was investigated using TGA to make sure that there will be no thermal degradation during BDS experiment. From the TGA thermograms, it is concluded that there is no thermal degradation during the temperature range studied using BDS.

From the DSC measurements, it is evident that probucol shows no crystallization during heating and cooling. The glass transition temperature, T_g of probucol was observed to be at 301.67 K. The melting peak of crystalline probucol appears at 400.44 K. Both these values are in close agreement with the earlier reports by Baird *et al.* The melting enthalpy is found to be 65.79 J/g. The sample as received is polymorphic Form I. DSC study of clofoctol and droperidol showed crystallization during reheating above T_g indicating its poor glass forming ability.

Dielectric measurements of the pharmaceuticals - probucol, clofoctol, droperidol were done using a Novocontrol Concept 40 broadband dielectric spectrometer in the frequency range of 10 mHz – 10 MHz. The temperature is controlled using dry nitrogen-flow in the Novocontrol Quatro cryosystem with temperature stability 0.1K. The sample to be measured is placed between the electrodes (made of stainless steel) of the capacitor. Width of the capacitor is 0.20mm and diameter is 30mm. Teflon with the width of 50 μm is used as spacer.

The sample is heated few degrees above the melting point and then fast cooling is carried out, which causes the vitrification of the sample. Dielectric spectra were measured isothermally, after stabilizing the temperature Data analysis is carried out using WinFIT Version 3.2 program provided by Novocontrol.

Based on the investigation of the molecular dynamics of the three glass forming APIs in the supercooled and glassy state using broadband dielectric spectroscopy, we are summarizing the important results.

DC conductivity is present at lower frequencies. The dielectric spectra are analyzed using Havriliak–Negami equation. Probucol, shows no signs of crystallization over the measured temperature ranges. Two types of relaxations are observed in the dielectric spectra, namely α-relaxation and β-relaxation. Clofoctol shows cooperative α-relaxation above T_g and γ- relaxation below T_g whereas Droperidol shows cooperative α-relaxation above T_g and two secondary relaxations *i.e.,* γ- relaxation and δ-relaxation below T_g. The α-relaxation follows non-Arrhenius behavior described by the Vogel-Fulchers-Tammanns equation and secondary relaxations shows Arrhenius temperature dependence. The values of T_g, m, T_0 are evaluated from the VFT fit.

Fragility of probucol is obtained as 87, for clofoctol, m = 95 and for droperidol the value of m is obtained as 85. Thus all the three APIs are fragile glass former. From VFT fit the value of T_0 is estimated which is often referred as the Kauzmann temperature, T_K, the hypothetical temperature at which the molecular motions cease. Storage of these APIs at a temperature lower than T_K provides better shelf life.

The β-relaxation in probucol is revealed to be as JG β-relaxation from the KWW fit of CM prediction. The observed secondary relaxation frequencies in clofoctol and droperidol are several orders of magnitude away from the predicted primitive relaxation frequency. Therefore these secondary relaxations are characterized as non JG relaxation originating from the intramolecular degrees of freedom.

Droperidol and clofoctol show crystallization while probucol doesn't show any signs crystallization during BDS experiment. For clofoctol crystallization begins at temperature 258.15 K and for droperidol, crystallization begins at temperature 330.15 K.

Isothermal crystallization kinetics of amorphous clofoctol were studied for crystallization temperatures-285.15 K and 288.15 K where isothermal crystallization kinetics of amorphous droperidol were studied for crystallization temperatures 330.15 K and 333.15 K. A new amorphous sample was prepared for each measurement. The complex dielectric permittivity was recorded throughout the crystallization process at specific interval of time.

Isothermal cold crystallization of clofoctol and droperidol is analyzed using Avrami and Avramov models. Both clofoctol and droperidol show evidence of homogeneous nucleation with two-dimensional crystal growth.

All the three samples studied showed very good correlation between the frequency dispersion of the α-relaxation (β_{KWW}) and the dielectric strength $\Delta\varepsilon(T_g)$ established in Van der Waals molecular glass formers explained in terms of dipole-dipole interaction potential to the attractive part of the intermolecular potential proposed by Paluch and co-workers.[83]

According to the Shamblin's criteria, as β_{KWW} decreases, the stability also decreases. But for our sample probucol, the value of β_{KWW} is 0.57, still did not show any tendency of crystallization during the experiment. For droperidol and clofoctol, the value of β_{KWW} is 0.56 and 0.46 respectively and they showed crystallization during experiments and are in accordance with Shamblin's criteria. Thus it is concluded that the value of the stretching parameter β_{KWW} cannot offer a meticulously reliable prediction about the amorphous stability of the systems.

8.2. Future plans

- Two of the samples studied are highly prone to crystallization. The stability can be enhanced by mixing with suitable apolar components. So we are planning to emphasize studies on methods to overcome crystallization and to improve the shelf life of pharmaceuticals. Binary route can give selective investigation of the probe dynamics to understand spectral shape dependence on different environments and comparing the results.
- We are planning to investigate the pharmaceuticals with biocompatible host systems using DSC to understand the binary phase diagram and stable composition of the drug in appropriate excipient to achieve longer shelf life. The study would be followed by solubility investigations to evaluate the bioavailability.
- We are planning to investigate more neat pharmaceutical systems of different physical and chemical properties, glass transition temperature, molecular complexity *etc*. using broadband dielectric spectroscopy to understand the physiochemical aspects of glass transition phenomena in pharmaceuticals using broadband dielectric spectroscopy and other experimental techniques live DSC, FTIR, XRD *etc*. We will investigate the different relaxation processes their properties, correlation with primary or structural relaxation.

- We can extend the experimental limits of our investigation. The frequency limit of our investigations is 10^{-2}Hz–10MHz. The high frequency limit can be extended to 100 GigaHertz by using impedance and network analyzers, in addition, the broadband dielectric spectrometer. This can give further information about the structural relaxation and secondary relaxations. The lower temperature limit is -150 °C. This can be extended to -190°C by making liquid nitrogen bath based cryosystem. In addition to these we are planning to explore some of the systems with elevated pressure experiments. High pressure investigations can give more light to the glass transition phenomena.
- We will devise techniques to apply these results in the future to understand and resolve issues in the areas of technological applications like designing of amorphous pharmaceuticals etc.

BIBLIOGRAPHY

1. Angell, C. A. Recent Developments in Fast Ion Transport in Glassy and Amorphous Materials. *Solid State Ionics* **18** & **19**, 72–88 (1986).

2. Zhang, B., Zhao, D. Q., Pan, M. X., Wang, W. H. & Greer, A. L. Amorphous Metallic Plastic. *Phys. Rev. Lett.* **94**, 205502 (2005).

3. Orita, M. Ohta, H.,Hirano, M., Narushima, S. & Hosono, H+. Amorphous transparent conductive oxide $InGaO_3$ (ZnO) m (m ≤ 4): a Zn4s Conductor. *Philos. Mag. B* **81,** 501–515 (2009).

4. Jansen, B. J. P., Rastogi, S., Meijer, H. E. H. & Lemstra, P. J. Rubber-Modified Glassy Amorphous Polymers Prepared via Chemically Induced Phase Separation . 4 . Comparison of Properties of Semi- and Full-IPNs , and Copolymers of Acrylate - Aliphatic Epoxy Systems. *Macromolecules* **32**, 6290–6297 (1999).

5. Eerdenbrugh, B. Van & Taylor, L. S. CrystEngComm An ab initio polymer selection methodology to prevent crystallization in amorphous solid dispersions by application of crystal engineering principles †. *Cryst. Growth Des.* **13**, 6171–6178 (2011).

6. Krause, B., Mettinkhof, R., Vegt, N. F. A. Van Der & Wessling, M. Microcellular Foaming of Amorphous High- T g Polymers Using Carbon Dioxide. *Macromolecules* **34**, 874–884 (2001).

7. Angell, C. A. Dynamic Processes in Ionic Glasses. *Chem. Rev.* **90**, 523–542 (1990).

8. Baranchugov, V., Markevich, E., Pollak, E., Salitra, G. & Aurbach, D. Amorphous silicon thin films as a high capacity anodes for Li-ion batteries in ionic liquid electrolytes. *Electrochem. commun.* **9**, 796–800 (2007).

9. Egami, T., Flanders, P. J. & Jr, C. D. G. Amorphous alloys as soft magnetic materials. *AIP Conf. Proc.* (1975). doi:10.1063/1.30243

10. Davis, E. A. & Mott, N. F. Conduction in non-crystalline systems V . Conductivity , optical absorption and photoconductivity in amorphous semiconductors. *Philos. Mag.* **22**, 903–922 (1970).

11. Hosono, H. Ionic amorphous oxide semiconductors : Material design , carrier transport and device application. *J. Non-Cryst. Solids* **352**, 851–858 (2006).

12. Amidon, G. L., Lennernäs, H., Shah, V. P. & Crison, J. R. A theoretical basis for a biopharmaceutic drug classification: the correlation of in vitro drug product dissolution and in vivo bioavailability. *Pharm Res.* **12**, 413–420 (1995).

13. Sachan, N. K., Bhattacharya, A., Pushkar, S. & Mishra, A. Biopharmaceutical classification system : A strategic tool for oral drug delivery technology. *Asian J. Pharm* 76–81 (2009). doi:10.4103/0973-8398.55042

14. Baird, J. A., Eerdenbrugh, B. V. A. N. & Taylor, L. S. A Classification System to Assess the Crystallization Tendency of Organic Molecules from Undercooled Melts. *J Pharm Sci* **99**, 3787–3806 (2010).

15. Kawabata, Y., Wada, K., Nakatani, M., Yamada, S. & Onoue, S. Formulation design for poorly water-soluble drugs based on biopharmaceutics classification system: Basic approaches and practical applications. *Int. J. Pharm.* **420**, 1–10 (2011).

16. Hu J, Johnston KP, W. R. Nanoparticle engineering processes for enhancing the dissolution rates of poorly water soluble drugs. *Drug Dev Ind Pharm* **30**, 233–245 (2004).

17. Costa P, S. L. J. Modeling and comparison of dissolution profiles. *Eur J Pharm Sci* **13**, 123–133 (2001).

18. Savjani, K. T., Gajjar, A. K. & Savjani, J. K. Drug Solubility : Importance and Enhancement Techniques. *ISRN Pharm.* 1–10 (2012). doi:10.5402/2012/195727

19. Hancock, B.C.; Parks, M. What is the True Solubility Advantage for Amorphous Pharmaceuticals? *Pharm. Res.* **17**, 397–404 (2000).

20. Vasconcelos, T.; Sarmento, B.; Costa, P. Solid dispersions as strategy to improve oral bioavailability of poor water soluble drugs. *Drug Discov. Today* **12**, 1068–1075 (2007).

21. Hancock, B. C. & Zografi, G. Characteristics and Significance of the Amorphous State in Pharmaceutical Systems. *J. Pharm. Sci.* **86**, 1–12 (1997).

22. Craig DQM, Royall PG, Kett VL, H. M. The relevance of the amorphous state to pharmaceutical dosage forms: glassy drugs and freeze dried systems. *Int J Pharm.* **179**, 179–207 (1999).

23. Yu, L. Amorphous pharmaceutical solids: Preparation, characterization and stabilization. *Adv. Drug Deliv. Rev.* **48**, 27–42 (2001).

24. Kaushal, A. M., Gupta, P. & Bansal, A. K. Amorphous Drug Delivery Systems: Molecular Aspects, Design, and Performance. *Crit. Rev. Ther. Drug Carrier Syst.* **21**, 133–193 (2004).

25. C. Bhugra & M. J. Pikal. Role of thermodynamic, molecular, and kinetic factors in crystallization from the amorphous state. *J. Pharm Sci* **97,** 1329–1350 (2008).

26. Sun, Y., Zhu. L., Wu, T., Cai. T., Gunn. E. M & Yu. L. Stability of Amorphous pharmaceutical solids: Crystal growth mechanisms and effect of polymer additives. *AAPS J.* **14,** 380–388 (2012).

27. Kothari, K., Ragoonanan, V. & Suryanarayanan, R. Influence of molecular mobility on the physical stability of amorphous pharmaceuticals in the supercooled and glassy states. *Mol. Pharm.* **11**, 3048–3055 (2014).

28. V. Caron, C. Bhugra, M. J. P. Prediction of onset of crystallization in amorphous pharmaceutical systems: Phenobarbital, nifedipine/PVP, and phenobarbital/PVP. *J. Pharm. Sci.* **99**, 3887–900 (2010).

29. Johari, G. P., Kim, S. & Shanker, R. M. Dielectric studies of molecular motions in amorphous solid and ultraviscous acetaminophen. *J. Pharm. Sci.* **94**, 2207–2223 (2005).

30. Johari, G. P., Kim, S. & Shanker, R. M. Dielectric Relaxation and Crystallization of Ultraviscous Melt and Glassy States of Aspirin, Ibuprofen, Progesterone, and Quinidine. *J Pharm Sci* **96**, 1159–1175 (2007).

31. Pan, X. H.,Julian, T. & Augsburger, L. Increasing the dissolution rate of a low-solubility drug through a crystalline-amorphous transition: A case study with indomethicin. *Drug Dev. Ind. Pharm.* **34**, 221–31 (2008).

32. Chono, S., Takeda, E., Seki, T. & Morimoto, K. Enhancement of the dissolution rate and gastrointestinal absorption of pranlukast as a model poorly water-soluble drug by grinding with gelatin. *Int. J. Pharm.* **347**, 71–8 (2008).

33. Hancock, B. C. Disordered drug delivery: destiny, dynamics and the Deborah number. *J. Pharm. Pharmacol.* **54**, 737–746 (2002).

34. Singhal, D. & Curatolo, W. Drug polymorphism and dosage form design: A practical perspective. *Adv. Drug Deliv. Rev.* **56**, 335–347 (2004).

35. Shamblin, S. L., Hancock, B. C. & Pikal, M. J. Coupling Between Chemical Reactivity and Structural Relaxation in Pharmaceutical Glasses. *Pharm. Res.* **23**, 2254–2268 (2006).

36. Lehto, V. & Laine, E. Assessment of physical stability of different forms of cefadroxil at high humidities. *Int. J. Pharm.* **163**, 49–62 (1998).

37. Datta, S., Grant, D. J. W. & Hall, W. Crystal structures of drugs : advances in determination, prediction and engineering. *Nat. Rev. Drug Discov.* **3,** 42–57 (2004).

38. Liu, J. Physical Characterization of Pharmaceutical Formulations in Frozen and Freeze-Dried Solid States : Techniques and Applications in Freeze- Drying Development Freeze-Dried Solid States : Techniques and Applications in Freeze-Drying. *Pharm. Dev. Technol.* **11**, 3–28 (2008).

39. Sailaja, U., Shahin Thayyil, M., Krishna Kumar, N. S. & Govindaraj, G. Molecular dynamics in liquid and glassy states of non-steroidal anti-inflammatory drug: Ketoprofen. *Eur. J. Pharm. Sci.* **49**, 333–340 (2013).

40. Adrjanowicz, K.,Grzybowska. K., Kaminski. K. & Hawelek. L. Comprehensive studies on physical and chemical stability in liquid and glassy states of telmisartan (TEL): Solubility advantages given by cryomilled and quenched material. (2011).

41. Chan, H., Clark. A. R., Feeley. J. C., Kuo. M. C., Lehrman. S. R., Pikal. C. K., Miller. D. P., Vehring. R. & Lechuga-Ballesteros D. Physical stability of Salmon Calcitonin spray-dried powders for inhalation. *J. Pharm. Sci.* **93,** 792–804 (2004).

42. Chiou, W. I. N. L. & Riegelmant, S. Pharmaceutical sciences Pharmaceutical Applications of Solid. *J. Pharm Sci* **60**, 1281–1302 (1971).

43. Yu, L.; Mishra, D.S.; Rigsbee, D. . Determination of the Glass Properties of D - Mannitol Using Sorbitol as an Impurity. *J Pharm Sci* **87**, 774–777 (1998).

44. Matteucci, M. E. Brettmann, B. K., Rogers, T.L., Elder. E. J., Williams. R. & Johnston. K.P. Design of Potent Amorphous Drug Nanoparticles for Rapid Generation of Highly Supersaturated Media.*Mol. Pharm.* **4,** 782–793 (2007).

45. Mu, M. & Meier, U. Experimental Study of the Effect of Process Parameters in the Recrystallization of an Organic Compound Using Compressed Carbon Dioxide as Antisolvent. *Ind. Eng. Chem. Res.* **39**, 2260–2268 (2000).

46. Gupta, M. K., Vanwert, A. & Bogner, R. H. Formation of Physically Stable Amorphous Drugs by Milling with Neusilin. *J. Pharm Sci* **92**, 536–551 (2003).

47. Mirza, S., Miroshnyk, I., Christiansen, L. & Karjalainen, M. Influence of Solvents on the Variety of Crystalline Forms of Erythromycin. *AAPS PharmSci* **5**, 39–47 (2003).

48. Melani, E., Bettinetti, G. E., Mura, E. & Manderioli, A. Interaction of Naproxen with 7-Hydroxypropyl Cyclodextrins in Solution and in the Solid State. *J. lnclusion Phenom. Mol. Recognit. Chem.* **22**, 131–143 (1995).

49. Schebor, C., Burin, L., Buera, P., Aguilera, M. & Chirife, J. Glassy State and Thermal Inactivation of Invertase and Lactase in Dried Amorphous Matrices. *Biotechnol.Prog* **13**, 857–863 (1997).

50. Zhou, D., Zhang, G. G. Z., Law, D., Grant, D. J. W. & Schmitt, E. A. Physical stability of amorphous pharmaceuticals: Importance of configurational thermodynamic quantities and molecular mobility. *J. Pharm. Sci.* **91**, 1863–1872 (2002).

51. Lechuga-Ballesteros, D., Bakri, A. & Miller, D. P. Microcalorimetric measurement of the interactions between water vapor and amorphous pharmaceutical solids. *Pharm. Res.* **20**, 308–318 (2003).

52. Brás, A. R.,Noronha, J. P., Antunes, A. M. M., Cardoso, M. M., Schönhals, A., Affouard, F., Dionísio, M. & Correia, N. T. Molecular motions in amorphous ibuprofen as studied by broadband dielectric spectroscopy. *J. Phys. Chem. B* **112,** 11087–11099 (2008).

53. Adrjanowicz, K., Kaminski, K., Wojnarowska, Z., Dulsik, M., Hawelek, L., Pawlus, S., Paluch, M. & Sawicki, W. Dielectric relaxation and crystallization kinetics of ibuprofen at ambient and elevated pressure. *J. Phys. Chem. B* **114,** 6579–6593 (2010).

54. El Goresy, T. & Böhmer, R. Dielectric study of the viscous and glassy states of a binary, nifedipine-based pharmaceutical alloy. *J. Non. Cryst. Solids* **352**, 4459–4463 (2006).

55. Rodrigues, A. C., Viciosa, M. T., Dane, F., A, F. & Correia, N. T. Molecular Mobility of Amorphous S- Flurbiprofen : A Dielectric Relaxation Spectroscopy Approach. *Mol. Pharm.* **11**, 112–130 (2014).

56. Adrjanowicz, K., Paluch, M. & Ngai, K. L. Determining the structural relaxation times deep in the glassy state of the pharmaceutical Telmisartan. *J. Phys. Condens. Matter* **22**, (2010).

57. Wojnarowska, Z. Adrjanowicz, K., Wlodarczyk, P., Kaminska, E., Kaminski, K., Grzybowska, K., Wrzalik, R., Paluch, M. & Ngai, K. L. Broadband dielectric relaxation study at ambient and elevated pressure of molecular dynamics of pharmaceutical: indomethacin. *J. Phys. Chem. B* **113,** 12536–12545 (2009).

58. Andronis, V. & Zografi, G. Crystal nucleation and growth of indomethacin polymorphs from the amorphous state. *J. Non. Cryst. Solids* **271**, 236–248 (2000).

59. Adrjanowicz, K. *et al.* Molecular dynamics in supercooled liquid and glassy states of antibiotics: Azithromycin, clarithromycin and roxithromycin studied by dielectric spectroscopy. Advantages given by the amorphous state. *Mol. Pharm.* **9,** 1748–1763 (2012).

60. Wojnarowska, Z., Zakowiecki, D., Kaminski, K., Hawelek, L.,Grzybowska, K., Tarnacka, M., Paluch, M. & Cal, K. Molecular dynamics studies on the water mixtures of pharmaceutically important ionic liquid lidocaine HCl. *Mol. Pharm.* **9,** 1250–1261 (2012).

61. Pajula, K., Taskinen, M., Lehto, V., Ketolainen, J. & Korhonen, O. Predicting the formation and stability of amorphous small molecule binary mixtures from computationally determined Flory-Huggins interaction parameter and phase diagram.*Mol. Parm* **7,** 795–804 (2010).

62. Nanakwani, K., Modi, S. R., Kumar, L. & Bansal, A. K. Role of thermodynamic, kinetic and structural factors in the recrystallization behavior of amorphous erythromycin salts. *Thermochim. Acta* **582**, 77–85 (2014).

63. Sailaja, U., Shahin Thayyil, M., Krishna Kumar, N. S., Govindaraj, G. & Ngai, K. L. Molecular mobility in the supercooled and glassy states of nizatidine and perphenazine. *Eur. J. Pharm. Sci.* **99**, 147–151 (2017).

64. Sailaja, U., Thayyil, M. S., Kumar, N. S. K. & Govindaraj, G. Molecular dynamics of amorphous pharmaceutical fenofibrate studied by broadband dielectric spectroscopy. *J. Pharm. Anal.* **6**, 165–170 (2016).

65. Sailaja, U. & Thayyil, M. S. Dielectric and Spectroscopic Investigations of Amorphous Captopril. *IOSR J. Pharm* **2**, 479–484 (2012).

66. Sailaja, U. & Thayyil, M. S. Fragility of Cimetidine Drug Probed by Broadband Dielectric Spectroscopy. *Transl. Med.* **4**, 2013–2015 (2014).

67. Viciosa, M. T., Ramos, J. J. M. & Diogo, H. P. The Slow Relaxation Dynamics in the Amorphous Pharmaceutical Drugs Cimetidine , Nizatidine , and Famotidine. 1–12 (2016).

68. Wojnarowska, Z., Hawelek, L., Paluch, M., Sawicki, W. & Ngai, K. L. Molecular dynamics at ambient and elevated pressure of the amorphous pharmaceutical: Nonivamide (pelargonic acid vanillylamide). *J. Chem. Phys.* **134**, (2011).

69. Knapik-Kowalczuk, J., Wojnarowska, Z., Rams-Baron, M., Jurkiewicz, K., Cielecka-Piontek, J., Ngai, K. L., & Paluch, M. Atorvastatin as a promising crystallization inhibitor of amorphous Probucol: Dielectric studies at ambient and elevated pressure. *Mol. Pharm.* **14** (8)**,** 2670–2680 (2017).

70. Wojnarowska, Z., Swiety-Pospiech, A., Grzybowska, K., Hawelek, L., Paluch, M. & Ngai, K. L. Fundamentals of ionic conductivity relaxation gained from study of procaine hydrochloride and procainamide hydrochloride at ambient and elevated pressure. *J. Chem. Phys.* **136,** (2012).

71. Chawla, G. Molecular Mobility and Physical Stability of Amorphous Irbesartan. *Sci. Pharm.* **77**, 695–709 (2009).

72. Surana, R., Pyne, A. & Suryanarayanan, R. Effect of Aging on the Physical Properties of Amorphous Trehalose. **21**, (2004).

73. Kaminski, K., Kaminska, E., Hensel-Bielowska, S., Pawlus, S., Paluch, M. & Ziolo, J. High pressure study on molecular mobility of leucrose. *J. Chem. Phys.* **129,** 1–6 (2008).

74. Knapik, J., Wojnarowska, Z., Grzybowska, K., Jurkiewicz, K., Tajber, L. & Paluch, M. Molecular dynamics and physical stability of coamorphous Ezetimib and Indapamide mixtures. *Mol. Pharm.* **12** (10|), 3610-3619 (2015).

75. Wojnarowska, Z., Grzybowska, K., Hawelek, L., Dulski, M., Wrzalik, R., Gruszka, I., Paluch, M., Pienkowska, K., Sawicki, W., Bujak, P., Palch, K. J., Tajber, L. & Markowski, J. Molecular dynamics, physical stability and solubility advantage from amorphous indapamide drug. *Mol. Pharm.* **10,** 3612–3627 (2013).

76. Adrjanowicz, K., Kaminski, K., Wlodarczyk, P., Grzybowska, K., Tarnacka, M., Zakowiecki, D, Garbacz, G., Paluch, M. & Jurga, S. Molecular dynamics of the supercooled pharmaceutical agent posaconazole studied via differential scanning calorimetry and dielectric and mechanical spectroscopies. *Mol. Pharm.* **10,** 3934–3945 (2013).

77. Kamiński, K., Paluch, M., Ziolo, J. & Ngai, K. L. Dielectric studies of molecular motions in glassy and liquid nicotine. *J. Phys. Condens. Matter* **18**, 5607–5615 (2006).

78. Shete, G., Khomane, K. S. & Bansal, A. K. Molecular relaxation behavior and isothermal crystallization above glass transition temperature of amorphous hesperetin. *J. Pharm. Sci.* **103**, 167–178 (2014).

79. Grzybowska, K., Paluch, M., Grzybowska, K., Wojnarowska, Z., Hawelek, L., Kolodziejczyk, K., Ngai, K. L. Molecular dynamics and physical stability of amorphous anti-inflammatory drug: celecoxib. *J. Phys. Chem. B* **114,** 12792–12801 (2010).

80. Knapik-kowalczuk, J., Tu, W., Chmiel, K., Rams-baron, M. & Paluch, M. Co-Stabilization of Amorphous Pharmaceuticals - The Case of Nifedipine and Nimodipine. *Mol. Pharm.* **15**, 2455–2465 (2018).

81. Dantuluri, A. K. R., Amin, A., Puri, V. & Bansal, A. K. Role of α-relaxation on crystallization of amorphous Celecoxib above T_g probed by dielectric spectroscopy. *Mol. Pharm.* **8,** 814–822 (2011).

82. Kolodziejczyk, K., Paluch, M., Grzybowska, K., Grzybowski, A., Wojnarowska, Z., Hawelek, L., & Ziolo, J. D. Relaxation dynamics and crystallization study of sildenafil in the liquid and glassy states. *Mol. Pharm.* **10,** 2270–2282 (2013).83. Paluch, M.; Knapik, J.; Wojnarowska, Z.; Grzybowski, A.; Ngai, K. L. Universal Behavior of Dielectric Responses of Glass Formers: Role of Dipole-Dipole Interactions. *Phys. Rev. Lett.* **116**, 25702 (2016).

84. Jedrzejowska, A., Ngai, K. L. & Paluch, M. Modifications of Structure and Intermolecular Potential of a Canonical Glassformer: Dynamics Changing with Dipole–Dipole Interaction. *J. Phys. Chem. A* **120**, 8781–8785 (2016).

85. Ediger, M. D. & Nagel, S. R. Supercooled Liquids and Glasses. **V**, 13200–13212 (1996).

86. Angell, C. A., Ngai, K. L., Mckenna, G. B., Mcmillan, P. F. & Martin, S. W. Relaxation in glassforming liquids and amorphous solids Relaxation in glassforming liquids and amorphous solids. **3113**, (2013).

87. Kremer, F. & Schönhals, A. Broadband Dielectric Spectroscopy. *Springer* (2003).

88. Lunkenheimer, P., Schneider, U., Brand, R. & Loidl, A. Glassy dynamics. *Contemp. Phys.* **41**, 15–36 (2000).

89. Lunkenheimer, P., Wehn, R., Köhler, M. & Loidl, A. Fast dynamics in glass-forming salol investigated by dielectric spectroscopy.

90. Richert, R. Heterogeneous dynamics in liquids: fluctuations in space and time. *J. Phys. Condens. Matter* **14**, 703–738 (2002).

91. Jackle, J. Models of the glass transition. *Reports Prog. Phys.* **49**, 171–231 (1986).

92. Ferguson, R., Arrighi, V., McEwen, I. J., Gagliardi, S. & Triolo, A. An improved algorithm for the fourier integral of the KWW function and its application to neutron scattering and dielectric data. *J. Macromol. Sci. Part B Phys.* **45 B**, 1065–1081 (2006).

93. Havriliak, S. & Havriliak, S. J. Comparison of the Havriliak-Negami and stretched exponential functions. *Polymer (Guildf).* **37**, 4107–4110 (1996).

94. Vogel, H. The law of the relation between the viscosity of liquids and the temperature. *Phys. Z* **22**, 645–646 (1921).

95. Fulcher, G. Analysis of recent measurements of the viscosity of glasses.—ii1. *J. Am. Ceram. Soc.* **8**, 789–794 (1925).

96. Fulcher, G. S. Analysis of recent measurements of the viscosity of glasses. *J. Am. Ceram. Soc.* **8**, 339–355 (1925).

97. Tammann, G.; Hesse, W. The dependence of viscosity upon the temperature of supercooled liquids. *Z.Anorg. Allg. Chem* **156**, 245–257 (1926).

98. Angell, C. A., Ngai, K. L., McKenna, G. B., McMillan, P. F. & Martin, S. W. Relaxation in glassforming liquids and amorphous solids. *J. Appl. Phys.* **88**, 3113–3157 (2000).

99. Ngai, K. L. Dynamic and thermodynamic properties of glass-forming substances. *J. Non-Cryst. Solids* **275**, 7–51 (2000).

100. Angell, C. A. Relaxation in liquids, polymers and plastic crystals - strong/fragile patterns and problems. *J. Non-Cryst. Solids* **133**, 13–31 (1991).

101. Tanaka, H. Relationship among glass-forming ability, fragility, and short-range bond ordering of liquids. *J. Non-Cryst. Solids* **351**, 678–690 (2005).

102. Lu, J., Rohani, S. Polymorphism and crystallization of active pharmaceutical ingredients (APIs). *Curr. Med. Chem.* **16**, 884–905 (2009).

103. Johari, G. P. & Goldstein, M. Viscous Liquids and the Glass Transition. II. Secondary Relaxations in Glasses of Rigid Molecules. *J. Chem. Phys.* **53**, 2372–2388 (1970).

104. Johari, G. P. Intrinsic mobility of molecular glasses. *J Chem. Phys* **58**, 1766–1770 (1973).

105. Johari, G. P. Localized molecular motions of b -relaxation and its energy landscape. *J. Non-Cryst. Solids* **307**–**310**, 317–325 (2002).

106. Williams, G. & Watts, D. C. in The Glassy. *Trans. Faraday Soc.* 1971–1979 (1971).

107. Thayyil, M. S., Capaccioli, S., Prevosto, D. & Ngai, K. L. Is the Johari-Goldstein β -relaxation universal ? *Philos. Mag.* **88**, 4007–4013 (2008).

108. Debye, P. *Polar Molecules*. *Chemical Catalog Company, New york* (1929).

109. Cole, K. S. & Cole, R. H. Dispersion and Absorption in Dielectrics I . Alternating Current Characteristics. *J Chem. Phys* **341**, (2004).

110. Davidson, D. W. & Cole, R. H. Dielectric Relaxation in Glycerine. *J. Chem. Phys* **1417**, 6–8 (1950).

111. Davidson, D. W. & Cole, R. H. Dielectric Relaxation in Glycerol, Propylene Glycol, and nPropanol. *J. Chem. Phys* **1484**, (1951).

112. Havriliak, S. & Negami, S. A Complex Plane Analysis of or-Dispersions in Some Polymer Systems. *J. Polym. Sci. Pt. C* **117**, 99–117 (1966).

113. Havriliak, S. & Negami, S. A Complex Plane Representation of Dielectric and Mechanical Relaxation Processes in Some Polymers. *Polymer (Guildf).* **8**, 161–210 (1967).

114. Jin, X., Zhang, S., Horvath, J. R. & Runt, J. Broadband Dielectric Investigation on 2 , 6-Dihydroxynaphthalene / Poly (vinyl ethyl ether) Mixtures. *J. Phy. Chem. B* **108**, 7681–7687 (2004).

115. Ngai, K. L. & Tsang, K. Y. From Chemical Structure to Viscoelastic Properties of Polymers. *Macromol. Symp.* **90**, 95–129 (1995).

116. Hensel-Bielowka, S., Pawlus, S., Roland, C. M. & Paluch, M. Effect of large hydrostatic pressure on the dielectric loss spectrum of type- A glass formers. *Phys. Rev. E.* **50501**, 19–22 (2004).

117. Ngai, K. L. Why the glass transition problem remains unsolved? *J. Non. Cryst. Solids* **353**, 709–718 (2007).

118. Zorn, R., Arbe, A., Colmenero, J., Frick, B., Richter, D. & Buchenau, U. Neutron scattering study of the picosecond dynamics of polybutadiene and polyisoprene. *Phys. Rev. E* **52**, 781–795 (1995).

119. Colmenero, J., Arbe, A. & Alegría, A. Crossover from Debye to non-Debye dynamical behavior of the alpha relaxation observed by quasielastic neutron scattering in a glass-forming polymer. *Phys. Rev. Lett.* **71**, 2603–2606 (1993).

120. Ngai, K. L. Relation between some secondary relaxations and the α relaxations in glass-forming materials according to the coupling model. *J. Chem. Phys.* **6982**, (1998).

121. Ngai, K. L. An extended coupling model description of the evolution of dynamics with time in supercooled liquids and ionic conductors. *J. Phys. Condens. Matter* **15**, S1107–S1125 (2003).

122. Capaccioli, S., Prevosto, D., Lucchesi, M., Rolla, P. A., Casalini, R. & Ngai, K. L. Identifying the genuine Johari–Goldstein β-relaxation by cooling, compressing, and aging small molecular glass-formers. *J. Non. Cryst. Solids* **351**, 2643–2651 (2005).

123. Kaminski, K.; Kaminska, E.; Adrjanowicz, K.; Grzybowiska, K.; Wlodarczyk, P.; Paluch, M.; Burian, A.; Ziolo, J.; Lepek, P.; Mazgalski, J. . S. Dielectric Relaxation Study on Tramadol Monohydrate and Its Hydrochloride Salt. *J. Pharm. Sci* **99**, 94–106 (2010).

124. Yinnon, H. & Uhlmann, D. R. Applications of thermoanalytical techniques to the study of crystallization kinetics in glass-forming liquids, Part I: Theory. *J. Non-Cryst. Solids* **54**, 253–275 (1983).

125. Bhattacharya, S. & Suryanarayanan, R. A. J. Local Mobility in Amorphous Pharmaceuticals — Characterization and Implications on Stability. *J. Pharm Sci* **98**, 2935–2953 (2009).

126. Vyazovkin, S. & Dranca, I. Effect of Physical Aging on Nucleation of Amorphous Indomethacin. *J. Phys. Chem. B* **111**, 7283–7287 (2007).

127. Schammé, B, Mignot, M., Couvrat, N., Tognetti, V., Joubert, L., Dupray, V., Joubert, L., Delbreilh, L., Dargent, E. & Coquerel, G. Molecular Relaxations in Supercooled Liquid and Glassy States of Amorphous Quinidine : Dielectric Spectroscopy and Density Functional Theory (DFT) Approaches. *J. Phys. Chem. B* **120,** 7579–7592 (2016).

128. Hédoux, A., Guinet, Y., Capet, F., Paccou, L. & Descamps, M. Evidence for a high-density amorphous form in indomethacin from Raman scattering investigations. *Phys. Rev. B* **77**, 94205-1–10 (2008).

129. Viel, Q., Cartigny, Y., Euse, M. E. S., Dargent, E. & Petit, S. Crystallization from the Amorphous State of a Pharmaceutical Compound : Impact of Chirality and Chemical Purity. *Cryst. Growth Des.* **17**, 337–346 (2017).

130. Legrand, V., Descamps, M. & Alba-simionesco, C. Glass-forming meta-toluidine: A thermal and structural analysis of its crystalline polymorphism and devitrification. *Thermochim. Acta* **307**, 77–83 (1997).

131. Chattoraj, S., Bhugra, C., Telang, C., Zhong, L., Wang, Z. & Sun, C. C. Origin of Two Modes of Non-isothermal Crystallization of Glasses Produced by Milling. *Pharm Res.* **29,** 1020–1032 (2012).

132. Willart, J. F. & Descamps, M. Solid State Amorphization of Pharmaceuticals. *Mol. Pharm.* **5**, 905–920 (2008).

133. Karmwar, P., Graeser, K., Gordon, K. C., Strachan, C. J. & Rades, T. Investigation of properties and recrystallisation behaviour of amorphous indomethacin samples prepared by different methods. *Int. J. Pharm.* **417**, 94–100 (2011).

134. Matusita, K. & Sakka, S. Kinetic Study on Non-Isothermal Crystallization of Glass by Thermal Analysis. *Bull. Inst. Chem. Res* **59**, 159–171 (1981).

135. Avrami, M. Kinetics of phase change. II Transformation-time relations for random distribution of nuclei. *J. Chem. Phys.* **8**, 212–224 (1940).

136. Avramov, I., Avramova, K. & Rüssel, C. New method to analyze data on overall crystallization kinetics. *J. Cryst. Growth* **285**, 394–399 (2005).

137. Ozawa, T. Kinetics of non-isothermal crystallization. *Polymer (Guildf).* **12**, 150–158 (1971).

138. Augis, J. A. & Bennett, J. E. Calculation of the Avrami parameters for heterogeneous solid state reactions using a modified the Kissingermethod. *J. Therm. Anal.* **13**, 283–292 (1978).

139. Marseglia, E. A. Kinetic Theory of Crystallization of Amorphous Materials. *J. Non-Cryst. Solids* **41**, 31–36 (1980).

140. Christian, J. W. *The theory of transformations in metals and alloys*. (Pergamon Press, 1975).

141. Avrami, M. Kinetics of phase change. I: General theory. *J. Chem. Phys.* **7**, 1103–1112 (1939).

142. Stocker, R. Molecular mechanisms underlying the antiatherosclerotic and antidiabetic effects of probucol, succinobucol, and other probucol analogues. *Curr. Opin. Lipidol.* **20**, 227–235 (2009).

143. Poirier, J. Apolipoprotein E and cholesterol metabolism in the pathogenesis and treatment of Alzheimer's disease. *Trends Mol. Med.* **9**, 94–101 (2003).

144. Champagne, D., Pearson, D., Dea, D., Rochford, J. & Poirier, J. The cholesterol-lowering drug Probucol increases apolipoprotein e production in the hippocampus of aged rats: implications for Alzheimer's disease. *Neuroscience* **121**, 99–110 (2003).

145. Dalsin, M. C.; Tale, S. & Reineke, T. M. Solution-State Polymer Assemblies Influence BCS Class II Drug Dissolution and Supersaturation Maintenance. *Biomacromolecules* **15**, 500–511 (2014).

146. Yagi, N.; Terashima, Y.; Kenmotsu, H.; Seikikawa, H. & Takada, M. Dissolution behavior of Probucol from solid dispersion systems of Probucol-Polyvinylpyrrolidone. *Chem. Pharm. Bull.* **44,** 241–244 (1996).

147. Benmore, C. J. & Weber, J. K. R. Amorphization of Molecular Liquids of Pharmaceutical Drugs by Acoustic Levitation. **11004**, 1–7 (2011).

148. Gerber, J. J., Caira, M. R. & Lötter, A. P. Structures of two conformational polymorphs of the cholesterol-lowering drug probucol. *J. Crystallogr. Spectrosc. Res.* **23**, 863–869. (1993).

149. Thybo, P., Pedersen, B. L., Hovgaard, L., Holm, R. & Müllertz, A. Characterization and Physical Stability of Spray Dried Solid Dispersions of Probucol and PVP-K30. *Pharm. Dev. Technol.* **13**, 375–386. (2008).

150. Broman, E., Khoo, C. & Taylor, L. S. A comparison of alternative polymer excipients and processing methods for making solid dispersions of a poorly water soluble drug. *Int. J. Pharm.* **222**, 139–151 (2001).

151. Zaghloul, A. A., Khattab, I., Nada, A. & Al-Saidan, S. Preparation, characterization and optimization of probucol self-emulsified drug delivery system to enhance solubility and dissolution. *Pharmazie* **63**, 654–660 (2008).

152. Adrjanowicz, K.; Wojnarowska, Z.; Wlodarczyk, P.; Kaminski, K.; Paluch, M.; Mazgalski, J. Molecular mobility in liquid and glassy states of Telmisartan (TEL) studied by Broadband Dielectric Spectroscopy. *Eur. J. Pharm. Sci.* **38**, 395–404 (2009).

153. https://pubchem.ncbi.nlm.nih.gov/compound/Probucol.

154. Fulcher, G. S. Analysis of Recent Measurements of the Viscosity of Glasses. *J. Am. Ceram. Soc.* **75**, 1043–1055 (1992).

155. Sahra, M. *et al.* Dielectric spectroscopic studies of three important active pharmaceutical ingredients - clofoctol , droperidol and probucol. *J. Non-Cryst. Solids* **505**, 28–36 (2019).

156. Patkowski, A., Paluch, M. & Gapiński, J. Relationship between T_0, T_g and their pressure dependence for supercooled liquids. *J. Non. Cryst. Solids* **330**, 259–263 (2003).

157. Ngai, K. L. & Capaccioli, S. Relation between the activation energy of the Johari-Goldstein β relaxation and T_g of glass formers. *Phys. Rev. E* **69,** 31501 (2004).

158. Mora, E., Diogo, H. P. & Moura, J. J. Thermochimica Acta The slow molecular dynamics in amorphous probucol. **595**, 83–88 (2014).

159. Tacca, M. Del., Danesi, R., Senesi, S., Gasperini, M., Mussi, A. & Angeletti, C. A. Penetration of clofoctol into human lung. *J. Antimicrob. Chemother.* **19** (5), 679–683 (1987).

160. Wang, M., Shim, J. S. & Li, R. Identification of an old antibiotic clofoctol as a novel activator of unfolded protein response pathways and an inhibitor of. (2014). doi:10.1111/bph.12800

161. https://pubchem.ncbi.nlm.nih.gov/compound/Clofoctol.

162. Christian, J. W. *The Theory of Transformations in Metals and Alloys*. (Pergamon Press, Oxford, 1965).

163. D. A. Porter, K. E. E. and M. Y. S. *'Phase Transformations in Metals and Alloys'*. (, CRC Press Taylor and Francis Group, New York., 1981).

164. Avrami, M. Granulation, phase change, and microstructure kinetics of phase change. III. *J. Chem. Phys.* **9**, 177–184 (1941).

165. Mittemeijer, E. J. Review Analysis of the kinetics of phase transformations. **27**, 3977–3987 (1992).

166. Kruger, P. On the relation between non-isothermal and isothermal Kolomogorov-Johnson-Mehl-Avrami crystallization kinetics*., J. Phys. Chem. Solids* **54,** 1549–1555 (1993).

167. Massalska-Arodz, M., Wiliiams, G., Smith, I. K., Conolly, C., Aldridge, G.A. & Dabrowski, R. Molecular-Dynamics and Crystallization Behavior of Isopentyl Cyanobiphenyl as Studied by Dielectric-Relaxation Spectroscopy. *J. Chem. Soc.-Faraday Trans.* **94**, 387–394 (1998).

168. Naffakh, M., Martín, Z., Marco, C., Gómez, M. A. & Jiménez, I. Isothermal crystallization kinetics of isotactic polypropylene with inorganic fullerene-like WS2 nanoparticles. *Thermochim. Acta* **472**, 11–16 (2008).

169. Domino, K. B., Anderson, E. A., Polissar, N. L., & Posner, K. L. Comparative Efficacy and Safety of Ondansetron, Droperidol, and Metoclopramide for Preventing Postoperative Nausea and Vomiting: A Meta-Analysis. *Anesth. Analg.* **88**, 1370–1379 (1999).

170. Richards, J., Derlet, R., & Duncan, D. Chemical restraint for the agitated patient in the emergency department: lorazepam versus droperidol. *J. Emerg. Med.* **16**, 567–573 (1998).

171. https://pubchem.ncbi.nlm.nih.gov/compound/Droperidol.

172. Hensel-bielowka, S., Wojnarowska, Z., Dzida, M., Zorębski, E., Zorębski, M., Geppert-Rybczyńska, M., Peppel, T., Grzybowska, K., Wang, Y., Sokolov, A.P. & Paluch, M. Heterogeneous Nature of Relaxation Dynamics of Room- Temperature Ionic Liquids (EMIm) 2 [Co(NCS) 4] and (BMIm) 2 [Co(NCS) 4]. (2015). doi:10.1021/acs.jpcc.5b07123

173. Yu, J. & He, J. Crystallization kinetics of maleic anhydride grafted polypropylene ionomers. *Polymer (Guildf).* **41**, 891–898 (2000).

174. Bordat, P., Affouard, F., Descamps, M. & Ngai, K. L. Does the interaction potential determine both the fragility of the liquid and the vibrational properties of its glassy state? *Phys. Rev. Lett.* **93**, 105502 (2004).

175. Shamblin, S. L., Hancock, B. C., Dupuis, Y. & Pikal, M. J. Pharmaceutical Systems. **89**, 417–427 (2000).

176. Shamblin, S. L., Tang, X., Chang, L., Hancock, B. C. & Pikal, M. J. Characterization of the Time Scales of Molecular Motion in Pharmaceutically Important Glasses. 4113–4121 (1999).

177. Grzybowska, K., Capaccioli, S. & Paluch, M. Recent developments in the experimental investigations of relaxations in pharmaceuticals by dielectric techniques at ambient and elevated pressure. *Adv. Drug Deliv. Rev.* **100**, 158–182 (2016).

178. Carpentier, L., Decressain, R., Desprez, S. & Descamps, M. Dynamics of the amorphous and crystalline α-, β-phases of indomethacin. *J. Phys. Chem. B* **110**, 457–464 (2006).

179. Adrjanowicz, K., Kaminski, K., Paluch, M., Wlodarczyk, P., Grzybowska, K., Wojnarowska, Z., Hawelek, L., Sawicki, W., Lepek, P. & Lunio, R. Dielectric relaxation studies and dissolution behavior of amorphous verapamil hydrochloride. *J. Pharm. Sci.* **99**, 828–839 (2010).

180. Kaminski, K., Maslanka, S., Ziolo, J. & Paluch, M. *et al.* Dielectric relaxation of α - tocopherol acetate (vitamin E). *Phys. Rev. E - Stat. Nonlinear, Soft Matter Phys.* **75**, 1–7 (2007).

181. Knapik J, Wojnarowska Z, Grzybowska K, Hawelek L, Sawicki W, Wlodarski K, Markowski J, P. M. Physical stability of the amorphous anticholesterol agent (ezetimibe): the role of molecular mobility. *Mol. Pharm.* **11**, 4280–4290 (2014).

182. Wlodarczyk, P., Paluch, M., Wojnarowska, Z., Hawelek, L., Kaminski, K. & Pilch, J. Theoretical and experimental studies on the internal mobility of two sulfonylurea agents: Glibenclamide and glimepiride. *J. Phys. Condens. Matter* **23**, 425901 (2011).

183. Wojnarowska, Z., Hawelek, L., Paluch, M., Sawicki, W. & Ngai, K. L. Molecular dynamics at ambient and elevated pressure of the amorphous pharmaceutical: Nonivamide (pelargonic acid vanillylamide). *J. Chem. Phys.* **134**, 44517 (2011).

184. *Disordered Pharmaceutical Materials*. (Wiley-VCH, 2016).

185. Kawakami, K., Usui, T., Hattori, M. Understanding the Glass-Forming Ability of Active Pharmaceutical Ingredients for Designing Supersaturating Dosage Forms. *J. Pharm. Sci* **101**, 3239–3248 (2012).

186. Correia, N. T., Moura Ramos, J. J., Descamps, M. & Collins, G. Molecular mobility and fragility in indomethacin: A thermally stimulated depolarization current study. *Pharm. Res.* **18**, 1767–1774 (2001).

187. Knapik, J., Wojnarowska, Z., Grzybowska K., Tajber, L., Mesallatti, H., Paluch, K. J. & Paluch, M. Molecular Dynamics and Physical Stability of Amorphous Nimesulide Drug and Its Binary Drug − Polymer Systems. *Mol. Pharm.* **13**, 1937–1946 (2016).

Journal of Non-Crystalline Solids 505 (2019) 28–36

Contents lists available at ScienceDirect

Journal of Non-Crystalline Solids

journal homepage: www.elsevier.com/locate/jnoncrysol

Dielectric spectroscopic studies of three important active pharmaceutical ingredients - clofoctol, droperidol and probucol

M. Sahra[a,*], M. Shahin Thayyil[a], Arvind Kumar Bansal[b], K.L. Ngai[c], M.K. Sulaiman[a,d], Ganesh Shete[b], Safna Hussan K.P.[a]

[a] Department of Physics, University of Calicut, Kerala 673635, India
[b] Department of Pharmaceutics, National Institute of Pharmaceutical Education and Research, Punjab 160062, India
[c] Dipartimento di Fisica, Universita di Pisa, Largo B Pontecorvo 3, I-56127 Pisa, Italy
[d] Department of Physics, S.A.R.B.T.M. Govt. College, Koyilandy, Kerala, India

ARTICLE INFO

Keywords:
Dielectric spectroscopy
Molecular dynamics
Amorphous pharmaceuticals
Active pharmaceutical ingredients
Bioavailability
Solubility

ABSTRACT

Nowadays the study of physiochemical stability of amorphous pharmaceuticals is of great interest in the field of medicinal application due to its enhanced water solubility and bioavailability than its crystalline counterpart. Molecular relaxations play an important role in understanding the physical stability of amorphous drugs. Hence herein, we investigated the molecular dynamics of three pharmaceutically important drugs, namely clofoctol, droperidol and probucol by means of broadband dielectric spectroscopy (BDS) and differential scanning calorimetry (DSC). The dielectric spectra in the supercooled state were fitted by Havriliak-Negami (HN) function, while in the glassy state with Cole-Cole equation. The structural relaxation followed non-Arrhenius temperature dependence and followed time-honored Vogel-Fulcher-Tamman (VFT) equation and the secondary relaxation followed Arrhenius equation. The Coupling model (CM) prediction was used to find the origin of the secondary relaxations. Although the three drugs were found to be fragile, clofoctol and droperidol showed recrystallization tendency. It was amazing that the three samples showed a good correlation between the stretch exponent β_{KWW} and the dielectric strength $\Delta\varepsilon(T_g)$. In addition, the molecular simulation was used to verify the presence of non-JG (Johari-Goldstein) secondary relaxation due to side chain rotation.

1. Introduction

Recently, the pharmaceutical industry has been focusing on the development of amorphous pharmaceutical due to its improved solubility and bioavailability than its crystalline counterpart [6,10,13,18,22,23,25,27,37,42]. However, the physical stability and shelf life of most of the amorphous drugs are incredibly low. The foremost important issue is the onset of crystallization during drug preparation, packaging or storage, which can initiate further growth and expansion of the crystal nuclei, and the drug gradually transforms to its thermodynamically favored crystalline state. This transformation ultimately nullifies all the attained benefits in preparing the active pharmaceutical ingredient [API] in amorphous form. Therefore, the understanding of the molecular dynamics and mechanism of crystallization from the amorphous state is inevitable in the development of amorphous pharmaceuticals for practical applications.

Moreover, the deep insight into the molecular dynamics of pharmaceuticals opens up a new research area for physicists, chemists, and material scientists, who are engaging in the research field of liquid-glass transition. The wide variety in physical and chemical structures of pharmaceuticals which are visibly different from the ordinary glassformers commonly used in the study of glass transition has contributed greatly to this field [2,3,8,11,14,17,36,41]. Both pharmaceuticals and ordinary glassformers follow the same traits in supercooled liquid and glassy phases. Hence, the knowledge gained from thermal and spectroscopic investigations of pharmaceuticals will not only benefit the practical applications of the pharmaceuticals, but also may shed light into the yet unresolved problems of glass transition phenomenon.

In this work we present, the thermal, spectroscopic and computational investigations of three hydrogen bonded APIs namely, clofoctol, droperidol and probucol to serve the dual purposes mentioned above. The relaxation dynamics of APIs were investigated in supercooled and

Abbreviations: API, Active pharmaceutical ingredient; CM, coupling model; JG, Johari-Goldstein; VFT, Vogel-Fulcher-Tamman; BCS, biopharmaceutical classification system

* Corresponding author.
E-mail address: sahratp@gmail.com (M. Sahra).

https://doi.org/10.1016/j.jnoncrysol.2018.10.046
Received 5 June 2018; Received in revised form 15 October 2018; Accepted 26 October 2018

Table 1
Physical properties of clofoctol, droperidol and probucol.

Samples	Chemical name	Molecular weight (g/mol)	Principal usage	T_g (K)	T_m (K)
Clofoctol	2-(2,4-dichlorobenzyl)-4-(tetramethyl-1, 1,3,3-butyl)phenol	365.33	Bacteriostatic antibiotic	269	361
Droperidol	1-{1-[4-(4-fluorophenyl)-4-oxobutyl]-1,2,3,6-tetrahydro-4-pyridyl}-1,3-dihydro-2H-benzimidazol-2-one	379.42	Antidopaminergic drug	302	416
Probucol	4,4′-[(1-methylethylidene) bis(thio)]-bis[2,6bis(1,1-dimethylethyl)]phenol.	516.84	Anti-hyper lipidemic drug	300	400

glassy states over a broad frequency and temperature ranges at ambient pressure. To find the origin of the secondary relaxations, CM predictions were used. It was further verified from the computational investigations with the help of density functional theory. The pharmaceuticals, chosen for study have significantly broader structural dispersion than the majority of the drugs investigated so far and thus we have carried out the anti-correlation study between the width of the structural loss peak at T_g to the polarity of the drugs [21,34] in the light of dipole-dipole interaction to the attractive part of the intermolecular potential. They are instrumental in testing the anti-correlation within the family of molecular pharmaceuticals as part of the totality of molecular glassformers studied by dielectric spectroscopy.

2. Materials and methods

2.1. Materials

The APIs and its use along with its physical properties [5] are listed in Table 1. The samples with analytical standard grade were purchased from Sigma Aldrich and used as received without further purification.

2.2. Methods

2.2.1. Differential scanning calorimetry (DSC)

DSC measurements were done using 821^e DSC (Mettler-Toledo, Switzerland) operating with STAR^e software version 9.1. The instrument was calibrated using high purity indium and zinc as standards. The sample weighing 3–5 mg was sealed into a pin holed aluminum pan and placed inside the calorimeter. The instrument was purged with dry nitrogen at the rate of 40 ml/min. The measurement was performed at a heating rate of 10 K/min. The sample was first heated to few degrees above the melting point and kept for a while. It was rapidly cooled at a rate of 20 K/min to ensure the smooth passage of the sample without any chance of crystallization to deep glassy state. The glassy sample was further heated at 10 K/min to get the glass transition temperature and other thermodynamic parameters.

2.2.2. Broadband dielectric spectroscopy (BDS)

Dielectric measurements were carried out using a broadband dielectric spectrometer (Novocontrol GmbH, Germany) for a frequency range of 10 mHz–10 MHz. The sample capacitor was made by keeping the sample between two stainless steel electrodes of 30 mm effective diameter and keeping two narrow Teflon spacers of 50 μm thickness to get an empty cell capacitance of approximately 100 pF. The temperature was controlled with the use of dry nitrogen-flow by the Novocontrol Quatro cryosystem achieving a temperature stability better than ± 0.1 K. As done for DSC, the pharmaceutical was kept in the melt state for a while and cooled fast across the melting region to deep glassy state to ensure complete vitrification. Then, the dielectric spectra were measured isothermally, after stabilizing the temperature for about 600 s. The real and imaginary parts of the dielectric susceptibility were further analyzed with non-linear curve fitting routine of Levenberg Marquadit algorithm using WINFIT software Version 3.2 provided by Novocontrol.

3. Results and discussion

3.1. Differential scanning calorimetry

From the DSC measurements, it was observed that all the three API's namely clofoctol, droperidol and probucol did not show any crystallization tendency during cooling. During subsequent heating from the glassy to their respective melting temperatures, as shown in Fig. 1, probucol showed no tendency of crystallization, while clofoctol and droperidol showed exothermic events indicating cold crystallization.

Our experimental results are in good agreement with the earlier

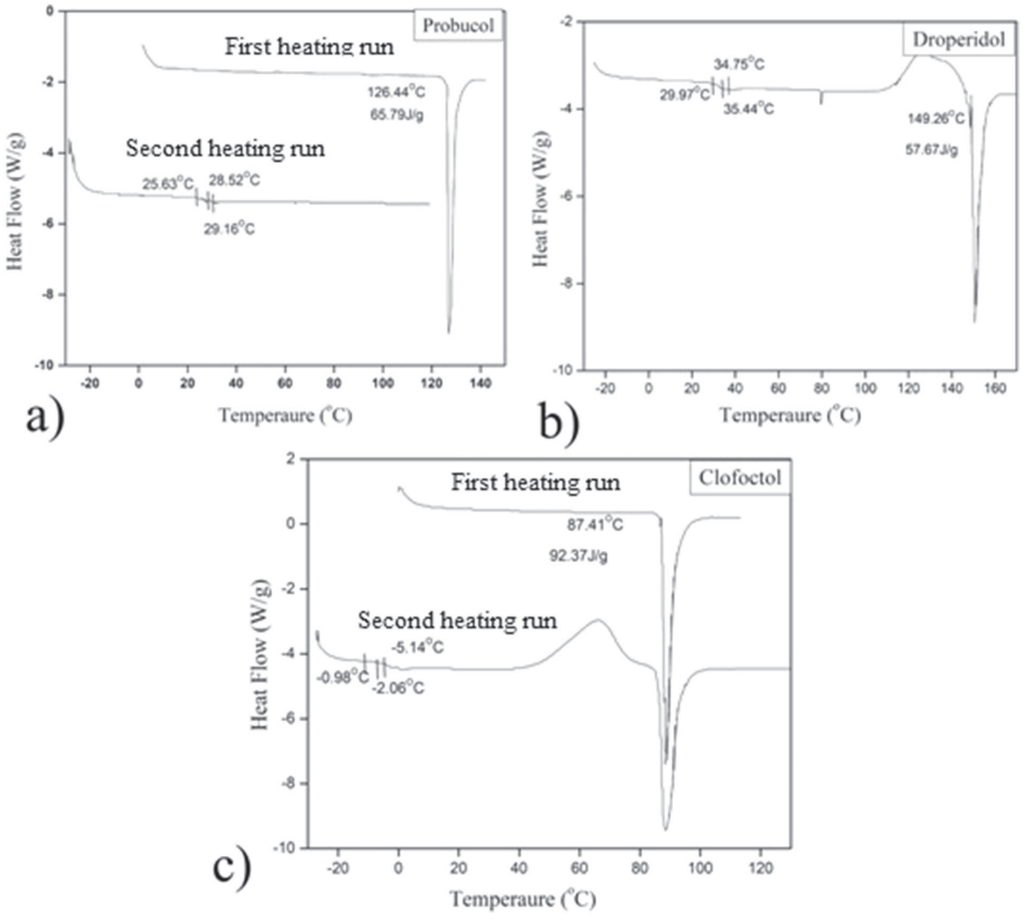

Fig. 1. DSC thermogram of a) probucol, b) droperidol and c) clofoctol.

report by Baird et al. (2010) [5]. Thus the thermal data confirms that probucol belongs to class (III) with high *glass forming ability* (during cooling) as well as high *glass stability* (upon reheating above T_g), while, clofoctol and droperidol belongs to class (II) according to Baird et al. (2010) [5]. Glass transition temperature (T_g) of amorphous drugs were observed as 271 K for clofoctol, 307.9 K for droperidol and 301.6 K for probucol. Consequently, the melting point reflected as the onset of melting endotherm in DSC and the corresponding enthalpy was measured to be 360.5 K (92.4 J/g) for clofoctol, 422.4 K (57.6 J/g) for droperidol and 399.5 K (65.7 J/g) for probucol. Among the three APIs, probucol is known to have at least two conformational polymorphs. Both have monoclinic space groups and the packing is determined by Van der Waals interactions [28]. Form I is thermodynamically stable and the onset melting point is at 399.15 K and for Form II, the onset melting point is at 389.15 K. The sample exhibited a melting point at 399.59 K and thus is Form I.

3.2. Dielectric relaxation

High glass forming ability of the three APIs from DSC measurements opened up an opportunity for detailed analysis of molecular dynamics in supercooled and glassy states using broadband dielectric spectroscopy. The isothermal complex dielectric response over wide frequency range $\varepsilon^*(f) = \varepsilon'(f) - i\varepsilon''(f)$ was recorded during heating of the amorphous APIs, where, ε' is the real and ε" is the imaginary part of dielectric permittivity. As shown in Fig. 2, the relaxation above T_g is the structural or α-relaxation which is due to the cooperative reorientation of the molecules and becomes kinetically frozen while cooling around T_g. The α-relaxation shows the signatures of typical glass forming systems, where the loss peaks shift towards higher frequencies as the temperature is increased. Further, the loss peaks show a rise at low frequencies resulting due to the presence of dc conductivity, whose magnitude increases on increase of temperature in an Arrhenius manner. The dc conductivity usually arises from the translational diffusion of ionic impurities in the material.

To get an idea about the temperature dependence of α-relaxation process for temperatures above T_g, the dielectric loss spectra of clofoctol, droperidol and probucol were shown after subtracting the conductivity. It is worth noting that the loss peaks shows a smooth trend over the entire range of temperature reported. The decrease in dielectric strength at the high temperature sideis due to the onset of crystallization in clofoctol and droperidol. We were unable to get the dielectric spectra at higher temperatures beyond the onset of crystallization during heating in the case of clofoctol and droperidol. We overcome this issue, by melting the samples and repeating the measurements during subsequent cooling. We could get the information about the peak loss frequency to fill the relaxation map up to 10^7 Hz for clofoctol, while we had difficulty in measuring the loss peaks for

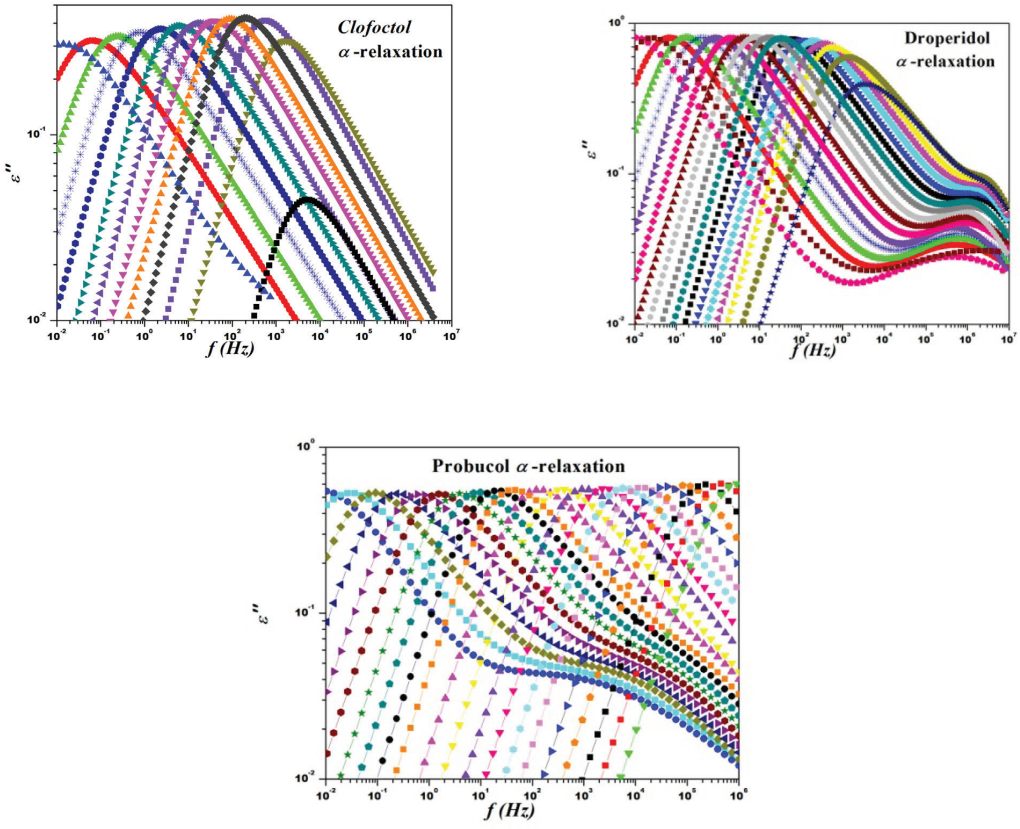

Fig. 2. HN fitted curves for the dielectric loss spectra of clofoctol (267.15 K–285.15 K, ΔT = 2 K and 288.15 K–294.15 K, ΔT = 3 K, from left to right), droperidol (303.15 K–333.15 K, ΔT = 2 K and 336.15 K–339.15 K, ΔT = 3 K, from left to right) and probucol (297.15 K–315.15 K, ΔT = 2 K; 318.15 K–333.15 K, ΔT = 3 K and 337.15 K to 353.15 K, ΔT = 4 K, from left to right) for temperatures above Tg after subtracting the conductivity.

frequencies higher than 10^5 Hz for droperidol due to the interference of crystallization even during cooling. Interestingly, probucol did not show any tendency of crystallization during heating from the deep glassy state. DSC measurement also showed the same behavior. Below T_g, the α-relaxation process is too slow to be measured in our experimental time scale retaining the secondary or β-process. The loss peaks of the secondary process (Fig. 3) moves towards lower frequencies on cooling at a much slower pace *vis a vis* to the structural relaxation. To get a clear understanding about the shape parameters, the dielectric spectra were analyzed using Havriliak–Negami equation [19] given by

$$\varepsilon^*_{HN}(\omega) = \varepsilon' - i\varepsilon'' = \varepsilon_\infty + \sum_k \left(\frac{\Delta\varepsilon}{(1 + (i\omega\tau_{HNk})^{\propto HNk})^{\beta HNk}} \right) - i\left(\frac{\sigma_0}{\omega\varepsilon_0} \right)^N \quad (1)$$

where ε_∞ is the permittivity at the high frequency limit, $\Delta\varepsilon = \varepsilon_s - \varepsilon_\alpha$ where ε_s is the static, low frequency permittivity, τ is the characteristic relaxation time of the medium corresponding to the maximal loss f_{max}, ω is the angular frequency and k denotes the summation over different relaxation processes. The exponents α and β describe the symmetric and asymmetric parameters responsible for deviation or broadening of the dielectric spectra from the classic Debye response. For secondary relaxations, β is taken to be 1 and the Havriliak–Negami equation reduces to the Cole–Cole equation.

The temperature dependence of the relaxation processes are depicted in Fig. 4. The α-process of the three APIs are very well described by the Vogel-Fulcher-Tammanns equation [4,15,16,38,40] given by,

$$f_\alpha = f_0^\alpha \, e^{(-B/(T-T_0))} \quad (2)$$

where T_0 is the limiting temperature which indicates the divergence of the relaxation time at infinite viscosity corresponding to the complete blocking of the structural relaxation, $f_0{}^\alpha$ is a constant and B = DT_0, D is the strength parameter whose value is related to the degree of deviation of the τ_α (T) curve from the Arrhenius equation [4]. For clofoctol, the fitted VFT parameters are B = 1596.2, and T_g obtained from VFT fit is 264.3 K and the estimated value of T_0 is equal to 220.6 K. This value of T_0 is approximately equal to the Kauzmann temperature, T_K [35], which is the hypothetical temperature at which the molecular motions cease completely and can be considered as the ideal high-temperature limit for storage without crystallization of pharmaceutical and is almost 50 degree below the T_g. In the vicinity of this temperature, the primary relaxation would have the time scale of exceeding years [1]. Below this temperature, the translational molecular motions are assumed to be negligible. So it is suggested that the storage of this particular API below 220.6 K would provide better shelf-life and stability. For droperidol, B = 1651.7, and T_g obtained from VFT fit is 300.8 K and the estimated value of T_0 is equal to 250.5 K and for probucol, the fitted parameters are B = 2360.4, T_g obtained from VFT fit is 294.7 K and the estimated value of T_0 is equal to 235.8 K. Our observations are comparable with the previous reports [26].

The fragility or steepness index, m can be calculated from VFT fit

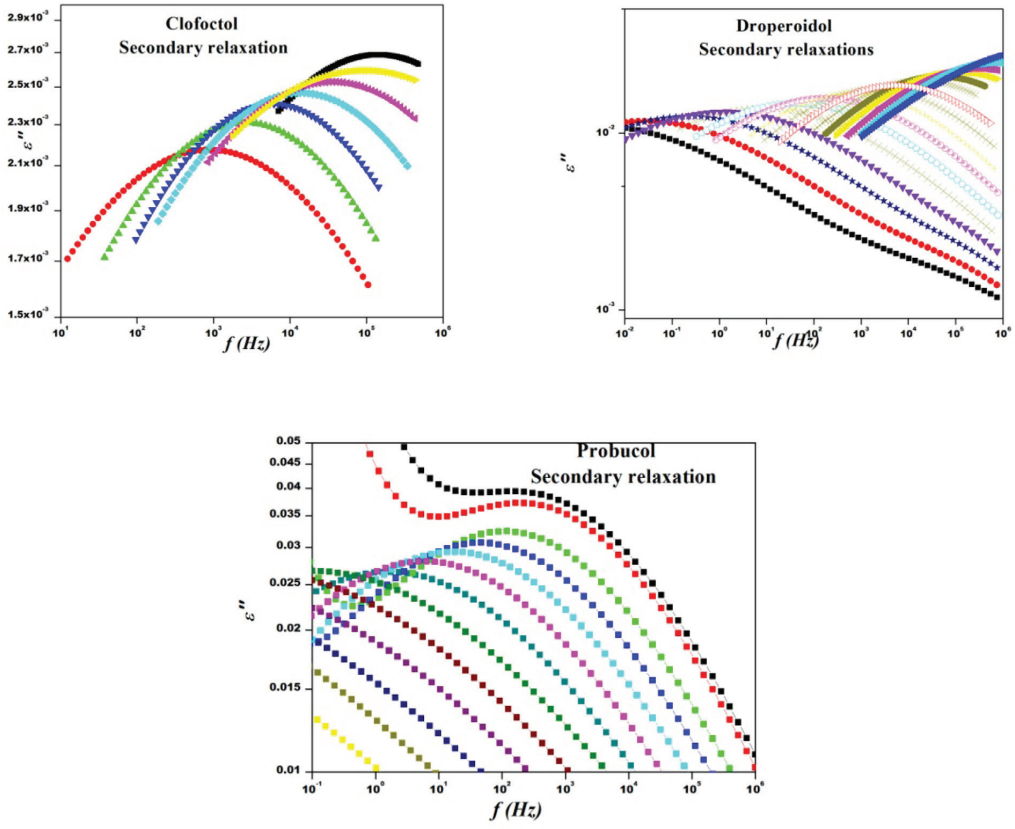

Fig. 3. HN fitted curves for the dielectric loss spectra of clofoctol (223.15 K–163.15 K, ΔT = 10 K from right to left), droperidol (283.15 K–133.15 K, ΔT = 10 K from right to left) and probucol (295.15 K–293.15 K, ΔT = 2 K and 283.15 K–183.15 K, ΔT = 10 K from right to left) for temperatures below T_g.

and is defined as the slope of the relaxation time curve vs. T_g/T at the glass transition temperature T_g in the Oldekop-Laughlin-Uhlmann-Angell (OLUA) plot, given by [39].

$$m = \frac{d\log(\tau)}{d\left(\frac{T_g}{T}\right)} |\mathrm{T} = \mathrm{T_g} \tag{3}$$

If the value of m is < 45 then such system belongs to strong liquids and if m is > 75 such system belongs to fragile liquids [29]. For clofoctol m = 95, for droperidol m = 85 and for probucol m = 87; hence all are fragile glass formers. We have compared the fragility indices of some of the drugs already investigated by other using broadband dielectric spectroscopy and are given in Table 2 and from that it is clear that most of the pharmaceuticals are fragile glass formers.

As further shown in Fig. 4, in the glassy state of the investigated pharmaceuticals, the evolution of secondary relaxation processes revealed linear temperature dependence and consequently be well described by the Arrhenius equation.

$$f_\beta = f_0^\beta \exp\left(\frac{-\Delta E_\beta}{\mathrm{RT}}\right) \tag{4}$$

where R is the gas constant (R = 8.314 J mol^{-1} K^{-1}), f_0^β is the pre-exponential factor related to the lattice vibrational frequency and ΔE_β is the activation energy to overcome the energy barrier. Both clofoctol and probucol showed only one resolved secondary relaxation, while droperidol has two processes in the glassy state. Since the cooperative relaxations remain frozen below T_g, the secondary relaxations originating from small angle rotations of whole or parts of molecules within their surroundings are still active. From the molecular origin, they are divided as inter or intra-molecular secondary processes. Intra-molecular secondary relaxations originating from the motions of a subset of the entire molecule were traditionally being ignored in the discussion of glass transition because of their trivial role in the glass transition phenomena. While, the local motions originating from the entire molecule were got attracted ever since the classic publications of Johari and Goldstein (also known as Johari−Goldstein (JG) relaxations) almost 4 decades ago highlighting their presence even in rigid glass formers lacking intra-molecular degrees of freedom. On further detailed studies pointed out that the JG relaxations might be the precursor of structural relaxation. Since, the motion that can induce intermolecular ordering in the glassy state is the JG, they are believed to be one of the important factors responsible for the recrystallization of amorphous drugs during storage. Apparently, it is significant to ascertain the nature and origin of the resolved secondary relaxations and to identify whether JG relaxation is present or not. For that purpose, coupling model (CM) predictions were used.

According to the CM predictions, the structural relaxation is correlated to its precursor, the JG relaxation through CM equation [32]. The corresponding correlation function of the model is the Kohlrausch-Williams-Watts (KWW) stretched exponential function that holds only for t > > t_c.

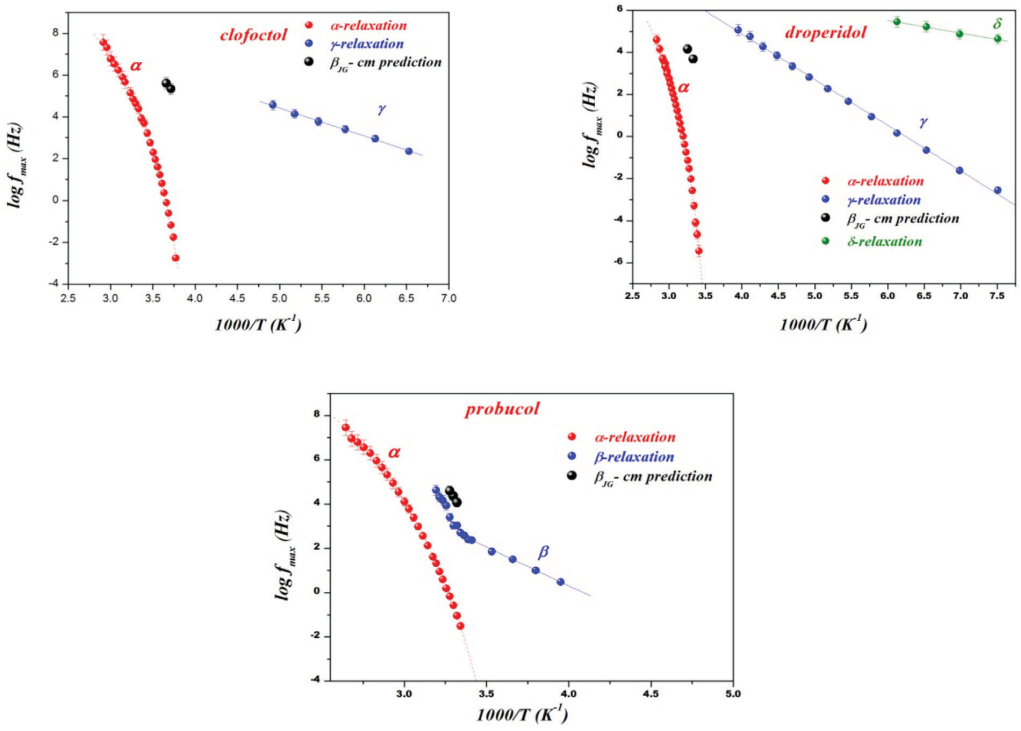

Fig. 4. Arrhenius map of clofoctol, droperidol and probucol. Red circles denote α-relaxation, blue and green circles for secondary relaxations and black circle denotes the CM prediction for JG β-relaxation. Solid red line represents the VFT fit for α-relaxation and solid blue and green lines represent the Arrhenius fit for secondary relaxations. (For interpretation of the references to colour in this figure legend, the reader is referred to the web version of this article.)

Table 2
Fragility indices of some pharmaceuticals.

Sl. no	Name	Fragility	Reference
1	Nifecupine	33	Biard et al. J. Pharm. Sci. 2010.
2	Carbamazepine	55.3	K. Kawakami et al. J. Pharm. Sci. 2012.
3	Indomethacin	67	Natalia. T et al. Phar. Res. 2001.
4	Procane	69	Biard et al. J. Pharm. Sci. 2010.
5	Haloperidol	72.8	K. Kawakami et al. J. Pharm. Sci. 2012
6	Ketoconazole	78	Biard et al. J. Pharm. Sci. 2010
7	Acetaminophen	79.5	Deliang Zhou et al. J.Pharm.Sci. 2002.
8	Ibuprofen	93	Bras A. R et al. J. Phy. Chem. B 2008.
9	Ketoprofen	86.57	Sailaja et al. Euro. J. Pharm. Sci. 2013.
10	Fenofibrate	83.4	Deliang Zhou et al. J.Pharm.Sci. 2002.
11	Captopril	84	Sailaja et al. IOSR J. Pharm. 2012.
12	Sildenafil	85	K. Kolodziejczyk et al. Mol. Pharm. 2013.
13	Nimesulid	85	Knapik. J et al. Mol. Pharm. 2016.
14	Droperidol	85	Present study
15	Probucol	87	"
16	Clofoctol	95	"
17	Sucrose	95.3	Deliang Zhou et al. J.Pharm.Sci. 2002.
18	Tolbutamide	101	K. Kawakami et al. J. Pharm. Sci. 2012.
19	Ritonavir	107.3	Deliang Zhou et al. J.Pharm.Sci. 2002.
20	Celecoxib	110	Grzybowska et al. J. Phy. Chem. B 2010.
21	Flurbiprofen	113	A. C. Rodrigues et al. Mol. Pharm. 2014.
22	Azithromycin	117	K. Adrjanowicz et al, Mol. Pharm. 2012.
23	Clarithromycin	118	"
24	ABT-229	119.4	Deliang Zhou et al. J.Pharm.Sci. 2002.
25	Roxithromycin	121	K. Adrjanowicz et al, Mol. Pharm. 2012.

$$\varphi(t) = \exp\left[-\left(\frac{t}{\tau_\alpha}\right)^{1-n}\right] \quad (5)$$

where $n = (1 - \beta_{KWW})$ is the coupling parameter of the CM and $0 < n < 1$, and the cross over at t_c leads to a relation between τ_α and τ_0 given by

$$\tau_\alpha = [t_c^{-n}\tau_0]^{\frac{1}{1-n}} \quad (6)$$

There are experimental evidences [12,43] that the cross-over from the primitive relaxation to Kohlrausch relaxation is at $t_c \approx 2$ ps for molecular systems. The correspondence between the independent (primitive) relaxation time of the coupling model (CM),τ_0, and the (JG) β-relaxation time, τ_β, was predicted and demonstrated by K.L Ngai [30]. The primitive and the JG relaxation processes are not identical, but they are closely related and are in good agreement for many molecular and polymeric glass formers [9,31] and for many APIs also [24].

The dielectric loss spectra of the samples were fitted using Fourier transform of the KWW function for the temperatures near to the T_g. In the case of clofoctol, as shown in Fig. 5, in the vicinity of T_g, we could only observe a deviation of loss at higher frequencies from the KWW fits. It also points that the resolved secondary relaxation (γ-) is non JG.

In the case of droperidol, as shown in Fig. 6, the well resolved secondary relaxation was found which does not shift much with the temperature. Also the calculated $\log f_0$ is located three-four orders lower to the resolved secondary relaxation. Further, there is clear deviation of the loss spectra around T_g from the fits of α-relaxation process to the KWW fits indicating that there could be an unresolved slower secondary relaxation process beneath the intense α-peaks. All these evidence points out that the resolved secondary relaxation is not the JG relaxation. In addition to the above, there is another faster relaxation (δ-process) which was resolved at much lower temperatures.

For probucol the n value for all the fitted spectra near to the glass transition temperature shows nearly invariant n values of 0.43 ($\beta_{KWW} = 0.57$) and a representative spectrum at 303.15 K is shown in

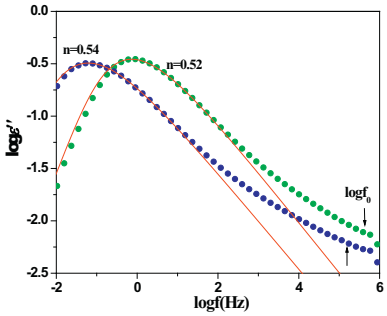

Fig. 5. KWW fit of clofoctol for temperatures 269.15 K and 273.15 K. The red line denotes the fitted data and the arrow denotes the position of Primitive relaxation frequency as predicted by Eq. (6). (For interpretation of the references to colour in this figure legend, the reader is referred to the web version of this article.)

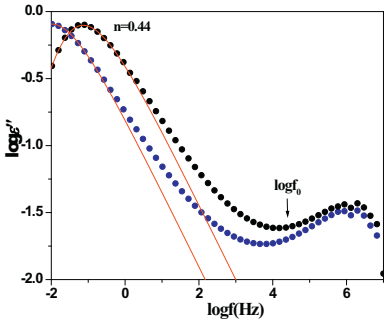

Fig. 6. KWW fit of droperidol for temperatures 303.15 K and 307.15 K. The red line denotes the fitted data and the arrow denotes the position of the primitive relaxation frequency as predicted by Eq. (6). (For interpretation of the references to colour in this figure legend, the reader is referred to the web version of this article.)

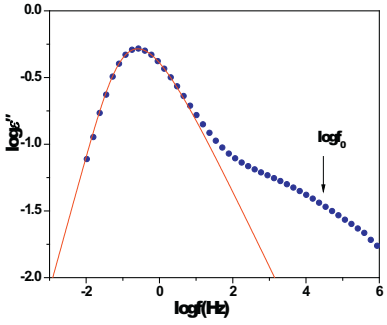

Fig. 7. KWW fit of probucol for the temperature 303.15 K. The red line denotes the fitted data and the arrow denotes the position of primitive relaxation frequency as predicted by Eq. (6). (For interpretation of the references to colour in this figure legend, the reader is referred to the web version of this article.)

Fig. 7. The value of β_{KWW} provides the deviation from the exponential behaviour of the relaxation function in time domain. The knowledge of the distribution function also helps to predict the resistance of the amorphous state against the crystallization and chemical degradation.

From the figure, the primitive relaxation time is calculated using Eq. (6) and the value of τ_0 for the above temperature is 7.1167×10^{-6} s and the corresponding frequency, $f_0 = (1/2\pi\ \tau_0) = 22.36$ kHz. It was found that the value of f_0 agrees well with the maximum of the secondary relaxation peak and thus it is JG secondary relaxation from the CM predictions. Therefore the secondary relaxation observed in this system was supposed to be intermolecular origin and is related to the local motion of the whole molecule. The same evidence was also reported by Knapik et at. by doing dielectric experiments at ambient and elevated pressure experiments [26].

For glass forming substances of all kinds, Ngai and Capaccioli [33] predicted the ratio E_β/RT_g quantitatively from the coupling model and arrived at the relation,

$$E_\beta/RT_g = 2.303(2\text{–}13.\ 7n - \log_{10}\tau_\alpha) \quad (7)$$

The ratio E_β/RT_g depends on the exponent n of α-relaxation and the pre-factor τ_α of the JG β- relaxation and the ratio fall within a broad neighborhood about 24 for most glass formers. For clofoctol the activation energy for γ-process was obtained as 25.6 kJ/mol and the value of $E_\gamma/RT_g = 11.6$ is too small for JG β-relaxation. This result supports that the JG β-relaxation is not resolved in the isothermal loss spectra. For the case of droperidol, the resolved secondary processes are γ-process (41.5 kJ/mol) and the δ-process (11.6 kJ/mol). The small values of the ratios, $E_\gamma/RT_g = 16.6$, $E_\delta/RT_g = 4.64$ indicates that none of the resolved secondary relaxations are JG. Interestingly, the ratio E_β/RT_g for probucol ($E_\beta = 67.9$ kJ/mol) was obtained as 27.4 from the experimental data and that calculated from (7) is 26.53 are matching nicely. This is further verification that the secondary relaxation obtained for probucol is JG β-relaxation.

In addition to the experimental investigations, we have pursued computational investigations of one of the title molecules, droperidol, using density functional theory calculation with the help of Gaussian 09 software. Here, we have checked the occurrence of intra-molecular secondary relaxations by incorporating all possible side-chain rotations about various dihedral angles. Among them, the rotation of droperidol shows a correlation with that of experimental results. The rotation around the oxygen atom labeled 3O of droperidol as shown in Fig. 8 has comparable barrier opposing energy of 11.14 kJ/mol with an experimental activation energy 11.6 ± 0.05 kJ/mol for the δ-process. The calculated value of activation energy may be slightly lower than that of observed experimental values since we considered only one single molecule for the simulation. Even though, the obtained results are quite comparable within a tolerance limit of few kJ/mol [20].

3.3. Test of correlation between β_K and $\Delta\varepsilon(T_g)$

Paluch and co-workers [34] examined the characteristics of structural α-relaxation in practically all Van der Waals molecular glass-formers reported so far by dielectric spectroscopy. They found that the width of the dielectric loss peak at the glass transition temperature T_g is strongly anti-correlated with the polarity of the molecule. The larger the dielectric relaxation strength $\Delta\varepsilon(T_g)$ of the system, the narrower is the α-loss peak. The frequency dispersion of the α-relaxation is obtained by fitting the complex dielectric permittivity data $\varepsilon^*(f)$ by the Fourier transform of the KWW function. Thus, narrower the width of the α-loss peak, larger is the value of β_{KWW}. They explained this remarkable property via the correlation between $\Delta\varepsilon(T_g)$ and β_{KWW} by the contribution from the dipole-dipole interaction potential $V_{dd}(r) = -Dr^{-6}$to the attractive part of the intermolecular potential, making the resultant potential more harmonic and the frequency dispersion of the α-relaxation narrower. The effect increases rapidly with the dipole moment μ and $\Delta\varepsilon(T_g)$ in view of the relation, $D \propto (\mu^4/kT_g) \propto kT_g[\Delta\varepsilon(T_g)]^2$. This trend is supported by molecular dynamics simulations of binary Lennard-Jones particles as model glass-formers [7]. Modifications of the repulsive part and/or the attractive part of the inter-particle potential resulted in different dynamic properties including non-exponentiality of the structural α-relaxation. The width of the frequency dispersion is a measure of the degrees of non-

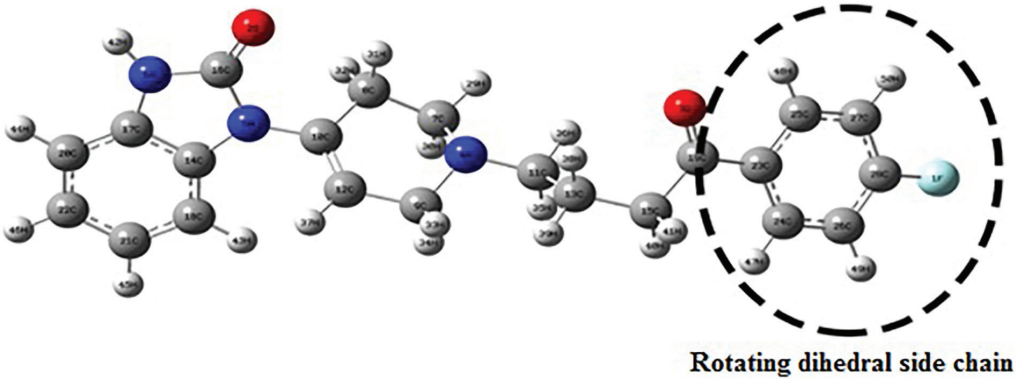

Fig. 8. Atomic arrangement of the droperidol structure, the rotated group is marked.

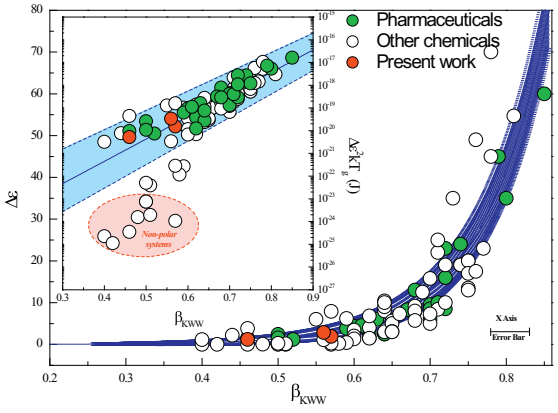

Fig. 9. β_{Kww} Vs $\Delta\varepsilon(T_g)$. The inset pictures β_{Kww} Vs $kT_g[\Delta\varepsilon(T_g)]^2$.

exponentiality and dynamic heterogeneity of the α-relaxation, and in turn the viscosity and diffusion coefficient. Therefore the correlation found is not only of fundamental interest but also of practical applications.

Among the 88 glass-formers considered by Paluch and co-workers, many are pharmaceuticals and were shown to conform well to the correlation. These pharmaceuticals are picked out in the original figures published in Ref. 34 by coloring them green in Fig. 9. Most of the pharmaceuticals studied by Paluch and coworkers [34] (green symbols) have larger values of β_{KWW} larger than 0.57. The exceptions are three, namely azithromycin (β_{KWW} = 0.52), itraconazol (β_{KWW} = 0.52), and posaconazone (β_{KWW} = 0.52). The three currently studied pharmaceutical, probucol, droperidol, and clofoctol, have values of β_{KWW} = 0.57, 0.56, and 0.46 respectively. On the lower end of the values of β_{KWW} of pharmaceuticals, these three new members afford a meaningful test of the correlation found by Paluch et al..... The data of $\Delta\varepsilon(T_g)$ and $kT_g[\Delta\varepsilon(T_g)]^2$ of the three are plotted against β_{KWW}, and shown by the circles colored red in Fig. 9 and the inset respectively. The results of the three (red) support well the correlation.

4. Conclusions

Molecular dynamics in glassy and supercooled phases of three important pharmaceuticals viz. clofoctol, droperidol and probucol were investigated in neat form using differential scanning calorimetry (DSC) and broadband dielectric spectroscopy (BDS). From the DSC measurements all the three samples showed good glass forming ability and the glass transition temperatures were recorded from the heating endotherm: clofoctol (271.0 K), droperidol (307.9 K) and probucol (301.6 K). Clofoctol and droperidol showed cold crystallization, while probucol showed smooth behaviour without indications of crystallization throughout its supercooled region till melting. Dielectric measurements show typical behaviour of glass forming systems showing structural relaxation above T_g and secondary relaxations below T_g originating from inter and intra-molecular degrees of freedom. Clofoctol and probucol revealed only single secondary relaxation, while droperidol showed two secondary relaxations. From the coupling model predictions, the resolved secondary relaxation in probucol is identified as JG in its origin and the resolved secondary relaxations in the other two samples were identified to be intramolecular in origin. The fastest secondary relaxation in droperidol was further investigated by density functional theory (DFT) calculations and the activation energy was found to be matching with the experimental values and the origin was identified to be from the rotation about the oxygen in the dihedral side chain. All the three samples showed very good correlation between the frequency dispersion of the α-relaxation (β_{KWW}) and the dielectric strength $\Delta\varepsilon(T_g)$ established in Van der Waals molecular glass formers explained in terms of dipole-dipole interaction potential to the attractive part of the intermolecular potential.

Acknowledgment

M Sahra gratefully acknowledges the U.G.C, Govt. of India for providing financial assistance through MANF scheme. G Shete acknowledges CSIR, Govt. of India for providing Senior Research Fellowship. MST acknowledges the financial assistances from KSCSTE (SRS, SARD), UGC (MRP) and DST FIST and CSIF University of Calicut.

References

[1] K. Adrjanowicz, Z. Wojnarowska, P. Wlodarczyk, K. Kaminski, M. Paluch, J. Mazgalski, molecular mobility in liquid and glassy states of telmisartan (TEL) studied by broadband dielectric spectroscopy, Eur. J. Pharm. Sci. 38 (4) (2009) 395–404.
[2] K. Adrjanowicz, Z. Wojnarowska, K. Grzybowska, L. Hawelek, K. Kaminski, M. Paluch, A. Kasprzycka, K. Walczak, Molecular dynamics and crystallization phenomenon of supercooled and glassy DNA and RNA nucleosides: β-adenosine, β-thymidine, and β-uridine, Phys. Rev. E 84 (2011) 51507.
[3] K. Adrjanowicz, K. Kaminski, M. Paluch, K.L. Ngai, L. Yu, Study of dynamics and crystallization kinetics of 5-methyl-2-(2- nitrophenyl)amino-3-thiophenecarbonitrile at ambient and elevated pressure, J. Chem. Phys. 136 (23) (2012).
[4] C.A. Angell, K.L. Ngai, G.B. McKenna, P.F. McMillan, S.W. Martin, Relaxation in glassforming liquids and amorphous solids, J. Appl. Phys. 88 (6) (2000) 3113–3157.
[5] J.A. Baird, B. Van Eerdenbrugh, L.S. Taylor, A classification system to assess the crystallization tendency of organic molecules from undercooled melts, J. Pharm. Sci. 99 (9) (2010) 3787–3806.

[6] C. Bhugra, M.J. Pikal, Role of Thermodynamic, Molecular, and Kinetic Factors in Crystallization from the Amorphous State, J. Pharm. Sci. 97 (4) (2008) 1329–1350.

[7] P. Bordat, F. Affouard, M. Descampes, K.L. Ngai, Does the interaction potential determine both the fragility of the liquid and the vibrational properties of its glassy state? Phys. Rev. Lett. 93 (2004) 105502.

[8] Bra, A. R.; Noronha, P.; Antunes, A. M. M.; Cardoso, M. M.; Dionı, M.; Correia, T.; De Physique, U. F. R.; Bat, P.; Uni, V. Molecular motions in amorphous ibuprofen as studied by broadband dielectric spectroscopy. J. Phys. Chem. B 2008, 112, 11087–11099.

[9] S. Capaccioli, D. Prevosto, M. Lucchesi, P.A. Rolla, R. Casalini, K.L. Ngai, Identifying the genuine Johari–Goldstein β-relaxation by cooling, compressing, and aging small molecular glass-formers, J. Non-Cryst. Solids 351 (33–36) (2005) 2643–2651.

[10] V. Caron, C. Bhugra, M.J. Pikal, Prediction of onset of crystallization in amorphous pharmaceutical systems: phenobarbital, nifedipine/PVP, and phenobarbital/PVP, J. Pharm. Sci. 99 (2010) 3887–3900.

[11] L. Carpentier, R. Decressain, A. De Gusseme, C. Neves, M. Descamps, Molecular mobility in glass forming fananserine: a dielectric, NMR, and TMDSC investigation, Pharm. Res. 23 (4) (2006) 798–805.

[12] J. Colmenero, A. Arbe, A. Alegría, Crossover from debye to non-debye dynamical behavior of the alpha relaxation observed by quasielastic neutron scattering in a glass-forming polymer, Phys. Rev. Lett. 71 (16) (1993) 2603–2606.

[13] D.Q.M. Craig, P.G. Royall, V.L. Kett, H. M, The relevance of the amorphous state to pharmaceutical dosage forms: glassy drugs and freeze dried systems, Int. J. Pharm. 179 (2) (1999) 179–207.

[14] T. El Goresy, R. B, Dielectric Relaxation Processes in Solid and Supercooled Liquid Solutions of Acetaminophen and Nifedipine, J. Phys. Condens. Matter 19 (2007).

[15] G. Fulcher, Analysis of recent measurements of the viscosity of glasses.—ii1, J. Am. Ceram. Soc. 8 (12) (1925) 789–794.

[16] G.S. Fulcher, Analysis of recent measurements of the viscosity of glasses, J. Am. Ceram. Soc. 8 (6) (1925) 339–355.

[17] K. Grzybowska, M. Paluch, a Grzybowski, Z. Wojnarowska, L. Hawelek, K. Kolodziejczyk, K.L. Ngai, Molecular dynamics and physical stability of amorphous anti-inflammatory drug: celecoxib, J. Phys. Chem. B 114 (40) (2010) 12792–12801.

[18] B.C. Hancock, G. Zografi, Characteristics and significance of the amorphous state in pharmaceutical systems, J. Pharm. Sci. 86 (1) (1997) 1–12.

[19] S. Havriliak, S. Negami, A complex plane representation of dielectric and mechanical relaxation processes in some polymers, Polymer (Guildf). 8 (1967) 161–210.

[20] Hensel-Bielowka, S.; Wojnarowska, Z.; Dzida, M.; Zor, E.; Geppert-Rybczyn, M.; Peppel, T.; Grzybowska, K.; Wang, Y.; Sokolov, A. P.; Paluch, M. Heterogeneous nature of relaxation dynamics of room-temperature ionic liquids (EMIm) 2 [Co (NCS) 4] and (BMIm) 2 [Co(NCS) 4]. 2015.

[21] A. Jedrzejowska, K.L. Ngai, M. Paluch, Modifications of structure and intermolecular potential of a canonical glassformer: dynamics changing with dipole–-dipole interaction, J. Phys. Chem. A 120 (44) (2016) 8781–8785.

[22] G.P. Johari, S. Kim, R.M. Shanker, Dielectric studies of molecular motions in amorphous solid and ultraviscous acetaminophen, J. Pharm. Sci. 94 (10) (2005) 2207–2223.

[23] G.P. Johari, S. Kim, S. Ravi, Dielectric relaxation and crystallization of ultraviscous melt and glassy states of aspirin, ibuprofen, progesterone, and quinidine, J. Pharm. Sci. 96 (2007) 1159–1175.

[24] K. Kaminski, E. Kaminska, K. Adrjanowicz, K. Grzybowiska, P. Wlodarczyk, M. Paluch, A. Burian, J. Ziolo, P. Lepek, J. Mazgalski, W. Sawicki, K. Kaminski, E. Kaminska, K. Adrjanowicz, K. Grzybowiska, P. Wlodarczyk, M. Paluch, A. Burian, W. Zio, Dielectric relaxation study on tramadol monohydrate and its hydrochloride salt, J. Pharm. Sci. 99 (1) (2010) 94–106.

[25] A.M. Kaushal, P. Gupta, A.K. Bansal, Amorphous drug delivery systems: molecular aspects, design, and performance, Crit. Rev. Ther. Drug Carrier Syst. 21 (3) (2004) 133–193.

[26] J. Knapik-Kowalczuk, Z. Wojnarowska, M. Rams-Baron, K. Jurkiewicz, J. Cielecka-Piontek, K.L. Ngai, M. Paluch, Atorvastatin as a promising crystallization inhibitor of amorphous probucol: dielectric studies at ambient and elevated pressure, Mol. Pharm. 14 (8) (2017) 2670–2680.

[27] K. Kothari, V. Ragoonanan, R. Suryanarayanan, Influence of molecular mobility on the physical stability of amorphous pharmaceuticals in the supercooled and glassy states, Mol. Pharm. 11 (9) (2014) 3048–3055.

[28] A.P. Lötter, J.J. Gerber, M.R. Caira, Structures of two conformational polymorphs of the cholesterol-lowering drug probucol, J. Crystallogr. Spectrosc. Res. 23 (11) (1993) 863–869.

[29] J. Lu, S. Rohani, Polymorphism and crystallization of active pharmaceutical ingredients (APIs), Curr. Med. Chem. 16 (7) (2009) 884–905.

[30] K.L. Ngai, Relation between some secondary relaxations and the α relaxations in glass-forming materials according to the coupling model, J. Chem. Phys. 109 (1998) 6982–6994.

[31] K.L. Ngai, An extended coupling model description of the evolution of dynamics with time in supercooled liquids and ionic conductors, J. Phys. Condens. Matter 15 (2003) S1107–S1125.

[32] K.L. Ngai, Why the glass transition problem remains unsolved? J. Non-Cryst. Solids 353 (8–10) (2007) 709–718.

[33] K. Ngai, S. Capaccioli, Relation between the activation energy of the Johari-Goldstein β relaxation and T_{g} of glass formers, Phys. Rev. E 69 (3) (2004) 31501.

[34] M. Paluch, J. Knapik, Z. Wojnarowska, A. Grzybowski, K.L. Ngai, Universal behavior of dielectric responses of glass formers: role of dipole-dipole interactions, Phys. Rev. Lett. 116 (2016) 25702.

[35] A. Patkowski, M. Paluch, J. Gapiński, Relationship between T0, Tgand their pressure dependence for supercooled liquids, J. Non-Cryst. Solids 330 (1–3) (2003) 259–263.

[36] U. Sailaja, M. Shahin Thayyil, N.S. Krishna Kumar, G. Govindaraj, Molecular dynamics in liquid and glassy states of non-steroidal anti-inflammatory drug: Ketoprofen, Eur. J. Pharm. Sci. 49 (2) (2013) 333–340.

[37] Y. Sun, L. Zhu, T. Wu, T. Cai, E.M. Gunn, L. Yu, Stability of amorphous pharmaceutical solids: crystal growth mechanisms and effect of polymer additives, AAPS J. 14 (3) (2012) 380–388.

[38] G. Tammann, W. Hesse, The dependence of viscosity upon the temperature of supercooled liquids, Z. Anorg. Allg. Chem. 156 (1926) 245–257.

[39] H. Tanaka, Relationship among glass-forming ability, fragility, and short-range bond ordering of liquids, J. Non-Cryst. Solids 351 (8–9) (2005) 678–690.

[40] H. Vogel, The law of the relation between the viscosity of liquids and the temperature, Phys. Z. Vol. 22 (1921) 645–646.

[41] Z. Wojnarowska, K. Adrjanowicz, P. Wlodarczyk, E. Kaminska, K. Kaminski, K. Grzybowska, R. Wrzalik, M. Paluch, K.L. Ngai, Broadband dielectric relaxation study at ambient and elevated pressure of molecular dynamics of pharmaceutical: indomethacin, J. Phys. Chem. B 113 (37) (2009) 12536–12545.

[42] L. Yu, Amorphous pharmaceutical solids: preparation, characterization and stabilization, Adv. Drug Deliv. Rev. 48 (1) (2001) 27–42.

[43] R. Zorn, A. Arbe, J. Colmenero, B. Frick, D. Richter, U. Buchenau, Neutron scattering study of the picosecond dynamics of polybutadiene and polyisoprene, Phys. Rev. E 52 (1) (1995) 781–795.

Molecular Relaxations in Amorphous Phenylbutazone

M. Sahra[1,*], M. Shahin Thayyil[1] and S. Capaccioli[2]

[1]*Department of Physics, University of Calicut, Malappuram-673635, Kerala, India,* [2]*Departmento di Fisica, Università di Pisa, Largo Bruno Pontecorvo 3, I-56127, Pisa, Italy, *Email:sahratp@gmail.com*

Abstract. Molecular dynamics of phenylbutazone in the supercooled liquid and glassy state is studied using broadband dielectric spectroscopy for test frequencies 1 kHz, 10 kHz and 100 kHz over a wide temperature range. Above the glass transition temperature T_g, the presence of the structural α- relaxation peak was observed which shifts towards lower frequencies as the temperature decreases and kinetically freezes at T_g. Besides the structural α- relaxation peak, a β-process which arises due to the localized molecular fluctuations is observed at lower temperature.

Keywords: Broadband dielectric spectroscopy, Molecular dynamics.
PACS: 77.22.Gm, 64.70.P-

INTRODUCTION

In recent years the development of amorphous pharmaceuticals has become one of the most important aspects of pharmaceutical research due to the fact that amorphous pharmaceuticals shows better solubility and bioavailability than their crystalline form [1]. As the amorphous state is having higher free energy than the crystalline state, the amorphous pharmaceuticals are thermodynamically unstable and quickly return to their crystalline form [2]. Stability of the amorphous phase is significantly affected by the molecular dynamics, intrinsic properties like Glass Forming Ability (GFA), fragility, viscosity, crystallization rate and storage temperature etc. According to recent studies molecular dynamics play a crucial role in determining the physical and chemical stability of amorphous pharmaceuticals. It is believed that initiation of crystallization can be triggered by intermolecular dynamics involving the β-relaxation mode. Thus it is very important to understand the nature and molecular mechanism responsible for the secondary relaxations observed in the glassy state.

To study the molecular relaxations in amorphous pharmaceuticals, broadband dielectric spectroscopy (BDS) proved to be one of the best tools. The unique advantage of broadband dielectric spectroscopy is its tremendous ability for monitoring the molecular mobility over broad frequency range and in a wide range of temperatures and pressures. Even the microscopic or molecular level information can be achieved by this technique.

EXPERIMENTAL

Phenylbutazone (synonyms: 4-Butyl-1,2-diphenyl-3,5-pyrazolidinedione) was purchased from Sigma Aldrich and used as received without any further purification, which is stable against crystallization during the experiment. Glassy pharmaceuticals were prepared by quench cooling the melt. Dielectric measurements were carried out using Novocontrol Alpha analyzer. Sample cell is made up of a parallel plate capacitor separated by silicon fiber spacers of 50 micron diameter with an empty cell capacitance of approximately 100 pF and the sample is filled between the plates. The temperature is controlled using dry nitrogen-flow in the Novocontrol Quatro cryosystem (-170°C – 125°C). The sample was heated to few degrees above the melting point and cooled rapidly to -170^0C, the achievable lowest temperature in this experimental setup. Dielectric spectra for different frequencies were measured during heating of the sample from deep glassy state.

Phenylbutazone is a non-steroidal anti-inflammatory drug (NSAID). It is a potent pain reliever, antipyretic and anti-inflammatory, usually used in animals.

RESULTS AND DISCUSSIONS

The chemical formula of phenylbutazone is $C_{19}H_{20}N_2O_2$ with a molecular weight of 308,37g/mol, melting point ranges between 379K-381K, according to manufacturer's specification. Boiling point is 675K.

DAE Solid State Physics Symposium 2015
AIP Conf. Proc. 1731, 070026-1–070026-3; doi: 10.1063/1.4947858

Relaxation Dynamics of Amorphous Dibucaine Using Dielectric Studies

M. Sahra[1,*], K. Jumailath[2], M. Shahin Thayyil[1] and S. Capaccioli[3]

[1]*Department of Physics, University of Calicut, Malappuram-673635, Kerala, India*
[2]*Department of Physics, MES Ponnani College, Ponnani-679586, Kerala, India*
[3]*Departmento di Fisica, Università di Pisa, Largo Bruno Pontecorvo 3, I-56127, Pisa, Italy*
**E-mail:sahratp@gmail.com*

Abstract. Using broadband dielectric spectroscopy the molecular mobility of dibucaine is investigated in the supercooled liquid and gassy states, over a wide temperature range for some test frequencies. Above the glass transition temperature T_g, the presence of structural α- relaxation peak was observed due to the cooperative motions of the molecule and upon cooling frozen kinetically to form the glass. The secondary relaxation process was perceivable below T_g due to localized motions. The peak loss frequency of α-relaxation process shows non-Arrhenius behavior and obeys Vogel-Fulcher-Tammann equation over the measured temperature range whereas the β- process shows Arrhenius behavior.

Keywords: Molecular mobility, Glass transition temperature, Broadband dielectric spectroscopy.
PACS: 77.22.Gm, 64.70.P-

INTRODUCTION

Investigating the molecular dynamics of amorphous pharmaceutical is very important for proposing an alternative way to achieve better solubility and bioavailability *via* oral route. One of the unique features of molecular dynamics of glass-forming systems is the continuous and dramatic increase of the structural relaxation time from values of the order of picoseconds in the liquid state to hundreds of seconds in the vicinity of the glass transition temperature. Drugs prepared in the amorphous forms are characterized by better bioavailability and solubility than their crystalline counterparts [1]. But the amorphous pharmaceuticals can quickly revert to their crystalline forms since supercooled and glassy states are thermodynamically unstable [2] and hence the stability of the amorphous phase against the physical and chemical degradation is a crucial issue to be addressed to determine the applicability of the amorphous active pharmaceutical ingredient (API) for practical application. Crystallization in amorphous materials can be triggered by the intermolecular relaxation modes [3] and these relaxations are very important in determining the shelf life of amorphous pharmaceuticals.

It is well accepted that broadband dielectric spectroscopy (BDS) is a useful tool for studying molecular dynamics in amorphous pharmaceuticals because of the rotational degrees of freedom enjoyed by supercooled and glassy materials. The relaxation properties over a very wide range of frequencies at different thermodynamic conditions (T, P) can be monitored using this technique.

EXPERIMENTAL

Dielectric relaxation spectroscopy probes the interaction of a macroscopic sample with a time dependent electric field. The resulting polarization is expressed by the frequency-dependent complex permittivity which characterizes the relaxation dynamics of the molecules within the sample.

Dibucaine with purity ≥ 99% was purchased from Sigma Aldrich, USA and used as received without further purification. Amorphous dibucaine was prepared by cooling the melt with very high cooling rate to avoid crystallization. Dielectric measurements were carried out using Novocontrol Alpha analyzer. The sample cell is made up of a parallel plate

Solid State Physics
AIP Conf. Proc. 1665, 070035-1–070035-3; doi: 10.1063/1.4917899

Molecular Dynamics in Amorphous Ergocalciferol

Sahra Mohamed[1] and M. Shahin Thayyil[1,*] and S. Capaccioli[2]

[1]*Department of Physics, University of Calicut, Malappuram-673635, Kerala, India*
[2]*Departmento di Fisica, Università di Pisa, Lungarno Paqconotti, 43, 565126 Pisa, Italy*
**E-mail:shahinth@gmail.com*

Abstract. While developing new pharmaceutical products based on drug substances in their amorphous form, the molecular mobility of amorphous active ingredients have to be characterized in detail. The molecular mobility in the supercooled liquid and glassy states of ergocalciferol is studied using broadband dielectric spectroscopy over wide frequency and temperature ranges. Dielectric studies revealed a number of relaxation process of different molecular origin.

Keywords: Amorphous pharmaceuticals, Broadband dielectric spectroscopy, Molecular dynamics, Glass transition.
PACS: 77.22.Gm, 64.70.P-

INTRODUCTION

When a liquid is cooled avoiding crystallization, we get supercooled liquid and on further decrease of temperature a glassy state can be reached. At glass transition temperature T_g, molecular motions slow down to the time scale of the order of few hundreds of seconds. Below T_g, the molecular rearrangement is extremely slow and the molecules cannot reach their equilibrium condition. Relaxation dynamic studies provide detailed information about molecular mobility above and below T_g. Amorphous Pharmaceuticals have greater solubility and dissolution rate than their crystalline counterpart [1]. Molecular mobility of the amorphous state forms a key factor responsible for the physical and chemical stability of the active pharmaceutical ingredient (API). Thus, understanding the nature and molecular mechanism responsible for the secondary relaxations observed in the glassy state is very crucial to ascertain the shelf life of these APIs. One of the best tools available to investigate the relaxation properties of the amorphous materials is the broadband dielectric spectroscopy (BDS) since it provides information about molecular dynamics in liquid and glassy states over a wide range of frequency, temperature and even at elevated pressures.

EXPERIMENTAL

Ergocalciferol with purity ≥ 98% was purchased from Sigma Aldrich, USA and used as received without further purification. It is stable against crystallization throughout the experiment. Glassy ergocalciferol was prepared by cooling the melt by exposing very high cooling rate to avoid crystallization. Dielectric measurements were carried out using Novocontrol Alpha analyzer in the frequency range of 10 mHz – 10 MHz. The temperature is controlled using dry nitrogen-flow in the Novocontrol Quatro cryosystem (-170°C – 125°C). The sample was heated to few degrees above the melting point cooled rapidly to -170^{0}C. Dielectric spectra were measured isothermally, after stabilizing the temperature.

RESULTS AND DISCUSSIONS

The chemical formula of ergocalciferol is ($C_{28}H_{44}O$) with a molecular weight of 396.65g/mol and melting point ranges between 114°C –118°C. The chemical structure of ergocalciferol is given below.

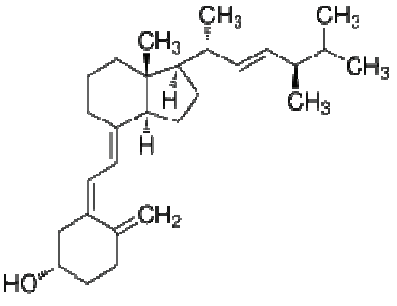

Solid State Physics
AIP Conf. Proc. 1591, 825-827 (2014); doi: 10.1063/1.4872769

Research Journal of Recent Sciences E-ISSN 2277-2502
Vol. **5(3),** 40-44, March **(2016)** *Res. J. Recent Sci.*

Molecular Dynamics in Amorphous Atropine and Tolnaftate

Sahra Mohamed[1], Jumailath Karuthedath[2], M. Shahin Thayyil[1*] and S. Capaccioli[3]
[1]Department of Physics, University of Calicut, Kerala, India
[2]MES Ponnani College, Ponnani, India
[3]Departmento di Fisica, Università di Pisa, Italy
shahinth@gmail.com

Available online at: www.isca.in, www.isca.me
Received 27th October 2015, revised 7th December 2015, accepted 10th January 2016

Abstract

During the development of new pharmaceutical products in amorphous form, the molecular mobility of amorphous active ingredients has to be characterized in detail. Here, using broadband dielectric spectroscopy, the molecular mobility in supercooled liquid and glassy states of two pharmaceuticals namely atropine and tolnaftate have been studied. The dielectric permittivity and loss spectra of glassy and ultraviscous states of the above two pharmaceuticals have been measured for some test frequencies over a wide temperature range. Above the glass transition temperature T_g, the presence of the structural α- relaxation peak was observed which shifts towards lower frequencies as the temperature decreases and kinetically freezes at T_g. The secondary relaxations perceivable below the glass transition temperature is due to intramolecular modes and are usually designated as β, γ and δ etc. are clearly observed in the ε" spectra of atropine, while in tolnaftate no secondary relaxation processes is observed in the loss spectra, but an excess contribution to the high-frequency tail of the α-peak, called excess wing is observed. The α- process shows non-Arrhenius behavior for both the samples. The dielectric relaxation time increases on cooling according to the Vogel-Fulcher-Tammann equation. The secondary relaxation process shows Arrhenius behavior.

Keywords: Amorphous pharmaceuticals, Broadband dielectric spectroscopy, Molecular dynamics.

Introduction

In the pharmaceutical industry, the characterization of drugs is very important. Several multitude analytical techniques are used for this purpose. The pharmaceutical industry is aiming to achieve drug preservation and administration via amorphous form because amorphous pharmaceuticals have the superiority in preservation, drug delivery, bioavailability and other advantages. Most of the water insoluble active pharmaceutical ingredients (APIs) exhibit low bioavailability. Thus in order to induce pharmaceutical effects, the dose of the used drug has to be increased which in turn results in the increase of the side effects of the pharmaceuticals. This can be avoided by the preparation of the pharmaceuticals in its amorphous form. Amorphous API has better solubility properties with body fluids and has higher bioavailability comparing to its crystalline counterpart. In many cases, the drug absorption time is four to five times faster than the crystalline form. Increasing the bioavailability of pharmaceutical compounds by solubility/dissolution enhancement is extremely important to the pharmaceutical industry. Bioavailability improvements that can be attained by using an amorphous form of a drug present a more significant challenge in pharmaceutical industry[1]. But the amorphous systems are not thermodynamically stable and they can revert to their crystalline form.

One of the major issues to be avoided during the preservation of amorphous pharmaceuticals is the crystallization of the samples. Crystallization can be triggered by the intermolecular dynamics involving the β-relaxation mode[2]. Intermolecular secondary relaxations also play an important role in deciding their shelf-life. Molecular mobility of the amorphous state appears as a key factor responsible for the physical and chemical stability of the amorphous API. Hence it's crucial to understand the nature and molecular mechanism responsible for the secondary relaxations observed in the glassy state. One of the best tools to investigate the relaxation properties of the amorphous materials is broadband dielectric spectroscopy (BDS). Application of this technique enables us to monitor the molecular dynamics of examined systems over a very wide range of frequencies at different thermodynamic conditions (P, T). Thus critical study of broadband dielectric spectroscopy and other phase information will give insight to the basic physics and give way to device better technology for these issues. In this work broad band dielectric data have been obtained for 2 well-known drugs.

Materials and Methods

Atropine (synonym: (RS)-(8-methyl-8-azabicyclo[3.2.1]oct-3-yl)3-hydroxy-2-phenylpropanoate) with purity ≥ 99% and tolnaftate (synonym: Methyl-(3-methylphenyl) carbamothioic acid O-2-naphthyl ester) were purchased from Sigma Aldrich and used without any further purification. Atropine occurs as white crystals or crystalline powder and is also known as Hyoscyamine. Tolnaftate is a white to creamy white crystalline odorless powder.